INTEGRATION OF NANOPARTICLES AS DRAW SOLUTE IN FORWARD OSMOSIS

LING MINGMING

NATIONAL UNIVERSITY OF SINGAPORE

2012

INTEGRATION OF NANOPARTICLES AS DRAW SOLUTE IN FORWARD OSMOSIS

LING MINGMING

(B. Eng, Dalian University of Technology,

P. R. China)

A THESIS SUBMITTED FOR THE DEGREE OF DOCTOR OF PHILOSOPHY

DEPARTMENT OF CHEMICAL AND BIOMOLECULAR ENGINEERING

NATIONAL UNIVERSITY OF SINGAPORE

2012

DECLARATION

I hereby declare that this thesis is my original work and it has been written by me in its entirety.

I have duly acknowledged all the sources of information which have been used in the thesis.

This thesis has also not been submitted for any degree in any university previously.

_____

Ling Mingming

May 28 2012

Acknowledgement

I wish to take this opportunity to express my heartfelt gratitude to all those who have supported me to complete this thesis. First of all, I would like to express my deepest appreciation to my academic supervisor, Professor Neal Chung Tai-Shung, for his invaluable guidance throughout this research project. Besides the knowledge and skills, I also learned the dedication and diligence from Prof. Chung, which is a life-long valuable asset for me in all aspects of life. I gratefully acknowledge National University of Singapore (NUS) and Department of Chemical and Biomolecular Engineering (ChBE) for providing me an opportunity to pursue my PhD degree and to utilize all the facilities for my PhD study.

I would like to thank the financial support of the research from NUS "The Initiative on Advanced Membranes for Pharmaceutical and Biomedical Application" with grant number of R-279-000-249-646, Environment and Water Industry Programme Office, Singapore (EWI) "Material Engineering and Fabrication of Nanofiltration-Based High-Performance FO Membranes for Water Reuses" with the grant numbers of R-279-000-218-305, KAUST via the grant number of R-279-000-265-597, as well as Singapore National Research Foundation (NRF) project entitled "New Advanced FO membranes and membrane systems for wastewater treatment, water reuse and seawater desalination" with the grant number of R-279-000-336-281.

I wish to take this opportunity to sincerely thank Dr. K. Y. Wang, Dr. Q. Yang and Dr. J. C. Su for their kindly help and discussions during my study. I would like to thank Dr. W. Wang for the discussion on nanoparticle synthesis. I acknowledge Prof. D. R. Paul from University of Texas for his enlightenment on the nanoparticle osmotic pressure calculation. I also thank all the sweet colleagues in our research group for their kind assistance and precious friendship.

Last but not least, I am most grateful to my grandparents, Mr. Quanxing Wang and Mrs. Yulan Wang, my parents and my fiancé for their endless love, encouragement and support that enable me to continue my academic pursuit.

Table of Contents

DECLARATION i

Acknowledgement ii

Table of Contents iv

Summary xiii

List of Tables xvi

Lists of Figures xvi

Nomenclature xxii

CHAPTER 1 1

INTRODUCTION AND LITERATURE REVIEW 1

1.1 Background 1

1.2 History of forward osmosis 4

1.3 Osmotic pressure 6

1.3.1 Osmotic pressure 6

1.3.2 Osmotic process 8

1.3.3 Concentration polarization 12

1.4 Draw solution 16

1.5 Applications of forward osmosis 19

1.6 Nanoparticles 22

1.6.1 Nanoparticles as draw solute in forward osmosis 22

1.7 Research objectives and project organization 24

1.71 Research objectives 24

1.72 Project organization 26

1.8 References 28

CHAPTER 2 33

EXPERIMENTAL 33

2.1 Synthesis of nanoparticles 33

2.1.1 Synthesis of 20 nm in diameter magnetic nanoparticles coated with triethylene glycol 33

2.1.2 Synthesis of 20 nm in diameter magnetic nanoparticles coated with 2-pyrrolidine 33

2.1.3 Synthesis of 20 nm in diameter magnetic nanoparticles coated with polyacrylic acid 34

2.1.4 Synthesis of 7 nm in diameter magnetic nanoparticles coated with polyacrylic acid..... 35

2.1.5 Synthesis of 5 nm in diameter magnetic nanoparticles coated with polyacrylic acid..... 35

2.1.6 Synthesis of 4 nm in diameter magnetic nanoparticles coated with polyacrylic acid..... 36

2.1.7 Synthesis of 20nm in diameter thermo-responsive magnetic nanoparticles..... 36

2.1.8 Synthesis of 20nm in diameter nanoparticles coated with polyacrylic acid and poly(N-isopropylacrylamide) 37

2.1.8 Surface dissociation of nanoparticles 38

2.2 Characterizations of nanoparticles 38

2.2.1 Field Emission Scanning Electron Microscope (FESEM) and Transmission Electron Microscope (TEM)..... 38

2.2.2 Thermogravimetric Analysis (TGA) 38

2.2.3 Fourier Transform Infrared spectroscopy (FTIR) 39

2.2.4 Nanoparticle size distribution..... 39

2.2.5 Vibrating Sample Magnetometer (VSM) 39

2.3 Forward osmosis performance test..... 40

CHAPTER 3 42

HIGHLY WATER SOLUBLE MAGNETIC NANOPARTICLES AS NOVEL DRAW SOLUTE IN FORWARD OSMOSIS 42

3.1 Introduction 42

3.2 Experimental 45

3.2.1 Synthesis of magnetic nanoparticles 45

3.2.2 Characterization of Magnetic Nanoparticles 47

3.2.3 Forward Osmosis using Surface Functionalized Magnetic Nanoparticles as Draw solutes 48

3.3 Results and discussion 50

3.3.1Characterizations of magnetic nanoparticles 50

3.3. 2 Forward osmosis performance evaluation of the membrane 53

3.3.3 Forward osmosis performance using Versatile Magnetic Nanoparticles as Draw Solutes 54

3.3.4 Facile Recovery of Magnetic Nanoparticles by Magnetic Field Capture 61

3.3.5 Forward osmosis performance using PAA-MNPs of Different Diameters as Draw Solute 63

3.4 Conclusion 66

3.5 References 67

CHAPTER 4 71

DESALINATION PROCESS USING SUPER HYDROPHILIC NANOPARTICLES VIA FORWARD OSMOSIS INTEGRATED WITH ULTRAFILTRATION REGENERATION 71

4.1 Introduction 71

4.2 Experimental 74

4.2.1 Preparation and Characterization of Highly Water-Soluble Nanoparticles 75

4.2.2 Ultrasonication Process to agglomerated magnetic nanoparticles 76

4.2.3 Forward Osmosis Process Integrated With Ultrafiltration for Desalination 76

4.2.4 Characterization of Pore Size Distribution of UF Membranes 79

4.3 Results and Discussion 80

4.3.1 Nanoparticles Characterization 80

4.3.2 Evaluation of Ultrasonication to Agglomerated Magnetic Nanoparticles 81

4.3.3 Integrated FO-UF System using Super Hydrophilic Nanoparticles as Draw Solutes 86

4.3.4 Desalination Process of Integrated FO-UF System with Super Hydrophilic Nanoparticles 93

4.4 Conclusion 95

4.5 References 96

CHAPTER 5 103

NOVEL DUAL-STAGE FORWARD OSMOSIS SYSTEM FOR SUSTAINABLE ENRICHEMENT USING NANOPARTICLES AS INTERMEDIATE DRAW SOLUTE 103

5.1 Introduction 103

5.2 Experimental 107

5.2.1 Preparation of Highly Hydrophilic Nanoparticle Draw Solutes 108

5.2.2 Characterization of Pore Size Distribution of FO Membranes 108

5.2.3 Forward Osmosis based on the HTI FO Membrane 110

5.2.4 Protein Enrichment via Dual-Stage FO system 111

5.3 Results and Discussion 113

5.3.1 Protein Enrichment in the Dual FO System 113

5.3.2 Size Effect in Protein Enrichment via Dual-Stage FO System 121

5.3.3 Charge Effect in Protein Enrichment via Dual-stage FO System 123

5.3.4 Comparison of BSA enrichment kinetics with improved performance 125

5.3.5 Effects of FO Membrane Orientation on Protein Enrichment Performance .. 127

5.4 Conclusion..... 131

5.5 References 132

CHAPTER 6 137

FACILE SYNTHESIS OF THERMOSENSITIVE MANGETIC NANOPARTICLES AS ‘SMART’ DRAW SOLUTE IN FORWARD OSMOSIS 137

6.1 Introduction 137

6.2 Thermosensitive magnetic nanoparticles as draw solute in forward osmosis..... 139

6.3 Evaluation of thermosensitive magnetic nanoparticles as draw solute in forward osmosis 147

6.4 Conclusion..... 149

6.5 References 150

CHAPTER 7 154

SURFACE-DISSOCIATED NANOPARTICLE DRAW SOLUTIONS INI FORWARD OSMOSIS AND THE REGENERATION IN AN INTEGRATED ELECTRIC FIELD AND NANOFILTRATION SYSTEM 154

7.1 Introduction 154

7.2 Experimental 157

7.2.1 Materials 157

7.2.2 Synthesis of Surface-dissociated Nanoparticles 157

7.2.3 Characterization of Surface-dissociated Nanoparticles 159

7.2.4 Forward Osmosis using Surface-Dissociated Nanoparticles as Draw Solutes 160

7.2.5 Nanoparticle Draw Solutes Regeneration via Integrated Eletrophresis-Nanofiltration System 160

7.3 Results and Discussion 161

7.3.1 Design strategies of surface-dissociated nanoparticles 161

7.3.2 Characterization of Surface-Dissociated Nanoparticles 163

7.3.3 Improved FO Performance using Surface-Dissociated Nanoparticles as Draw Solute 166

7.3.4 Effect of Different Ions and Ligand Compositions of Nanoparticle Draw Solutes on FO Performance 169

7.4 Conclusions 177

7.5 References 178

CHAPTER 8 183

CONCLUSION AND RECOMMENDATIONS 183

8.1 Conclusion 183

8.2 Recommendations 186

Publication list 189

Summary

This dissertation is about the exploration and investigation of using nanoparticles as novel draw solute in forward osmosis (FO); the science and engineering in FO using nanoparticles as draw solute and their regenerations in integrated systems for different applications.

Highly water soluble magnetic nanoparticles have been molecularly designed. For the first time, the application of highly hydrophilic magnetic nanoparticles as novel draw solutes in FO was systematically investigated. Magnetic nanoparticles functionalized by various groups were synthesized to explore the correlation between surface chemistry of magnetic nanoparticles and the achieved osmolality. The magnetic nanoparticles can be captured by the magnetic field and recycled back into the stream as draw solutes in the FO process. In addition, magnetic nanoparticles of different diameters were also synthesized to study the effect of particles size on FO performance. It is demonstrated that the engineering of surface hydrophilicity and magnetic nanoparticle size are both crucial in their application as draw solutes in FO. It is believed that magnetic nanoparticles will soon find great use in this area.

A potentially sustainable integrated FO-UF (forward osmosis - ultrafiltration) system for water reuse and desalination with the aid of super hydrophilic nanoparticles as draw

solutes has been proposed. The system uses a FO membrane as the semi-permeable membrane to reject salts, super hydrophilic nanoparticles as draw solutes to induce water across the FO membrane, and UF membranes to regenerate the draw solutes. The novel FO-UF process was tested for 5 continuous runs for the purpose of desalination without increasing nanoparticle draw solute size or reducing osmotic functionality. The proposed FO-UF integrated system using super hydrophilic nanoparticles as draw solutes is a promising technology to desalinate seawater and brackish water as well as wastewater reclamation.

Novel dual-stage FO system was conceptually demonstrated its applications, for the first time, to enrich proteins without causing protein structural changes. Highly hydrophilic nanoparticles were utilized as the draw solute to dehydrate protein solutions in the up-stage FO, while model reverse osmosis (RO) retentate as the draw solute to regenerate the nanoparticle solution in the down-stage FO. To explore the universal applicability of the dual-stage FO system for protein enrichment, various types of proteins of different sizes and charge characteristics were studied under different membrane orientations and testing modes. Excellent enrichment performance can be achieved by increasing membrane surface area and osmotic pressure of nanoparticles under the pressure retarded mode in both up-stage and down-stage FO systems. It is believed that the dual-stage FO system has great potential in future applications of protein and pharmaceutical enrichments because of its simplicity, practicality, and economy.

Thermo-sensitive superparamagnetic nanoparticles were synthesized in one-step thermal decomposition method and successfully recycled as a ‘smart’ draw solute in forward osmosis processes for water reuse without losing performance efficiency. The ‘smart’ draw solutes exhibit improved recyclability with the aid of thermo-responsive property compared to the nanoparticle draw solutes of the first generation. These enhancements show the perspectives for the development of nanoparticle draw solutes in the future research.

Surface-dissociated PAA@NPs and PAA-PNIPAM@NPs have been prepared and applied successfully as draw solutes in FO for water reuse. Nanoparticle draw solutions exhibited higher water fluxes and osmotic pressures after enhanced surface-dissociation using alkaline solutions. Surface-dissociated nanoparticle draw solutions with NaOH added performed superior to $Ca(OH)_2$ surface-dissociated nanoparticles of the same ligand compositions on nanoparticle surface. Draw solutions of surface-dissociated PAA nanoparticles can create a higher driving force than PAA-PNIPAM nanoparticles. The integrated electric field and nanofiltration system was proven to be effective in the regeneration of nanoparticle draw solutes. Future work will be focused on the optimization and energy evaluation of the regeneration system in the application of water reclamation.

List of Tables

Table 5.1 Secondary structure of original BSA and concentrated BSA

Table 7.1 Illustration of nanoparticles prepared in the work

Lists of Figures

Figure 1.1 Schematic drawings of osmotic processes

Figure 1.2 Schematic drawing of forward osmosis (draw solution and feed solution)

Figure 1.3 Schematic drawing of operational orientations of forward osmosis

Figure 1.4 Schematic illustrations of osmotic processes in terms of water flux and the driving force

Figure 1.5 Illustrations of CPs in FO mode and PRO mode

Figure 1.6 Illustrations of CPs in double-skinned FO membrane under different membrane orientations

Figure 1.7 SEM image of HTI FO membrane

Figure 1.8 Schematic drawing of hydration bag

Figure 1.9 Illustration of hydration bag

Figure 1.10 Cross-section of osmotic drug-delivery system

Figure 1.11 Illustration of different magnetic properties

Figure 2.1 Schematic diagram of a laboratory-scale FO set-up combined with a magnetic separator

Figure 3.1 Synthesis routes of surface functionalized magnetic nanoparticles

Figure 3.2 TGA graph of magnetic nanoparticles

Figure 3.3 FESEM and size distribution of magnetic nanoparticles

Figure 3.4 FTIR spectra of magnetic nanoparticles

Figure 3.5 Hysteresis loops of magnetic nanoparticles at 300 K.

Figure3.6 Water flux and salt reverse flux using a HTI FO membrane (NaCl as the draw solution)

Figure 3.7 Water flux of surface capping groups and magnetic nanoparticles

Figure 3.8 Osmolality of surface capping groups and magnetic nanoparticles in water

Figure 3.9 Potential energy to explain water flux differences

Figure 3.10 Summary of (a) highest water flux and (b) osmolality of magnetic nanoparticles of different surface chemistries

Figure 3.11 Water flux of magnetic nanoparticles before and after recycle

Figure 3.12 Size distributions of recycled magnetic nanoparticles (a) 2-Pyrol-MNPs (b) TREG-MNPs (c) PAA-MNPs

Figure 3.13 Size distributions of PAA-MNPs synthesized by adding (a) 2.5g (b) 2.0g (c) 1.5g and (d) 1.0g of polyacrylic acid in 25.0 ml solvent

Figure 3.14 Effect of PAA-MNP particle sizes on (a) water flux and (b) osmolality

Figure 4.1 Schematic diagram of the laboratory-scale integrated FO-UF system

Figure 4.2 TEM images of regenerated PAA-NPs.

Figure 4.3 Size distributions (a) and FTIR spectra (b) of TRGE-NPs

Figure 4.4 Hysteresis loops (a) and water flux (b) of TREG-NPs

Figure 4.5 Osmotic pressure (a) and water flux of FO process (b) comparisons of PAA-NPs draw solutions regenerated by UF membranes (MWCO 1K & 4K), DI water as feed solution in FO, PRO mode

Figure 4.6 Size distributions of PAA-NPs in draw solutions and filtrate water

Figure 4.7 (a) Solute rejection plotted on the log-normal probability co-ordinate system, (b) cumulative pore size distribution curves, and (c) pore size distribution density curves

Figure 4.8 Images of PAA-NPs draw solutions and filtrate water. a. Draw solute; b. Filtrate water by UF, MWCO 4K, one stage; c. Filtrate water by UF, MWCO 4K, two stages; d. Filtrate water by UF, MWCO1K, one stage

Figure 4.9 FO performance using PAA-NPs as draw solutes, DI water and model seawater as feed solution

Figure 4.10 Normalized water flux comparison of PAA-NPs draw solutions, DI water and model seawater as feed solution in FO

Figure 5.1 Schematic diagram of the laboratory-scale dual FO system for protein enrichment

Figure 5.2 a. pore size distribution of HTI FO membrane; b. diameter distribution of PAA-NPs

Figure 5.3 Water flux and salt flux of HTI FO memebrane, using NaCl as draw solute

Figure 5.4 Kinetics of protein enrichment in single and dual FO systems

Figure 5.5 Gel track of BSA of original and concentrated

Figure 5.6 CD spectra of BSA of original and concentrated

Figure 5.7 Salt flux of single and dual FO system during protein enrichment

Figure 5.8 Comparison of enlarged kinetics using PAA-NPs in single and dual FO systems

Figure 5.9 Comparison of protein enrichment kinetics for proteins of different sizes

Figure 5.10 Comparison of protein enrichment kinetics for proteins of different charges

Figure 5.11 Illustration of interactions between charged proteins and negatively charged membrane surface

Figure 5.12 Comparison of protein enrichment kinetics with increased PAA-NPs concentration. (Ic: initial PAA-NPs solution of 6 atm osmotic pressure; 2c: double-concentrationed PAA-NPs solution of 13 atm)

Figure 5.13 Comparison of protein enrichment kinetics with increased membrane area

Figure5.14 Improved protein enrichment kinetics with increased PAA-NPs concentration and membrane area

Figure 5.15 Illustrations of CPs in dual-stage FO in all membrane orientations

Figure 6.1 XRD patterns for PNIPAM/TRI-MNP

Figure 6.2 TEM images of PNIPAM/TRI-MNP before (a,b) and after magnetic separation for times (c,d)

Figure 6.3 Size distributions of PNIPAM/TRI-MNP after each regeneration

Figure 6.4 TGA profiles of PNIPAM/TRI-MNP and TRI-MNP

Figure 6.5 VSM loops of PNIPAM/TRI-MNP and TRI-MNP

Figure 6.6 PNIPAM/TRI-MNP size changes at different temperatures

Figure6.7 Schematic diagram of laboratory-scale FO set-up using thermosensitive magnetic nanoparticles as draw solute

Figure 6.8 FO performance of recycled PNIPAM/TRI-MNP

Figure 7.1 Schematic diagram of an electric field and nanofiltration integrated system

Figure 7.2 Size distributions of surface-dissociated nanoparticles and their originals

Figure 7.3 TEM imagines: A (Na/PAA@NPs), B (Ca/PAA@NPs), C (PAA@NPs), D (Na/PAA-PNIPAM@NPs) and E (Ca/PAA-PNIPAM@NPs

Figure 7.4 FTIR spectra of nanoparticles before and after dissociation

Figure 7.5 Osmotic pressure comparisons of PAA series NPs before and after dissociation

Figure 7.6 A comparison in water flux between surface-dissociated nanoparticles of different ions on PAA@NPs. (a) DI water as feed solution. (b) synthetic brackish water as feed solution

Figure 7.7 A comparison in water flux between surface-dissociated nanoparticles of different ions on PAA-PNIPAM@NPs. (a) DI water as feed solution. (b) synthetic brackish water as feed solution

Figure 7.8 A comparison in osmotic pressure comparison between surface-dissociated nanoparticles of Na^+ and Ca^{2+} in (a) PAA series and (b) PAA-PNIPAM series

Figure 7.9 A comparison in water flux between surface-dissociated nanoparticles of Na^+ capped with PAA-PNIPAM and PAA. (a) DI water as feed solution. (b) synthetic brackish water as feed solution

Figure 7.10 A comparison in water flux between surface-dissociated nanoparticles of Ca^{2+} capped with PAA-PNIPAM and PAA (a) DI water as feed solution. (b) synthetic brackish water as feed solution

Figure 7.11 A comparison in osmotic pressure between surface-dissociated nanoparticles of different ligand compositions with (a) Na^+ and (b) Ca^{2+}

Figure 7.12 Water flux of recycled Na surface-dissociated nanoparticles using synthetic brackish water as feed solution

Figure 7.13 Size distribution of recycled NPs (a) Na/PAA@NPs. (b) Na/PAA-PNIPAM@NPs

Nomenclature

A	effective membrane surface area, m^2
J_v	product water flux, $L \cdot m^{-2} \cdot h^{-1}$
Δt	operation time interval, h
ΔV	water permeation volume, L
M_w	molecular weight of surface capping material, g mol^{-1}
r_s	solute Stokes radius, nm
C_f	solute concentration in the feed solution, mol L^{-1}
C_p	solute concentration in the permeate, mol L^{-1}
R_E	effective solute rejection coefficient, %
C	molar concentration of surface capping material on nanoparticle, mol L^{-1}
M_w	molecular weight of surface capping material, g mol^{-1}
w	weight percentage of surface capping material on magnetic nanoparticle
ρ	density of magnetic nanoparticle solution, g L^{-1}
ΔH_f	molar heat of water, 80 cal g^{-1}
T_f	freezing temperature of water, 273k

T room temperature, 298k

ΔT freezing point depression

a water activity

V_w molar volume of water, $1cm^3g^{-1}$

R ideal gas constant

Greek

μ_p the mean effective pore radius, nm

μ_s the geometric mean radius of the solute at $R_E = 50\%$

σ_p the geometric standard deviation

σ_s the geometric standard deviation defined as the ratio of the r_s at $R_E = 84.13\%$ over that at $R_E = 50$

π osmotic pressure, atm

CHAPTER 1

INTRODUCTION AND LITERATURE REVIEW

1.1 Background

Energy related problems have already become worldwide problems and are getting increasingly serious. The global population is expected to increase from 6.5 billion today to 9.1 billion in 2050 according to United Union Press Release [1]. Thus, the demand for fossil fuels including petroleum, coal and natural gas rises proportionately each day in heat generation, production, commerce, transportation, and residential facilities. The US Department of Energy revealed that the world's available fossil fuels will be depleted in the early 22nd century [2]. Furthermore, greenhouse gases, mostly carbon dioxide released during fossil fuel combustion, significantly contribute to global warming with the consequences of widespread melting of ice, noticeable climate changes, and rising sea levels. The instability of oil price further influences the global political and economical structures. Renewable energy such as solar power, wind power, hydroelectric power and hydrogen power has been strongly advocated recently, but affordability has limited their adoption.

Given the global demand for energy and the limitations of current resources to produce that energy, we must emphasize the research and development of finding energy-efficient

processes for various applications. Two major applications which necessarily require energy-efficient processes are water production and protein production.

Looking for low-energy consumption process for water production has been very urgent as the water crisis is the second worldwide concern. A water crisis is when the available water within a region is less than the region's demand. Water covers more than 70% of the Earth's surface, but the problem is more than surface deep [3]. Water crisis affects 700 million people in 43 countries across every continent on Earth [4]. Although 70% of the earth is covered with water, most of it is inedible besides the limited freshwater is distributed unevenly and too much of it is wasted, polluted and unsustainably managed [5]. To solve the water crisis, we must solve the problems of inadequate access, excessive use, and pollution of water resources. Desalination is one solution to solve the inadequate accessibility of fresh water. Historically, technology to desalinate seawater has included multi-stage flash (MSF), multi-effect distillation (MED), and reverse osmosis (RO) [6-7]. However, the drawbacks of these technologies are very energy inefficient. MSF and MED require high temperatures to evaporate seawater while RO requires large amounts of electricity and extremely high hydraulic pressures to force water across the RO membrane while rejecting salt and other contaminants. As population increases drive up the demand for fresh water, these inefficient technologies are becoming less and less feasible. Only the most energy efficient technologies will prevail in solving the water crisis.

Low-cost healthcare and medicine is another global concern, relating with all mankind. A suitable energy-efficient process can benefit pharmaceutical production industry. Proteins, as the most important biopolymer in nature, have a wide range of commercial applications in nutraceutical, medical and pharmaceutical markets [8]. The price of protein based medicine has been increasing as the production cost keeps pace with the energy. In protein production, the process of protein enrichment plays a very important role and is companied with protein separations. In order to render medicine products more affordable, searching for innovative energy-efficient protein enrichment processes has become important and it provides strong incentives for protein production industries.

Forward osmosis (FO) technology has emerged as one of the most promising technologies being to address the global demands for clean water and low-cost medicines because it offers significant advantages over traditional processes. The osmotic pressure difference generated between two solutions separated by a semi-permeable membrane serves as the driving force for the FO process. FO can essentially reduce the energy consumption as it operates under the osmotic driving force which is the intrinsic energy source among molecules without any external aid, such as heat or hydraulic pressure. The advantages of FO will be detailed in later chapters.

1.2 History of forward osmosis

Forward osmosis (FO) is also referred to as direct osmosis (DO) in literature. The development of FO can be stemmed from the phenomenon of osmosis. The history of FO involves membranes, draw solutions, processes and energy generations. Osmosis is a ubiquitous physical observation, which can be found in all the living cells. Primarily, the osmosis process has been exploited to desiccate food for long term preservation in the early days of mankind [9]. The first report regarding the observation of osmosis was found in early 1700s [10]. Between 1827 and 1832, Renè Dutrochet proposed the terms "endosmosis" and "exosmosis" to name this phenomenon [10]. In 1864, the first artificial membrane made in copper ferrocyanide $Cu_2Fe(CN)_6$ was invented by M. Traube [11]; and in 1877, W.F.P. Pfeffer made membranes of good mechanical resistance by precipitating copper ferrocyanide in a porous material [10]. In 1886, an analogy between aqueous solutions and perfect gases was published by van't Hoff; he applied thermodynamics to osmosis and established a law similar to the Gay-Lussac law and proposed the adjective "semipermeable" [12], owing to which, van't Hoff was awarded by the Nobel Prize of chemistry in 1901. The early scientists were interested in the mechanism of osmosis and it was gradually developing in the 19th centuries [13-15]. At the same time, early membrane researchers have tried many possible materials, that were dense, non-porous, selectively permeable, to be tested as the membranes for various applications of FO [9]. Not until 1960s when the Loeb–Sourirajan process for making defect-free, high-flux, anisotropic RO membranes was successfully discovered, has the disciplines of science and engineering in membrane fabrication been fully followed [16].

Meanwhile, the test and evaluation of Pressure Retarded Osmosis (PRO), which utilizes the concept of FO for power generation, has also been disclosed to public since 1960s [17]. From 1970s, more and more efforts and attention were given in the research area of FO applications, such as food processing [18] and wastewater treatment [19-20]. However, researchers tested the FO performance in different configurations using mostly RO membranes and the results were lower than the anticipation [19-22]. The reason behind was progressively understood with the development of FO and other closely related processes [23-25]. RO membranes may induce severe internal concentration polarization (ICP) within the membrane when operated in no hydraulic pressure environment. The inevitable ICP can greatly lower the effective driving force of a FO process and thus using RO membranes tested in FO environment, the FO performance in terms of water flux was never satisfactory. Understanding the crucial role of FO membrane structure, which determines the degree of concentration polarization (CP), the predecessor of Hydration Technologies Inc. (HTI) successfully commercialized FO membrane with much improved FO performance in a group of applications 1990s [9]. In the 21st century, more FO membranes designed with novel structures spring up in publications. Wang et al reports doubled-skinned FO membranes of reduced ICP within porous sublayer, which was a breakthrough in the development of FO membranes [26]. Later, Zhang et al investigated the fabrication of double-skinned FO membrane using different substrates [27]. Su et al reports the broad studies of FO membrane made from cellulose acetate, which is a promising material for FO applications [28-30]. In terms of osmotic energy generation, Statkraft (Norway) in 2009 built up the first osmotic power

plant [31]. The energy was generated from the spontaneous mixing between seawater and fresh water across a semi-permeable membrane; this is an environmentally friendly industrial system without chemical discharging [32]. The rapid development of osmotic power generation in recent years is believed to play an important role as the future renewable and eco-friendly energy. The content of draw solution is specified in a later section 1.4.

1.3 Osmotic pressure

1.3.1 Osmotic pressure

Osmosis is a ubiquitous physical phenomenon found in all of biology and involving the great power of molecular transport that is water can automatically diffuse through a semi-permeable membrane without any external aid. The semi-permeable membrane is defined that a membrane allows water molecules to pass through but rejects the solutes in the solution, such as ions. The driven force of the osmosis is the osmotic pressure difference of the two solutions across the membrane. The origins and essence and other facts regarding osmotic pressure have been controversial among curious researchers since osmosis was studied. But when water molecules transfer from a lower-concentration (osmolality, to be exact) solution to a higher-concentration (osmolality, to be exact) solution across the membrane, it is generally agreed that there is an energy gap of chemical potential for water molecules between the two solutions. The higher-

concentration solution possesses lower water chemical potential while the lower-concentration solution has the higher water chemical potential.

The water chemical potential μ_1 in the concentrated solution is given by the relationship [10]:

$$\mu_1 = \mu_{01} + RT \ln a_1 + (P - 1) V_1 \quad (1)$$

where μ_{01} is the chemical potential of water in lower-concentration solution (J/mol), R is gas constant (8.314 J/mol · K), T is thermodynamic temperature (K), a_1 is solvent (water) activity which decreases when solute concentration increases, P is pressure upon the solution (Pa) and V_1 is solvent molar volume (m^3/mol).

When the equilibrium is reached, the chemical potential of water between the initial lower-concentration solution and higher-concentration solution are even.

$$\mu_1 = \mu_{01} + RT \ln a_1 + \pi V_1 = 0 \quad (2)$$

The expression of the osmotic pressure is:

$$\pi = - (RT/V_1) \ln a_1 \quad (3)$$

This relationship was deduced in assuming the solvent is incompressible. The activity can be further derived and simplified in different solution conditions; therefore the osmotic pressure can be calculated.

In the case of a diluted solution (a solution where the concentration of solutes is much lower than the concentration of solvent), the above equation can be derived to:

$$\pi = CRT \quad (4)$$

where C is the molar concentration of the impermeable solutes in the solution (mol/m^3).

It is important to note that osmosis is a colligative property: it does not depend on the specific nature of the solute (such as the exact size of the solute molecules), only on its concentration. Therefore, the calculation of osmotic pressure can be related with other colligatives properties of a solution, such as freezing point. When solutes are added in a solution, the osmotic pressure increases while its freezing point decreases. By measuring its freezing point depression, the osmotic pressure can be correlated.

The relationship between activity and freezing point depression is as below [33, 34]:

$$-\ln a = \frac{\Delta H_f^0}{\mathrm{RT_f^2}} \Delta T \quad (5)$$

The relationship between activity and osmotic pressure is as below [33, 34]:

$$\ln a = -\frac{\pi V_w}{\mathrm{RT}} \quad (6)$$

Where a is the water activity; ΔH_f is the molar heat of water, 80 cal g^{-1}; R is the ideal gas constant; T_f is the freezing temperature of water, 273k; ΔT *(k)* is the freezing point depression; π *(atm)* is the osmotic pressure; V_w is the molar volume of water, 1cm^3g^{-1}; and T is room temperature, 298k.

1.3.2 Osmotic process

Osmosis happens in a system composed of two compartments of solutions, separated by semi-permeable membrane. Based on that, there exists three osmotic processes, namely

forward osmosis (FO), reverse osmosis (RO) and pressure retarded osmosis (PRO), as shown in Figure 1.1. [9]

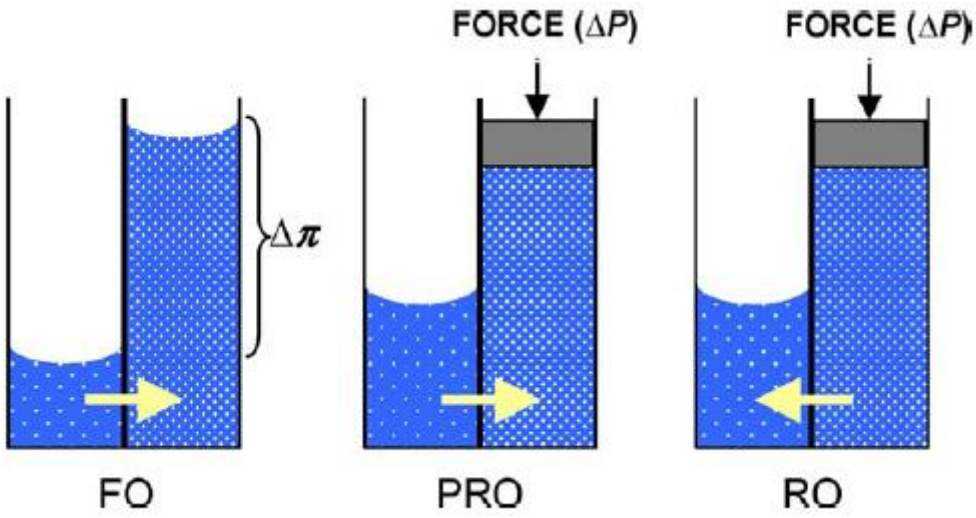

Figure 1.1 Schematic drawings of osmotic processes

In FO processes, the only driving force observed is the inherent osmotic pressure difference between the two solutions. In FO, no hydraulic pressure is needed; therefore it requires very low energy consumption during the process. In FO, the solution of lower osmotic pressure is referred to as feed solution, while the solution of higher osmotic pressure is referred to as draw solution, as depicted in Figure 1.2. Because FO membranes have different structures in its two faces, it results in different FO performance (water flux) when the solutions facing the different layers. Conventionally, when the draw solution encounters the relatively dense selective layer while the feed solution faces in the relatively porous and supporting layer, it is called as pressure retarded osmosis mode (PRO). When the feed solution encounters the relatively dense selective layer while the draw solution faces in the relatively porous and supporting layer,

it is called as forward osmosis mode (FO). The PRO mode and the FO mode are schematically illustrated in Figure 1.3.

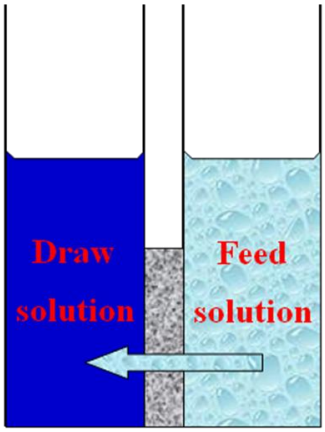

Figure 1.2 Schematic drawing of forward osmosis (draw solution and feed solution)

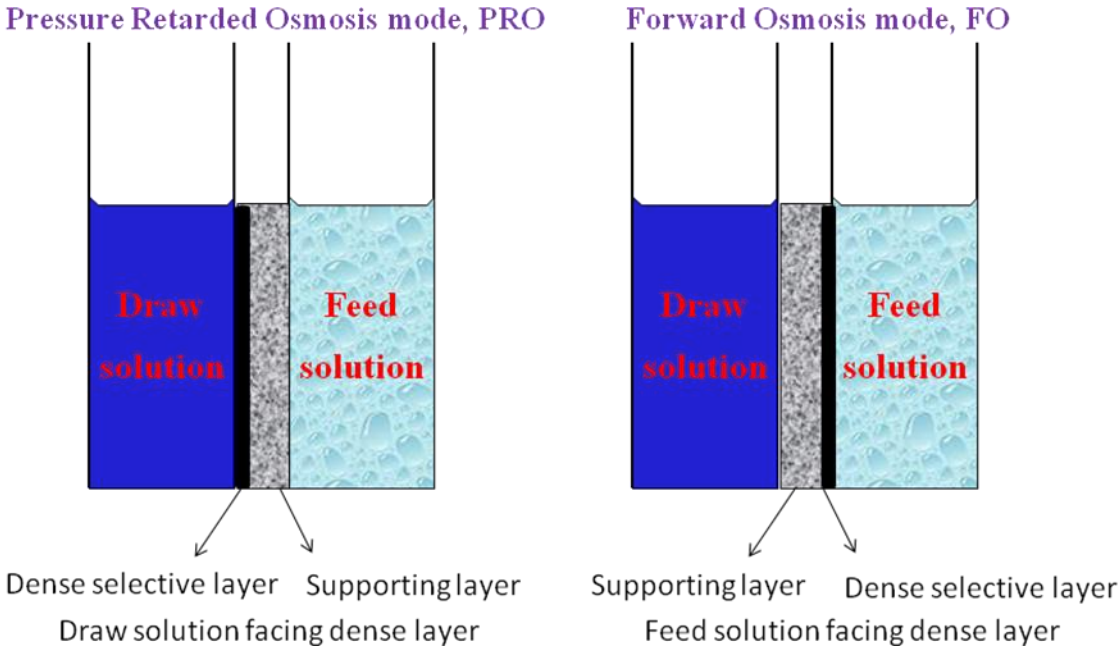

Figure 1.3 Schematic drawing of operational orientations of forward osmosis

The osmotic pressure difference triggers water molecules to transfer from the solution of lower osmotic pressure to the higher. When a hydraulic pressure higher than the osmotic pressure difference is applied on the solution of high osmotic pressure, the water molecules will move backwards from the solution of higher osmotic pressure to the solution of lower osmotic pressure. With the hydraulic pressure increasing, the water flux through the membrane will increase accordingly. This process is called RO, as in the reverse of ordinary osmosis. The driving force in RO process is the value of the hydraulic pressure minus the osmotic pressure difference of the two solutions. If the hydraulic pressure applied is lower the osmotic pressure difference, the water molecules still transfer from the solution of lower osmotic pressure to the higher. In this condition, it is called PRO. When the hydraulic pressure on the solution of higher osmotic pressure increases from zero to the osmotic pressure difference, the water flow rate through the membrane from the solution of lower osmotic pressure to the higher will be gradually decreased. It is because the driving force which is the value of the osmotic pressure difference minus the hydraulic pressure on the solution of higher osmotic pressure gradually decreases with the hydraulic pressure increases. The above statements can be summarized in the scheme below, Figure 1.4.

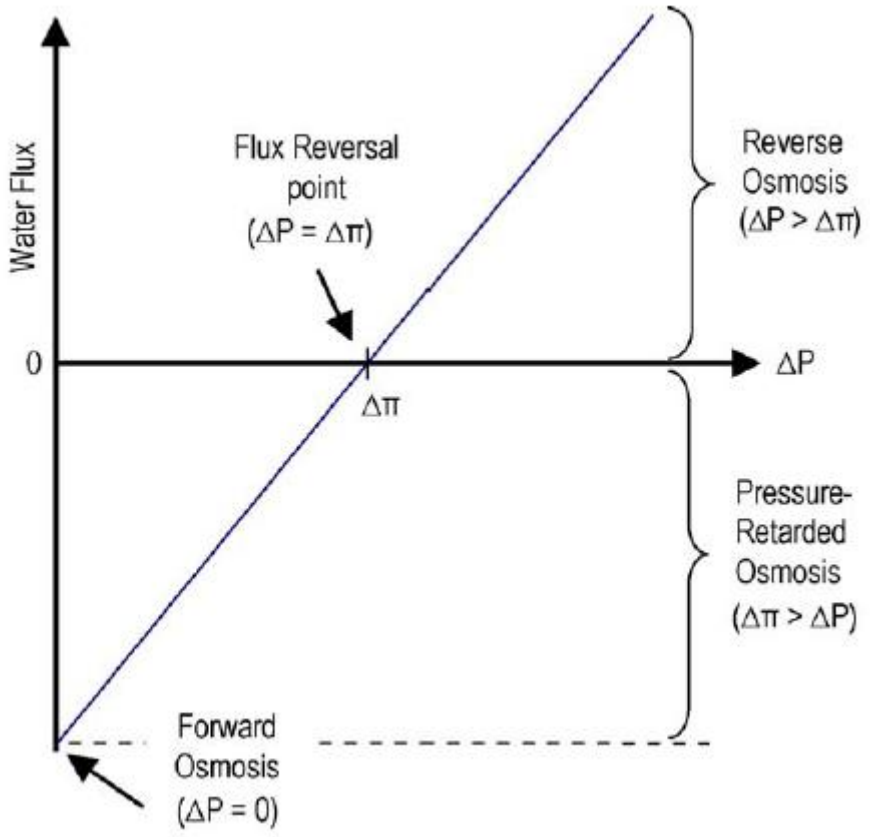

Figure 1.4 Schematic illustration of osmotic processes in terms of water flux and the driving force

1.3.3 Concentration polarization

Concentration polarization (CP) can be found in almost all the pressure driven and osmosis driven processes. In pressure driven processes, the CP is referred to the phenomenon that the concentration of solutes near the membrane surface is higher than that in the bulk of solution. It is induced by the pressure on the solution and the solutes are accumulated near membrane surface, resulting in the reduced driving force and lower

water flux. In osmosis driven process, the CP exists under the influence of osmotic pressure, because of which, the solutes may accumulate inside the membrane and the concentrations on membrane surface are different from the bulk concentration. The driving force can be significantly decreased owing to CP, which further attributes to lower water flux. The CP in forward osmosis process is relatively complicated and it is composed of external concentration polarization (ECP) and internal concentration polarization (ICP). The effective osmotic pressure is defined as the osmotic pressure difference across the two sides of the membrane and it equals to the osmotic pressure difference between the feed solution and the draw solution in an ideal condition.

When FO process is operated at FO mode (feed solution facing dense layer), water molecules in feed solution will flow through the membrane to the draw solution under the osmotic pressure, which will cause a built-up of solutes outside the dense layer. The accumulated solutes near the dense layer induce the higher osmotic pressure than the osmotic pressure of the bulk feed solution. Thus, the effective osmotic pressure is lowered as illustrated in Figure 1.5. This condition is defined as concentrative ECP. When FO process is operated at PRO mode (draw solution facing the dense layer), the concentration of the draw solute near the dense layer of the membrane surface is lower than that of the bulk draw solution because of the dilution of water from the feed solution, as depicted in Figure 1.5. This observation is therefore called as dilutive ECP. Both concentrative and dilutive ECPs can reduce the effective osmotic pressure and water flux than expectation. ECP can be alleviated by increasing the water flow rate and the addition

of turbulence near membrane surface. But the degree to reduce ECP is still limited. Nonetheless, ECP is not the main reason to cause the FO performance lower than theoretical value in an ideal case.

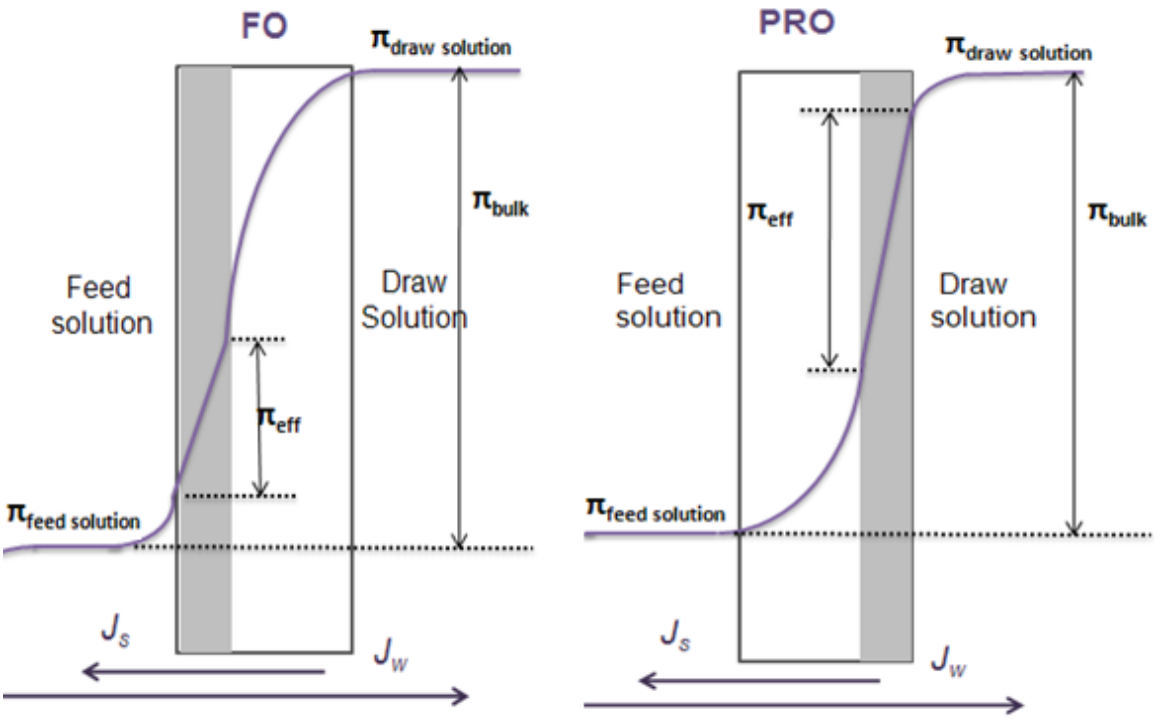

Figure 1.5 Illustrations of CPs in FO mode and PRO mode

ICP refers to the phenomenon that solutes propagate inside the porous layer of membrane, which reduced the effective driving force in a FO process. ICP is relatively inevitable because most of the FO membranes are asymmetric with porous layer. In PRO mode, the solutes may accumulate inside the porous layer and the concentration in porous layer higher than bulk solution with the osmotic flow through the membrane that is referred to as concentrative ICP, as shown in Figure1.5. In FO mode, the concentration of draw

solution near the dense layer is lower than the bulk with the water dilution from the feed solution, which is referred to as dilutive ICP, as displayed in Figure 1.5. ICP is one major issue for FO process and it can greatly lower the water flux. Due to the ICPs happen inside the membrane, it is difficult to diminish ICP by conventional methods such as increasing water velocity and turbulence. But with engineered membrane structure, the ICP can be minimized, such as the FO membrane of double dense layers on each side. The dense layer on each side can effectively reject solutes to propagate inside the membrane against ICP, as shown in Figure 1.6 [26].

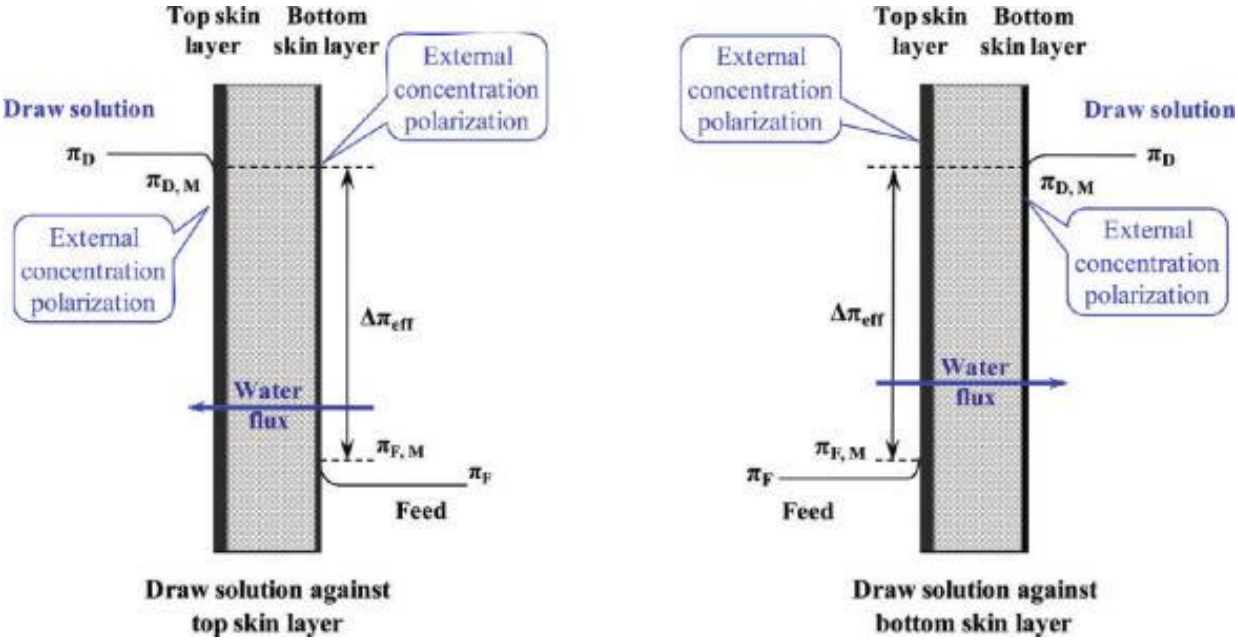

Figure 1.6 Illustrations of CPs in double-skinned FO membrane under different membrane orientations

1.4 Draw solution

In order to use FO for a variety of applications, two issues need to be addressed: one is the fabrication of excellent membranes for high water flux and low salt leakage and the other is the production of eligible draw solutions which possess high osmotic pressure and the drawn water can be easily separated from. The FO membranes are rigorously delicate and many researchers have put a great deal of effort in the study of FO membrane fabrications. However, the study on the production of draw solutions in FO is much less found.

Searching for an excellent draw solutes can be challenging especially for the application of water production. In order to induce high osmotic pressure, the size of draw solutes is supposed to be as small as possible because osmotic pressure is a colligative property. In principle, the use of small molecules such as salts and electrolytes may not be economical and practical because of the difficulties of recovery and salt leakage, clogging induced in the supporting layer and severe fouling and internal concentration polarization [35, 36]. In addition, the smaller draw solutes can easily generate high osmotic pressure but make the draw solute regeneration process more difficult and consume more energy no matter what regeneration methods are used. There should be a balance between the choices of high osmotic pressure and high regeneration efficiency. A suitable regeneration process also determines the efficiency and the application of the draw solutes. Although the FO process alone barely consumes energy, the regeneration process to separate the drawn water from draw solution may require large amount of energy if the regeneration process

is not chosen wisely. Researchers have proposed to use RO for draw solution regeneration. This proposal is technically feasible but economically and industrially unpractical, because high hydraulic pressure similar to RO may be needed to obtain the FO drawn water from the draw solution. Magnetic field, membrane distillation (MD) and ultrafiltration/nanofiltration (UF/NF) are feasible and popular candidates as draw solution regeneration methods and they can be applied on specific draw solutions only. If recovered by a magnetic field, the draw solutes must process superparamagnetic property. For using MD as the regeneration method, the draw solutes must have low-fouling propensity as the scaling and crystallization can easily deteriorate the MD process. UF/NF requires the larger draw solutes than the pores size and the draws solutes have opposite charge to the membrane surface to guarantee a high solute rejection and regeneration efficiency. The exploration of renewable energy can also be incorporated into the regeneration process to make the overall system more energy-friendly. In short, the advancement of FO relies on the development of both the FO membrane and draw solutions.

Different FO applications may have different emphases on the requirement of draw solutions. For the purpose of desalination and water reclamation, the ideal draw solutes for osmosis driven desalination must have the characteristics of high osmotic pressure, zero toxicity, easy recovery and low cost. Many efforts have been devoted to discovering suitable draw solutes [37–45]. Batchelder patented that volatile solutes, such as sulfur dioxide, were used as draw solutions in 1965 and could be removed by a heated gas

stripping operation [37]. Later in 1972, a draw solution made of aqueous aluminum sulfate was developed as an osmotic agent. Calcium hydroxide was added in solutions to facilitate the separation of salts via precipitation (calcium sulphate and aluminium hydroxide). Sulfuric acid or carbon dioxide was also added to neutralize the solution [38]. During 1975-1989 [39-40], scientists have used various sugars, such as glucose and fructose, to draw water from seawater and the obtained draw solution were used as nutritious solution directly without regeneration. In 1992, the sugar mixtures were explored as draw solutes and could be recovered by RO [41]. In the early 2000's, a water-soluble mixture of ammonium bicarbonate was discovered as draw solute and a high water flux was obtained due to its low molecular weight and high solubility. The draw solute can be recovered and decomposed to ammonia and carbon dioxide upon heating at 65 °C [42]. The discovery of using ammonium bicarbonate as draw solute has been novel and neat. However, due to the high solubility of the draw solute in water and its inherent strong chemical odor, it is not favored for edible water production process. In 2007, water-soluble magnetoferritin surrounded by polyethylene glycol [43] or hollow protein spheres [44], were tested as draw solute in FO as the magnetic nanoparticles could be recovered using a magnetic separator. Superabsorbent polymer was also studied as draw solute in FO [45]. By applying pressure over the osmotic pressure of the polymer which absorbed water, the water can be released.

1.5 Applications of forward osmosis

FO processes the advantages of low energy consumption, low fouling propensity compared to other pressure driven processes. Therefore, FO is intensively investigated in the applications of desalination and water reuse in recent years [9, 32]. In the 1990s, Hydration Technologies Inc. (HTI) first invented a high performance FO membrane superior to others. The membrane is made of cellulose triacetate (CTA) with the thickness less than 50 μm, as shown in Figure 1.7 [42]. This membrane is supported by embedded polyester mesh, which provides mechanical support different from traditional porous supporting layer as in RO membranes. With this FO membrane, commercial applications of water purification for military, emergency relief, and recreational purposes were successfully accomplished [9]. Hydration bag is one of the commercial FO products, which can be used when reliable drinking water is scarce or not available [9]. The interior of hydration bag is made of FO membrane, which can reject microorganisms, most macromolecules, and most ions; and it is filled with draw solution (e.g., nutrients and minerals) and the exterior is a sealed plastic bag containing the FO bag as shown in Figure 1.8. Upon immersion of the bag in aqueous solution even muddy water, water will diffuse into the bag under the osmotic pressure difference and slowly dilutes the draw solution. At the end of the process the diluted draw solution can be consumed as a sweet drink directly [9], as shown in Figure 1.9.

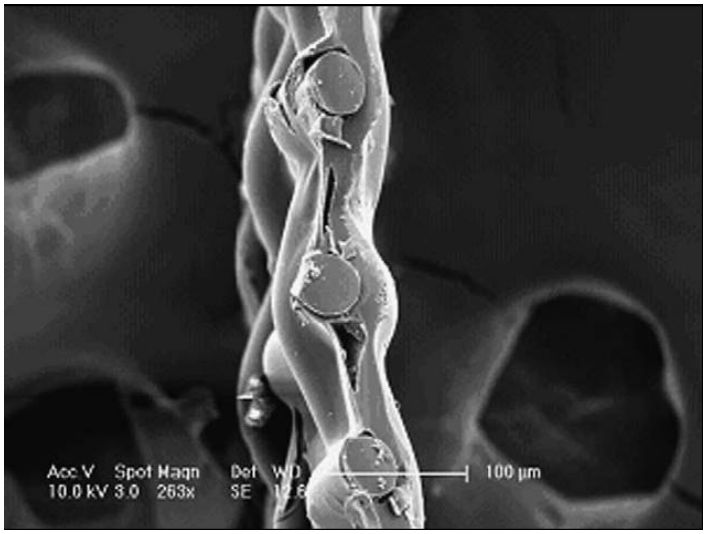

Figure 1.7 SEM image of HTI FO membrane

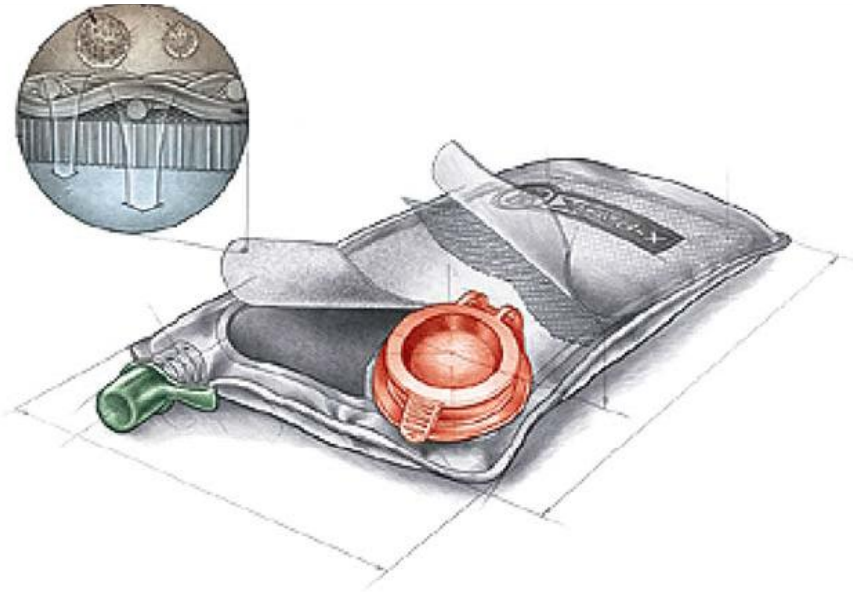

Figure 1.8 Schematic drawing of hydration bag

Figure 1.9 Illustration of hydration bag

As FO is operated under the conditions of no heat, pressure or chemicals added, pharmaceuticals and proteins can be processed through FO with high resolution and low energy consumption. For example, it has been demonstrated that proteins can be enriched in a FO process using magnesium chloride as the draw solute [46]. Another typical example using FO concept for pharmaceutical application is osmotic drug-delivery system are illustrated in Figure 1.10 [47]. The osmotic pump is contained in a titanium alloy cylindrical reservoir which protects the drug molecules from the components that might deactivate the drug prior to release [47]. A polyurethane membrane which is permeable to water but almost completely impermeable to ions seals one end of the reservoir. The draw solution occupies a portion of the cylinder behind the membrane. An elastomeric piston separates the draw solution from the drug formulation in the drug

reservoir. The drug may either be a solution or a suspension and either aqueous or non-aqueous in nature. The drug exit port is a small orifice located at the opposite end of the titanium cylinder. This system can be implanted into body for medical purpose. With volume of osmotic engine (draw solution) increases from the dilution, the drug will be gradually released through drug outlet into the body environment.

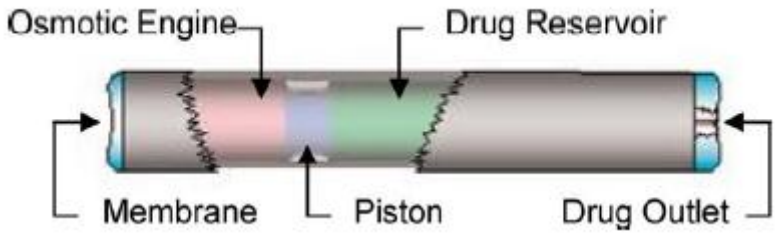

Figure 1.10 Cross-section of osmotic drug-delivery system

1.6 Nanoparticles

1.6.1 Nanoparticles as draw solute in forward osmosis

Inorganic salts and organic compounds can easily induce high osmotic pressures but their recovery via RO or heat is relatively energy intensive. It is difficult for nanoparticles to generate high osmotic pressure owing to their large size compared to salts or organic molecules. Nevertheless, one of the superiorities of hydrophilic nanoparticles is their extremely high surface-area-to-volume ratio that minimizes drawback of large particle sizes. In order to induce a high osmotic pressure, the size of draw solutes should be as small as possible since osmotic pressure is a colligative property. Not only can these

nanoparticles induce reasonable water fluxes and osmotic pressures through engineering their surface hydrophilicity and particle size, but also be recovered by various methods including magnetic field, UF, FO and electric field, depending on the applications. Therefore, nanoparticles can be a very promising class of draw solutes in FO.

Magnetic nanoparticles can be regenerated in a magnetic field with the aid of the magnetic core and the osmotic pressure will be induced by the functional groups on the nanoparticle surface. For magnetic nanoparticles, their magnetic properties can be classified to three kinds, including ferromagnetism, paramagnetisme and superparamagnetism, as shown in Figure 1.11. Ferromagnetism refers to the phenomenon that the materials always exhibit magnetic respond with and without a magnetic field, such as permanent magnet. Paramagetism refers to the phenomenon the material can only exhibit a relatively low magnetic property with a magnetic field. When the magnetic field is removed, the material does not possess magnetic propensity. Superparamagnetism is very similar to paramagnetism but can exhibit much stronger response to the magnetic field.

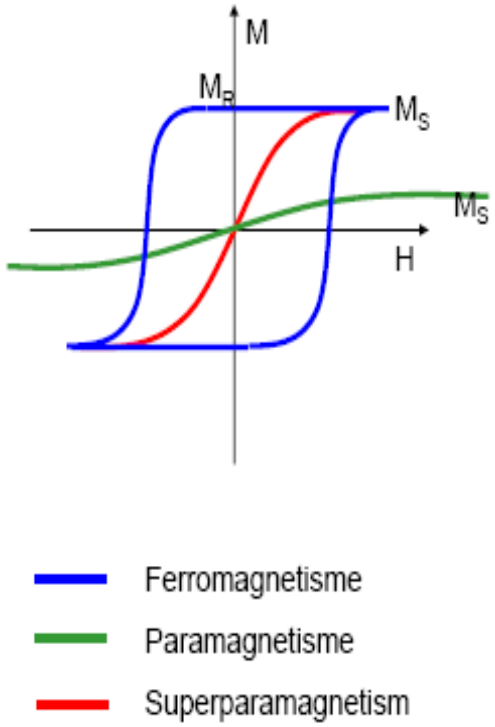

Figure 1.11 Illustration of different magnetic properties

1.7 Research objectives and project organization

1.71 Research objectives

It is important to explore FO technology as an energy-efficient process in various applications. Two key elements in FO process, namely FO membranes and draw solute, play a very important role in their realizations in different applications. The FO membranes are rigorously delicate and many researchers have put a great deal of effort in the study of FO membrane fabrications. However, not much study on the production of

draw solutions in FO has been done and the progress of draw solutes in FO has been minimal, especially the development of nanoparticle draw solutes in FO. Moreover, the studies on the fundamental science and engineering of nanoparticle draw solutes in FO need to be conducted to obtain a better understanding of the characteristics of nanoparticle draw solutes in terms of the induced osmotic pressure and regeneration methods and applications. Our ultimate goal was to develop novel nanoparticle draw solutes together with their most feasible regeneration methods for various applications, especially for water reclamation and desalination.

Therefore, the objectives of this research project were:

1. To explore hydrophilic magnetic nanoparticles as draw solutes in FO and the regeneration method by magnetic separator.
2. To investigate the effect of nanoparticle surface chemistry and particle size on the osmotic pressure and FO performance of the nanoparticle draw solutes
3. To examine ultrasonication used to recover agglomerated magnetic nanoparticles size as well as their FO performance
4. To study hydrophilic nanoparticles as draw solutes in FO and the regeneration method by ultrafiltration
5. To investigate dual-stage FO system using hydrophilic nanoparticles as intermediate draw solutes for protein enrichment
6. To evaluate of thermosensitive magnetic nanoparticles as ‘smart’ draw solutes in FO

7. To investigate performance-enhanced surface-dissociated nanoparticles and the regeneration method by electric field.

1.72 Project organization

This dissertation is about the exploration and investigation of using nanoparticles as novel draw solute in FO. Chapter 1 provides the background of this project conducted and literature review of FO technology. Given the global demand for energy and the limitations of current resources to produce that energy, it is crucial and urgent to develop energy-efficient processes for various applications. FO meets the requirements of low energy consumption as it is operated under osmotic pressure without external aid. Under the global crisis of water shortage and low-cost medicine, water production and protein production are two emphases with FO technology applied using nanoparticles as draw solutes. The detailed descriptions of experiments conducted in the project are given in Chapter 2. The first work of using magnetic nanoparticles as draw solute in FO for water reuse is reported in Chapter 3. Effects of different surface chemistry and particle size on nanoparticles draw solutes were studied in this chapter. It was demonstrated that water-soluble magnetic nanoparticles can be used as draw solutes in FO and recycled through a magnetic separator. However, it was observed that magnetic nanoparticles agglomerated after passing though magnetic separator. In order eliminate the agglomeration, an Ultra-Filtration (UF) process was attempted to regenerated diluted nanoparticle draw solutions, as reported in Chapter 4. It was shown that UF process can recycle nanoparticle draw solutions through several runs without increasing nanoparticle size. Different UF

membranes for regenerating nanoparticle draw solutions were investigated in this chapter. Chapter 5 presents the work of dual-stage FO system using nanoparticles as intermediate draw solutes to enrich protein solutions. The dual-stage FO system can be used to concentrate proteins of different sizes and charges. Reverse Osmosis (RO) retentate as draw solution to re-concentrate nanoparticle solutions in the dual-stage FO system alleviated its disposal and pollution problem. In order to further advance the technology of FO using nanoparticles as draw solutes, thermo-responsive magnetic nanoparticles were studied in Chapter 6. In this chapter, thermo-responsive magnetic nanoparticles were applied as draw solutes. After that, they were pre-heated above their critical temperature and therefore agglomerated together with their surface polymer configuration changes. At the same time, they went through a low-strength magnetic separator where they were regenerated and then recycled as draw solutes. Thermo-responsive magnetic nanoparticles exhibited improved regeneration efficiency. Nonetheless, their FO performance was not satisfactory. Therefore, in Chapter 7, surface-dissociated nanoparticles were prepared and studied as draw solutes in FO. Electric field and nanofiltration system also provided a facile method and was used to regenerate surface-dissociated nanoparticles with enhanced FO performance. Chapter 8 includes conclusions of this project and recommendations in the future.

1.8 References

1. http://www.ucsusa.org/ssi/biodiversity/population-and-environment-series/population-and-water-linkage.html

2. http://www.fe.doe.gov/

3. M. A. Shannon, P. W. Bohn, M.Elimelech, J. G. Georgiadis, B. J. Marias, A. M. Mayes, Science and technology for water purification in the coming decades, Nature, 452(2008)301.

4.http://www.stakeholderforum.org/fileadmin/files/Key%20stats%20and%20facts%20041110%20FINAL.pdf

5. L. Robert, M. Elimelech, Global challenges in energy and water supply: the promise of engineered osmosis, Environ. Sci. Tech., 42(2008)8625.

6. O.J. Morin, Design and operating comparison of MSF and MED systems, Desalination, 93(1993)69.

7. N. M. Wade, Distillation plant development in dual–purpose power and desalination plants. Desalination, 123(1999)115.

8. S. Jones, J. M. Thornton, Principles of protein-protein interactions. Proc.Natl.Acad.Sci. 93(1996) 13.

9. T. Y.Cath, A. E. Childress, M. Elimelech, Forward osmosis: principles, applications, and recent developments, J. Membr. Sci. 281(2006)70.

10. A. Jacob, A critical review of the history, development and future prospects for Forward Osmosis, Elesevier 2006

11. G. N. Ling, The new cell physiology: an outline, presented against its full historical background, beginning from the beginning. Physiol. Chern. Phys. & Med. 26(1994)121.

12. http://urila.tripod.com/evidence.htm

13. Lord Rayleigh, "The theory of solutions", Nature, 55(1897)253

14. Lord Kelvin, "On Osmotic Pressure against an Ideal Semi-Permeable Membrane", Nature, 55(1897)272

15. J.W. Gibbs, "Semi-Permeable Films and Osmotic Pressure", Nature, 55(1897)461

16. R.W. Baker, Membrane Technology and Applications, 2nd ed., John Wiley & Sons, Ltd., New York, NY, 2004

17. R.J. Aaberg, Osmotic power—a new and powerful renewable energy source, ReFocus 4 (2003) 48.

18. K. Popper, W.M. Camirand, F. Nury, W.L. Stanley, Dialyzer concentrates beverages, Food Eng. 38 (1966) 102.

19. F. Votta, S.M. Barnett, D.K. Anderson, Concentration of industrial waste by direct osmosis: completion report, Providence, RI, 1974.

20. D.K. Anderson, Concentration of Dilute Industrial Wastes by Direct Osmosis, University of Rhode Island, Providence, 1977.

21. G.D. Mehta, S. Loeb, Internal polarization in the porous substructure of a semi-permeable membrane under pressure-retarded osmosis, J. Membr. Sci. 4 (1978) 261.

22. G.D. Mehta, S. Loeb, Performance of Permasep B-9 and B-10 membranes in various osmotic regions and at high osmotic pressures, J. Membr. Sci. 4 (1979) 335.

23. G.D. Mehta, S. Loeb, Internal polarization in the porous substructure of a semi-permeable membrane under pressure-retarded osmosis, J. Membr.Sci. 4 (1978) 261.

24. K.L. Lee, R.W. Baker, H.K. Lonsdale, Membranes for power generation by pressure-retarded osmosis, J. Membr. Sci. 8 (1981) 141

25. L. Song, M. Elimelech, Theory of concentration polarization in crossflow filtration, J. Chem. Soc., Faraday Trans. 91 (1995) 3389.

31. http://www.statkraft.com/energy-sources/osmotic-power/

32. T.S. Chung, S. Zhang, J.C. Su, K.Y. Wang, M.M. Ling, Forward osmosis processes: Yesterday, today and tomorrow, doi:10.1016/j.desal.2010.12.019

33. R.H. Boyd, P.J. Phillips, The science of polymer molecules. Combridge University Press, 1996

34. P.R. Bergethon, The physical basis of biochemistry: the foundations of molecular. Springer, 2010

35. N.T. Hancock, T.Y. Cath, Solute coupled diffusion in osmotically driven membrane processes, Environ. Sci. Technol. 43 (2009) 6769.

36. W.A. Phillip, J. Yong, M. Elimelech, Reverse draw solute permeation in forward osmosis: modeling and experiments, Environ. Sci. Technol. 44 (2010) 5170.

37. G.W. Batchelder, Process for the Demineralization of Water, US Patent, 3,117, 799(1965)

38. B.S. Frank, Desalination of Sea Water, US Patent, 3,670, 897(1972).

39. J.O. Kessler and C.D. Moody, Drinking water from sea water by forward osmosis, Desalination, 18 (1976) 297.

40. K. Stache, Apparatus for transforming seawater, brackish water, polluted water or the like into a nutrious drink by means of osmosis. US Patent 4,879,030. (1989).

41. J. Yaeli, Method and apparatus for processing liquid solutions of suspensions particularly useful in the desalination of saline water. US Patent 5,098,575. (1992).

42. J.R. McCutcheon, R.L. McGinnis, M. Elimelech, A novel ammonia-carbon dioxide forward (direct) osmosis desalination process, Desalination 174 (2005) 1

43. S. Adham, J. Oppenheimer, L. Liu, M. Kumar, Dewatering reverse osmosis concentrate from water reuse using forward osmosis, WateReuse Foundation Research Report. Product No. 05-009-01 (2007) 1-52.

44. T.M. Oriard, P.D. Haggerty, Forward osmosis utilizing a controllable osmotic agent. US Patent 0278153. (2007).

45. R. A. L. Jones, A. J. Ryan, H. Storey, M. Butler, C. J. Crook, Apparatus and method for purifying water by forward osmosis, WO/2008/059219, 2008.

46. Q. Yang, K.Y. Wang, T.S. Chung, A novel dual-layer forward osmosis membrane for protein enrichment and concentration. Sep. Purif. Technol., 69 (2009)269.

47. J. Wright, S. Yum, RM. Johnson, DUROS® Osmotic Pharmaceutical Systems for Parenteral & Site-Directed Therapy. Drug Delivery Technology Magazine 3(2003) 64-73.

CHAPTER 2

EXPERIMENTAL

2.1 Synthesis of nanoparticles

2.1.1 Synthesis of 20 nm in diameter magnetic nanoparticles coated with triethylene glycol

2.0 mmol $Fe(acac)_3$ was added 25.0 ml triethylene glycol under a flow of argon and magnetically stirring. The mixture was slowly heated to 190°C for 30min and then quickly heated to reflux at 275°C under a blanket of argon for 30 min. By removing the heat source, the black homogeneous colloidal suspension was cooled down to room temperature. 30.0 ml ethyl acetate was added to the reaction solution and then separated via centrifugation, resulting in black precipitation. The black precipitation was dissolved in DI water and re-precipitated in ethanol and ethyl acetate for three times to remove residuals thoroughly.

2.1.2 Synthesis of 20 nm in diameter magnetic nanoparticles coated with 2-pyrrolidine

2.0 mmol $Fe(acac)_3$ was added 25.0 ml 2-pyrrolidine under a flow of argon and magnetically stirring. The mixture was slowly heated to 190°C for 30min and then quickly heated to reflux at 275°C under a blanket of argon for 30 min. By removing the

heat source, the black homogeneous colloidal suspension was cooled down to room temperature. 30.0 ml ethyl acetate was added to the reaction solution and then separated via centrifugation, resulting in black precipitation. The black precipitation was dissolved in DI water and re-precipitated in ethanol and ethyl acetate for three times to remove residuals thoroughly.

2.1.3 Synthesis of 20 nm in diameter magnetic nanoparticles coated with polyacrylic acid

1.0 g of polyacrylic acid was firstly mixed with 25.0 ml triethylene glycol under a flow of argon and magnetically stirring. 2.0 mmol $Fe(acac)_3$ was added when polyacrylic acid was complete dissolved in triethylene glycol. The mixture was slowly heated to 190°C for 30min and then quickly heated to reflux at 275°C under a blanket of argon for 30 min. By removing the heat source, the black homogeneous colloidal suspension was cooled down to room temperature. 30.0 ml ethyl acetate was added to the reaction solution and then separated via centrifugation, resulting in black precipitation. The black precipitation was dissolved in DI water and re-precipitated in ethanol and ethyl acetate for three times to remove residuals thoroughly.

2.1.4 Synthesis of 7 nm in diameter magnetic nanoparticles coated with polyacrylic acid

1.5 g of polyacrylic acid was firstly mixed with 25.0 ml triethylene glycol under a flow of argon and magnetically stirring. 2.0 mmol $Fe(acac)_3$ was added when polyacrylic acid was complete dissolved in triethylene glycol. The mixture was slowly heated to 190°C for 30min and then quickly heated to reflux at 275°C under a blanket of argon for 30 min. By removing the heat source, the black homogeneous colloidal suspension was cooled down to room temperature. 30.0 ml ethyl acetate was added to the reaction solution and then separated via centrifugation, resulting in black precipitation. The black precipitation was dissolved in DI water and re-precipitated in ethanol and ethyl acetate for three times to remove residuals thoroughly.

2.1.5 Synthesis of 5 nm in diameter magnetic nanoparticles coated with polyacrylic acid

2.0 g of polyacrylic acid was firstly mixed with 25.0 ml triethylene glycol under a flow of argon and magnetically stirring. 2.0 mmol $Fe(acac)_3$ was added when polyacrylic acid was complete dissolved in triethylene glycol. The mixture was slowly heated to 190°C for 30min and then quickly heated to reflux at 275°C under a blanket of argon for 30 min. By removing the heat source, the black homogeneous colloidal suspension was cooled down to room temperature. 30.0 ml ethyl acetate was added to the reaction solution and then separated via centrifugation, resulting in black precipitation. The black precipitation

was dissolved in DI water and re-precipitated in ethanol and ethyl acetate for three times to remove residuals thoroughly.

2.1.6 Synthesis of 4 nm in diameter magnetic nanoparticles coated with polyacrylic acid

2.5 g of polyacrylic acid was firstly mixed with 25.0 ml triethylene glycol under a flow of argon and magnetically stirring. 2.0 mmol $Fe(acac)_3$ was added when polyacrylic acid was complete dissolved in triethylene glycol. The mixture was slowly heated to 190°C for 30min and then quickly heated to reflux at 275°C under a blanket of argon for 30 min. By removing the heat source, the black homogeneous colloidal suspension was cooled down to room temperature. 30.0 ml ethyl acetate was added to the reaction solution and then separated via centrifugation, resulting in black precipitation. The black precipitation was dissolved in DI water and re-precipitated in ethanol and ethyl acetate for three times to remove residuals thoroughly.

2.1.7 Synthesis of 20nm in diameter thermo-responsive magnetic nanoparticles

1g poly(N-isopropylacrylamide) was firstly mixed with 30 ml triethylene glycol under a flow of argon and magnetically stirring. 2 mmol $Fe(acac)_3$ was added when poly acrylic acid was complete dissolved in triethylene glycol. The mixture was slowly heated to 190°C for 30min and then quickly heated to reflux at 275 °C under a blanket of argon. By

removing the heat source, the black homogeneous colloidal suspension was cooled down to room temperature. An excess amount of ethyl acetate was added to the mixture resulting in black precipitation that was separated via centrifugation. The black product was re-dissolved in ethanol and re-precipitated in ethyl acetate to remove residuals thoroughly. The residue was redispersed in DI water and for further characterizations.

2.1.8 Synthesis of 20nm in diameter nanoparticles coated with polyacrylic acid and poly(N-isopropylacrylamide)

0.28 mmol of PAA and 0.05mmol of PNIPAM were mechanically stirred in 30 ml triethylene glycol under a flow of argon. 2 mmol $Fe(acac)_3$ was added when poly acrylic acid was complete dissolved in triethylene glycol. The mixture was slowly heated to 190°C for 30min and then quickly heated to reflux at 275 °C under a blanket of argon. By removing the heat source, the black homogeneous colloidal suspension was cooled down to room temperature. An excess amount of ethyl acetate was added to the mixture resulting in black precipitation that was separated via centrifugation. The black product was re-dissolved in ethanol and re-precipitated in ethyl acetate to remove residuals thoroughly. The residue was redispersed in DI water and for further characterizations.

2.1.8 Surface dissociation of nanoparticles

The alkaline solution of either NaOH or $Ca(OH)_2$ was added dropwise in the nanoparticle solution until a constant neutral solution was obtained under mechanical stirring. After that, the resultant nanoparticle solutions were dialyzed for 36 hours to completely remove impurities prior to applications.

2.2 Characterizations of nanoparticles

2.2.1 Field Emission Scanning Electron Microscope (FESEM) and Transmission Electron Microscope (TEM)

FESEM and TEM are well-established methods to observe the morphological properties of nanoparticles. The sample is prepared by drying a dispersion of magnetic nanoparticles on amorphous carboncoated copper grids. Magnetic nanoparticles were imaged using Field Emission Scanning Electronic Microscopy (FESEM, JEOL JSM-6700) and Transmission Electron Microscope (TEM, JEOL: JEM-2010 model). For each nanoparticle solution, three samples were prepared.

2.2.2 Thermogravimetric Analysis (TGA)

TGA 2050 Themogravimetric Analyzer (TA Instruments) was used to quantify the weight percent of polymer coating on nanoparticles. TGA was conducted using a Perkin-

Elmer TGA 7 at a constant heating rate of 5 °C/min from room temperature to 650 °C in a nitrogen environment.

2.2.3 Fourier Transform Infrared spectroscopy (FTIR)

FTIR measurements of magnetic nanoparticles were conducted to understand the surface chemistry on nanoparticles. The samples were prepared by pressing nanoparticles into KBr pellets and the results were obtained on a Bio-Rad Spectrometer of FTS 135.

2.2.4 Nanoparticle size distribution

The nanoparticle size is crucial parameter for nanoparticles to be used as draw solute in FO. The particle size plays an important role in determining FO performace. By dissolving little amount of nanoparticles in water, the size distribution of nanoparticles would be obtained in Nanoparticle Size Analyzer (Nano ZS, ZEN3600).

2.2.5 Vibrating Sample Magnetometer (VSM)

For nanoparticles which are composed of magnetic core, the magnetic property was examined through VSM (LakeShore 450-10) with a saturating field of 1 T. Their superparamagnetic property was confirmed by VSM.

2.3 Forward osmosis performance test

The performance of magnetic nanoparticles and others as draw solutes in the FO system was carried out on a lab-scale circulating filtration unit, as depicted in Figure 2.1. The commercially available HTI FO membrane (Batch No. 060327-3; Hydration Technologies Inc. previously Osmotek Inc.) was used. Either synthetic seawater (3.5% w/w sodium chloride solution) or DI water were employed as feed solution. The crossflow permeation cell was designed in a plate and frame configuration with a rectangular channel on either side of the membrane. The velocities of both draw and feed solutions, which co-currently flowed through the permeation cell channel, were maintained at certain rate during the FO testing. The temperatures of the whole FO system were kept at 22 ± 0.5ºC.

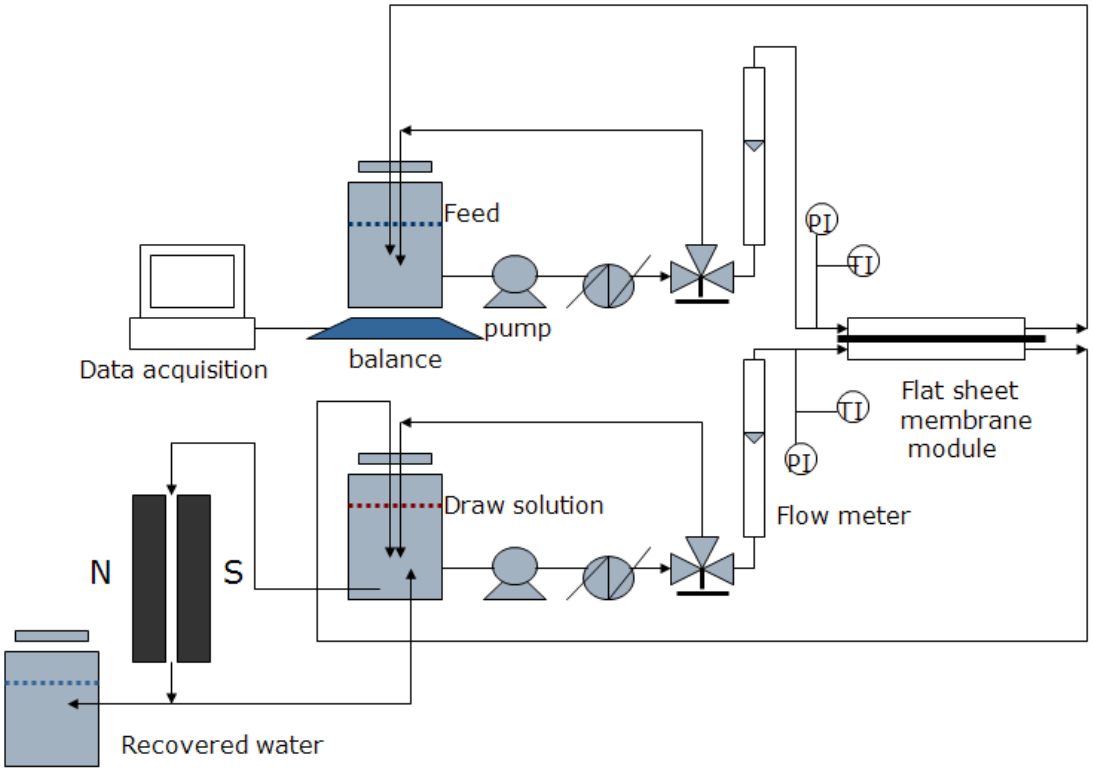

Figure 2.1 Schematic diagram of a laboratory-scale FO set-up combined with a magnetic separator

CHAPTER 3

HIGHLY WATER SOLUBLE MAGNETIC NANOPARTICLES AS NOVEL DRAW SOLUTE IN FORWARD OSMOSIS

3.1 Introduction

Water scarcity is gradually emerging as a worldwide problem due to accelerating population growth and environmental pollution [1]. More and more regions are considered water-poor and face associated problems of food production and public health issues [2]. Demands for clean water impel an emphasis on research in clean water reuse to avert a potential disaster. Previously, multistage flash (MSF), multi-effect distillation (MED) and especially reverse osmosis (RO) have been the flagships of seawater desalination [3-5]. However, MSF and MED are energy intensive processes that require high temperatures to evaporate water from ocean water, while RO is an electricity intensive process that needs extremely high hydraulic pressures to push water across the RO membrane but reject salts and other contaminants. MSF, MED and RO in this century are no longer as pragmatic as previously, especially in light of expected exponential population increase and the limited energy resources. Alternative low-energy desalination technologies are urgently needed to facilitate water reuse processes.

Osmosis is a ubiquitous physical phenomenon found in all of biology and involving the great power of molecular transport. Though it has been observed for a long time, only since the 1960s has it been explored as power generation as Pressure Retarded Osmosis (PRO) [6]. In FO, the osmotic pressure across the semi-permeable membrane provides the driving force that draws water from a higher water chemical potential side to a lower water chemical potential side without the aid of hydraulic pressure [7]. By comparison, the hydraulic pressure used in RO must exceed the required threshold osmotic pressure to move water from lower to higher water chemical potential. The significant advantages of osmotic pressure requiring no external energy source as its drawing force in FO together with a lower membrane fouling propensity than pressure-driven processes explains intensive investigative efforts for further exploitations, such as wastewater treatment, drug release and protein enrichment [8-9]. However, the challenges of FO still lie in the fabrication of eligible FO membranes and the readily separable draw solutes of high osmotic pressures. The FO membranes are rigorously delicate and many researchers have put a lot of effort in it [10-11]. The selected draw solutes vary across present-day studies that include sugar and ammonium carbon dioxide complex [12-13]. Nonetheless, there is a long way to go to fulfill the criteria of draw solutes in FO including (1) high osmolality to generate high osmotic pressures, and (2) easy and efficient separation from water.

According to the criteria of draw solutes in FO, superparamagnetic nanoparticles, which can be easily collected and separated from water by means of magnetic field, shall be considered as the draw solute in FO, assuming high osmotic pressures can be induced by

magnetic nanoparticles or some other means. Magnetic nanoparticles have assumed an important place in this research due to their high surface-area-to-volume ratio and special magnetic behavior [14]. So far, they are mainly studied in the field of biomedical applications, such as drug delivery and biocatalysis [15, 16]. However, many researchers in related areas have put forward the idea of using magnetic nanoparticles in FO, concerning the global water shortage problem [7, 17-18].

Herein, we synthesize highly hydrophilic magnetic nanoparticles and investigate the application of magnetic nanoparticles as draw solutes in FO. In previously published studies, magnetic nanoparticles were found to be of high molecular weight and low solubility in water thus of questionable suitability for use as a draw solute [19]. We report fine magnetic nanoparticles synthesized by a thermal decomposition method in one step with surfaces capped with super hydrophilic groups to implement draw solution of high osmotic pressure. Three different kinds of functional groups were used to functionalize the magnetic nanoparticles, resulting in different osmolalities when they reached the highest solubility. After the facile separation from water via magnetic field, magnetic nanoparticles were reused in FO processes. Magnetic nanoparticles of different diameters were also synthesized and tested to investigate possible factors that affect the performance of magnetic nanoparticles as draw solute in FO. Our results demonstrate that functionalized magnetic nanoparticles used as draw solute are attainable and suggest great potential in a variety of FO applications.

3.2 Experimental

3.2.1 Synthesis of magnetic nanoparticles

Materials

Iron (III) acetylacetonate ($Fe(acac)_3$, 99.9%), triethylene glycol (98%), 2-pyrrolidone(99%) and polyacrylic acid (PAA, Mw=1800, 98%) were purchased from Sigma-Aldrich. Ethyl acetate (98%) was obtained from Tedia. All the chemicals above were used as received. The deionized (DI) water used in experiments was produced by a Milli-Q unit (Millipore, USA) with the resistivity of 18 MΩ /cm

Synthesis of Magnetic Nanoparticles

Three kinds of water-soluble magnetic nanoparticles capped with different surface functional groups such as 2-pyrrolidone, triethylene glycol and polyacrylic acid were synthesized by the thermal decomposition method. Figure 3.1 illustrates the synthetic routes. 2-Pyrrolidone-magnetic nanoparticles (2-Pyrol-MNPs) and triethylene glycol-magnetic nanoparticles (TREG-MNPs) were prepared in hydrophilic and high boiling point organic solvents according to literature and the detail could be found in this thesis 2.1.

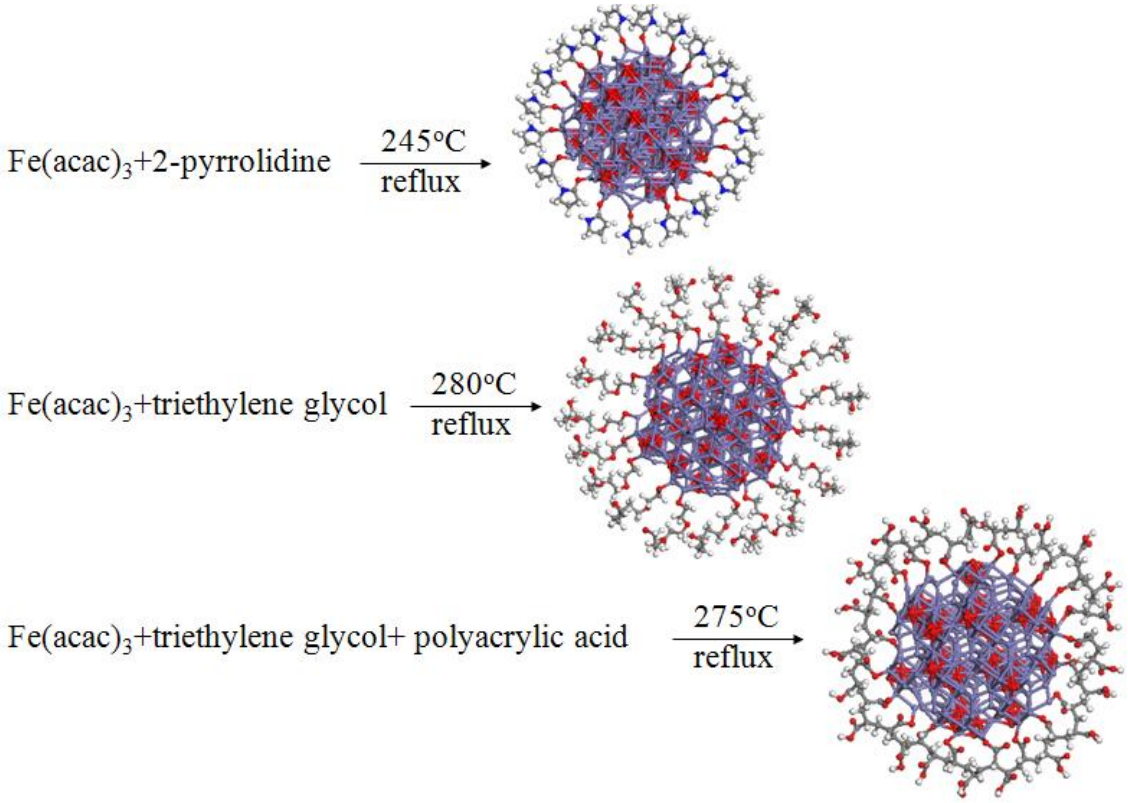

Figure 3.1 Synthesis routes of surface functionalized magnetic nanoparticles

In order to investigate and improve the hydrophilicity, polyacrylic acid was selected to functionalize the magnetic nanoparticle surface owing to the copious carboxylate groups along the polymer chain. These functional groups may enhance the interaction between water and magnetic nanoparticles because the free carboxylate groups extended in water may facilitate the dispersibility of polyacrylic acid-magnetic nanoparticles (PAA-MNPs) in the aqueous solution [22-23, 24], and increase the driving force for FO. The synthesis of PAA-MNPs for biomedical applications has been studied using the ligand exchange method that transfers the nanoparticle's surface property from hydrophobicity to

hydrophilicity [22-23]. However, compared to 2-Pyrol-MNPs and TREG-MNPs, the route of ligand exchange of polyacrylic acid onto initially hydrophobic magnetic nanoparticles was very complicated and tedious.

Inspired by the Sun's facile method [25] to synthesize fine hydrophobic magnetic nanoparticles using appropriate surfactants and high-boiling point solvents, we chose polyacrylic acid as the surfactant and triethylene glycol as the solvent to produce highly hydrophilic PAA-MNPs. To our best knowledge, PAA-MNPs prepared by this route have not been reported previously. The synthesis was carried out as the description in this thesis 2.1. By adjusting the reaction conditions, 2-Pyrol-MNPs, TREG-MNPs and PAA-MNPs were prepared with a similar size range (20~30 nm). All three kinds of magnetic nanoparticles show very hydrophilic properties and are stably dissolved in water even after storage for 3 months. The newly synthesized magnetic nanoparticle solutions were dialyzed for 36 hours to completely remove impurities prior to application.

3.2.2 Characterization of Magnetic Nanoparticles

Magnetic nanoparticles were imaged using Field Emission Scanning Electronic Microscopy (FESEM, JEOL JSM-6700) by drying a dispersion of magnetic nanoparticles on amorphous carbon coated copper grids. The measurements of size distribution of magnetic nanoparticles were conducted in Nanoparticle Size Analyzer (Nano ZS,

ZEN3600). The magnetic properties of functionalized magnetic nanoparticles were recorded in a vibrating sample magnetometer (VSM, LakeShore 450-10) with a saturating field of 1 T. Fourier transform infrared spectroscopy (FTIR) of magnetic nanoparticles, pressed into KBr pellets, were obtained on a Bio-Rad Spectrometer of FTS 135. Thermogravimetric analysis (TGA) was conducted to determine the weight percentage of surface capping groups covalently bonding to magnetic nanoparticles core, using a Perkin-Elmer TGA 7 at a constant heating rate of 5°C/min from room temperature to 600°C in a nitrogen environment.

3.2.3 Forward Osmosis using Surface Functionalized Magnetic Nanoparticles as Draw solutes

The performance of highly water-soluble magnetic nanoparticles as draw solutes in the FO system was carried out on a lab-scale circulating filtration unit, as depicted in this thesis 2.3. The draw solutions of magnetic nanoparticles were prepared by dissolving certain amount of nanoparticles in water. In the case of using magnetic nanoparticles as draw solutes in FO, the magnetic nanoparticles could be 100% intercepted by FO membranes in the draw solution side for the diameter of magnetic nanoparticles was much larger than the pore size of FO membranes. Therefore, the mass of magnetic nanoparticles remained constant in draw solutions. The dilution of draw solution was negligible because the volumes of draw solutions increased less than 2% during the FO testing.

The water permeation flux (J_v, $L \cdot m^{-2} \cdot hr^{-1}$, abbreviated as LMH) was calculated from the volume change of feed solution.

$$J_v = \Delta V/(A\Delta t) \quad (1)$$

where ΔV (L) is the permeation water collected over a predetermined time Δt (hr) in the FO process duration; A is the effective membrane surface area (m^2).

The concentration of surface capping groups surrounding each magnetic nanoparticle was calculated using the formula below:

$$C = \frac{(\rho - 1000) \cdot w}{M_w} \quad (2)$$

Where C is the molar concentration of surface capping groups on magnetic nanoparticles in water (mol/L); ρ is the density of magnetic nanoparticles solution (g/L) while the water density is assumed to be 1000 g/L; w is the mass percentage of the surface capping groups upon magnetic nanoparticles obtained by TGA via weight percentage change before and after burning magnetic nanoparticles at high temperatures, as shown in Figure 3.2; V is the volume of the draw solution; M_w is the molecular weight of the surface capping groups (g/mol). Here we assume no additional volume change in the draw solution after adding magnetic nanoparticles except their own individual volumes.

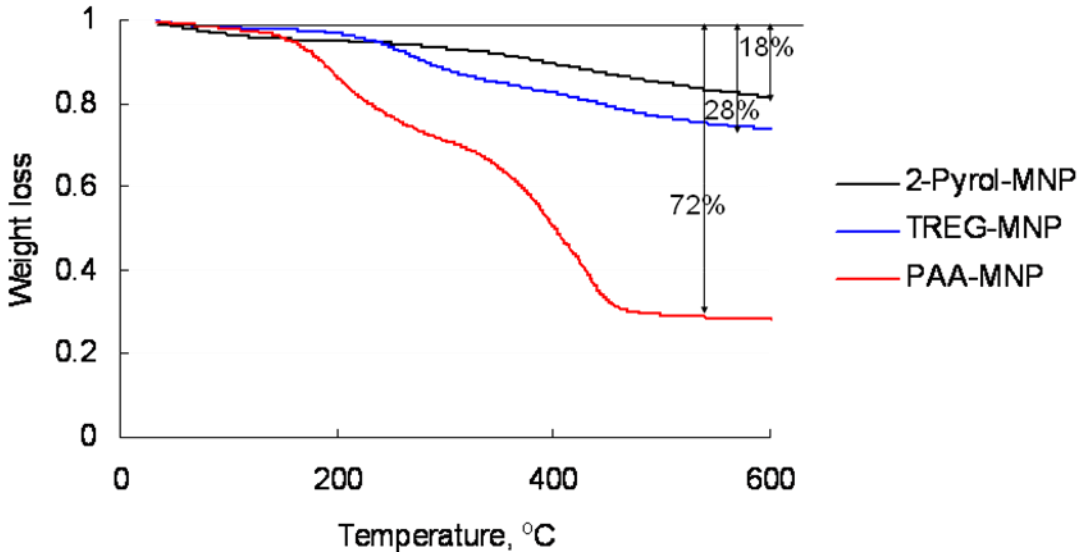

Figure3.2 TGA graph of magnetic nanoparticles

3.3 Results and discussion

3.3.1Characterizations of magnetic nanoparticles

The newly synthesized PAA-MNPs show narrow size distributions with superparamagnetic and super hydrophilic characteristics. These unique properties may arise from the close matching between the carboxylate groups of polyacrylic and magnetite nanocrystal surface [16, 22-23]. By increasing the amount of polyacrylic acid in reactions, one can effectively control the growth of magnetic nanoparticle cores and the resultant PAA-MNPs have average diameters of 4~30 nm.

Figure 3.3 shows FESEM images and particle size distributions of 2-Pyrol-MNPs, TREG-MNPs and PAA-MNPs. They are almost monodispersed in water with an average diameter of 20 ~ 30nm. Importantly, even though the particles are very small, no agglomeration can be observed in these magnetic nanoparticles.

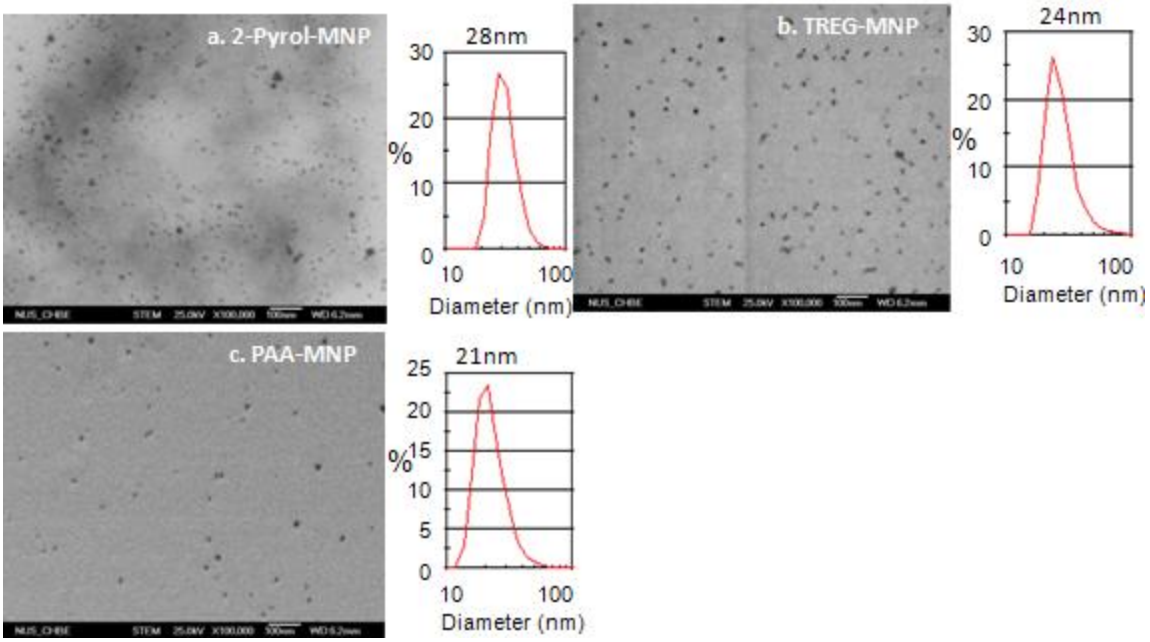

Figure 3.3 FESEM and size distribution of magnetic nanoparticles

Figure 3.4 displays the FTIR spectra of the surface chemistry of these magnetic nanoparticles. The characteristic peaks located at 590 cm^{-1} can be attributed to the lattice absorption of iron oxide [19-23], while the peaks around 1660 cm^{-1} due to the vibrating mode of C-O bond. Clearly, the O in C-O bond anchors to Fe on the surface of magnetic nanoparticles [19-23]. The characteristic bands at 2950–2900 cm^{-1} are typical C–H stretching. For 2-Pyrol-MNPs, the broad band peak at 3350cm^{-1} is ascribed to N-H stretching of 2-pyrrolidone [19, 26]. In the spectra of TREG-MNPs and PAA-MNPs,

peaks at 1121–1080 cm−1 are referred to as C–O stretching [20-22]. A strong absorption band of 1736 cm−1 is found in the spectrum of PAA-MNP, which is a characteristic of the C=O stretching mode for carboxylate groups [21-22]. The peaks at 1459~1395 cm^{-1} and 1621 cm^{-1} of symmetric and asymmetric C-O stretching modes of carboxylate groups further confirm a large amount of polyacrylic acid attached on the surface of magnetic nanoparticles[21-22].

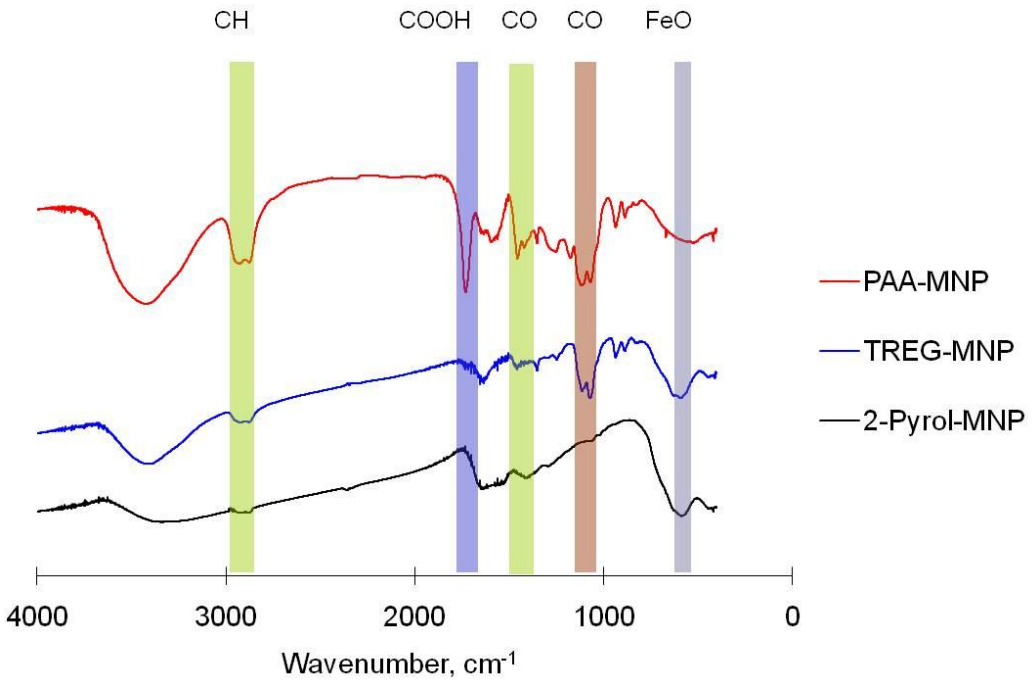

Figure 3.4 FTIR spectra of magnetic nanoparticles

Magnetic behaviors of 2-Pyrol-MNPs, TREG-MNPs and PAA-MNPs were investigated using VSM at room temperature. The magnetization curves in Figure 3.5 show the superparamagnetic properties of the three kinds of magnetic nanoparticles. Coericivity and remanence are not observed by magnetic measurements. For PAA-MNPs synthesized

in triethylene glycol as solvent, its saturation magnetization is greatly decreased comparing to TREG-MNPs. This phenomenon further confirms that polyacrylic acid was successfully bonded to the surface of magnetic nanoparticles in the competition with triethylene glycol in reactions and multilayer of polyacrylic acid might be formed [27].

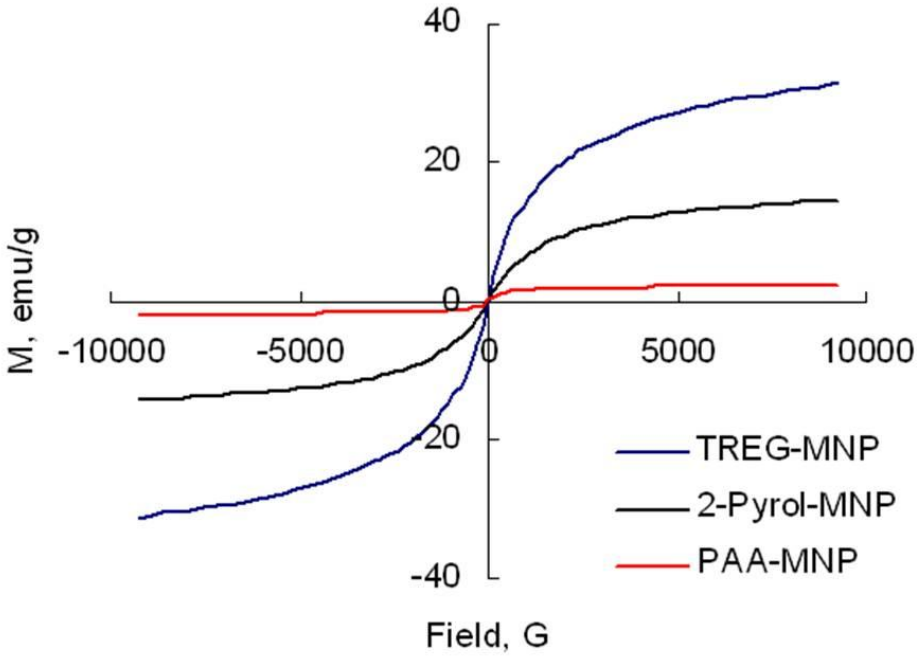

Figure 3.5. Hysteresis loops of magnetic nanoparticles at 300 K.

3.3. 2 Forward osmosis performance evaluation of the membrane

The FO performance of HTI FO membranes was first tested using sodium chloride as draw solute and Figure 3.6 shows the water flux and salt leakage. The water flux in the FO mode (the draw solution against the porous layer) is less than the PRO mode (the draw solution against the dense selective layer) due to the internal concentration polarization. In other words, more solutes are rejected by the dense layer in the PRO

mode, while more solutes could be accumulated inside the membrane pores in the FO mode and retard the flux [28, 29].

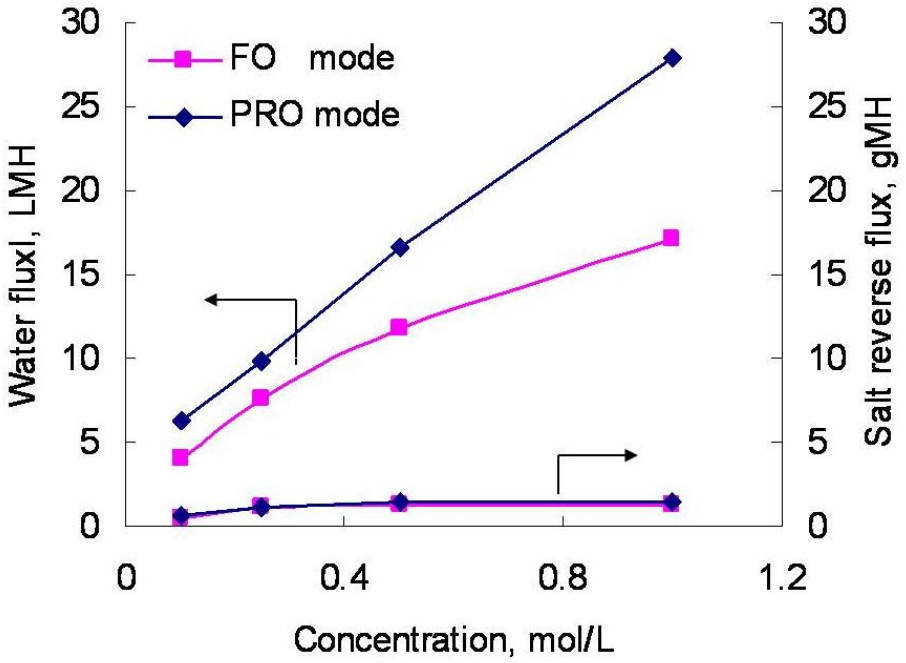

Figure 3.6 Water flux and salt reverse flux using a HTI FO membrane (NaCl as the draw solution)

3.3.3 Forward osmosis performance using Versatile Magnetic Nanoparticles as Draw Solutes

To investigate the effect of different surface chemistry of magnetic nanoparticles as draw solutes on water flux, 2-Pyrol-MNPs, TREG-MNPs and PAA-MNPs with diameters in a similar range of 20-30 nm were first examined. Figures 3.7 and 3.8 (in the next page) show the water flux and osmolalities as function of surface chemistry and draw solute concentration in PRO and FO modes. For comparison, the surface capping groups were

also tested as draw solutes and their performance are included in Figures 3.7 and 3.8. To elucidate the water flux discrepancy between different draw solutes in water, the chemical potential energy of surface capping groups in water was calculated with the aid of Material Studio 4.4 [30]. Figure 3.9 displays the calculated results. There is the smallest potential energy gap between water and 2-pyrrolidone solution; followed by water and triethylene glycol solution; then a much larger potential energy gap is exemplified between water and polyacrylic acid solution. A larger potential chemical gap bespeaks a higher osmotic pressure and a driving force.

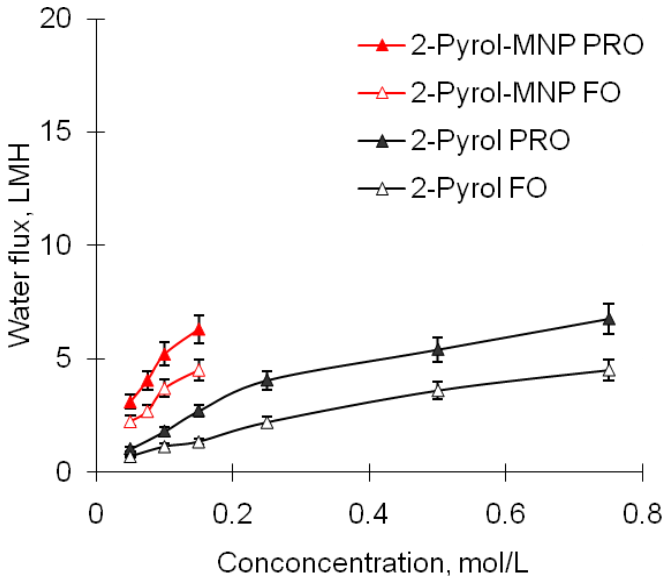

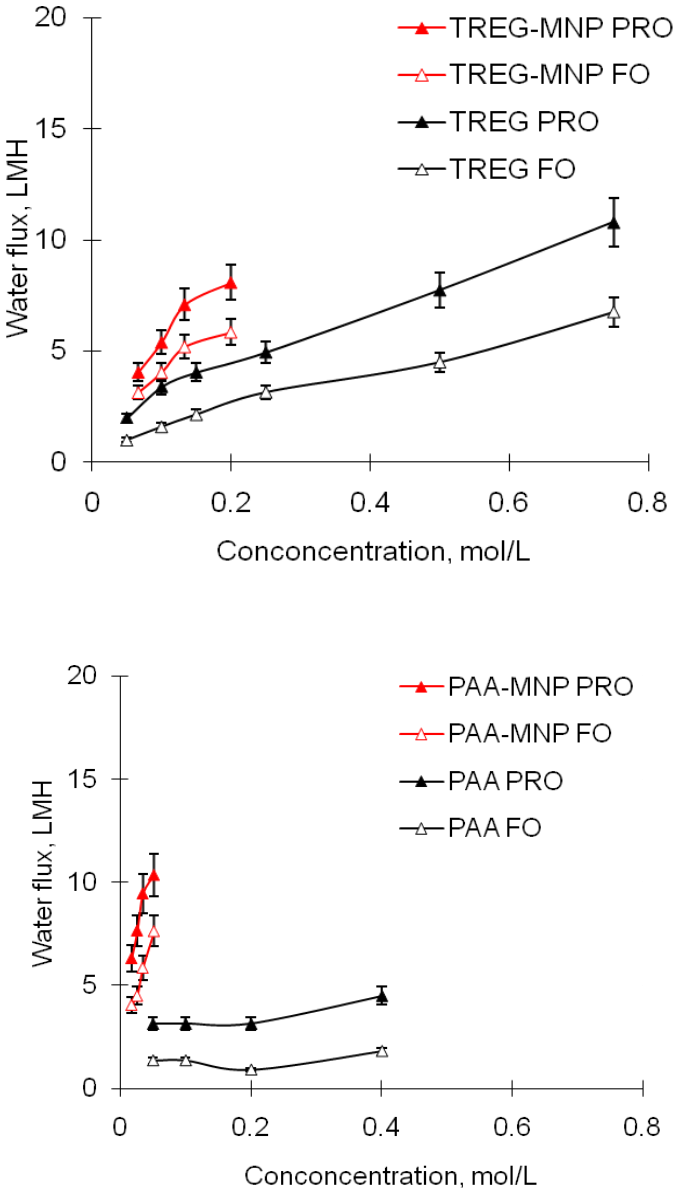

Figure 3.7 Water flux of surface capping groups and magnetic nanoparticles

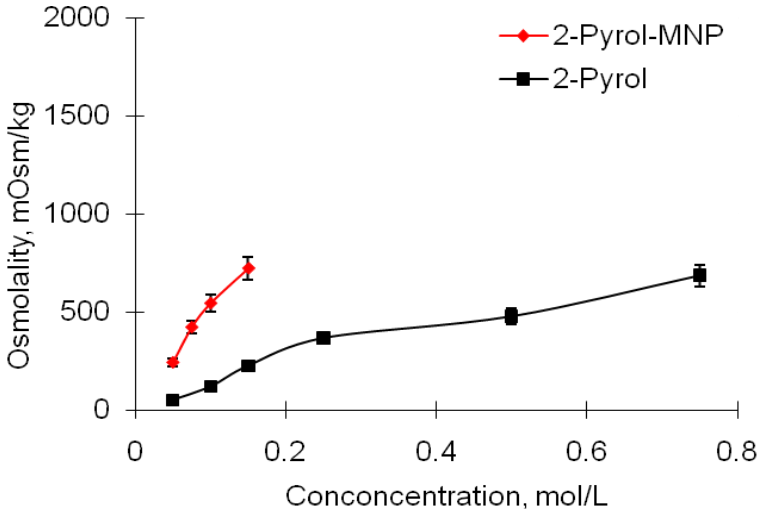
2000
1500
1000
500
0
Osmolality, mOsm/kg
0
0.2
0.4
0.6
0.8
Conconcentration, mol/L
2-Pyrol-MNP
2-Pyrol

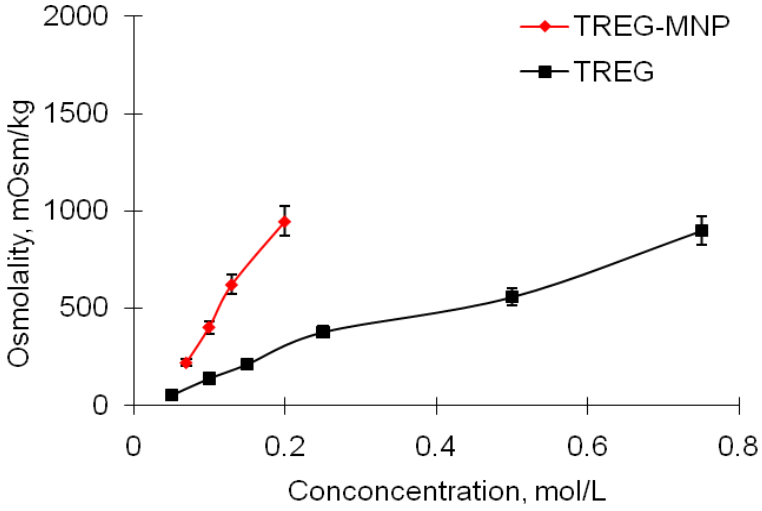
2000
1500
1000
500
0
Osmolality, mOsm/kg
0
0.2
0.4
0.6
0.8
Conconcentration, mol/L
TREG-MNP
TREG

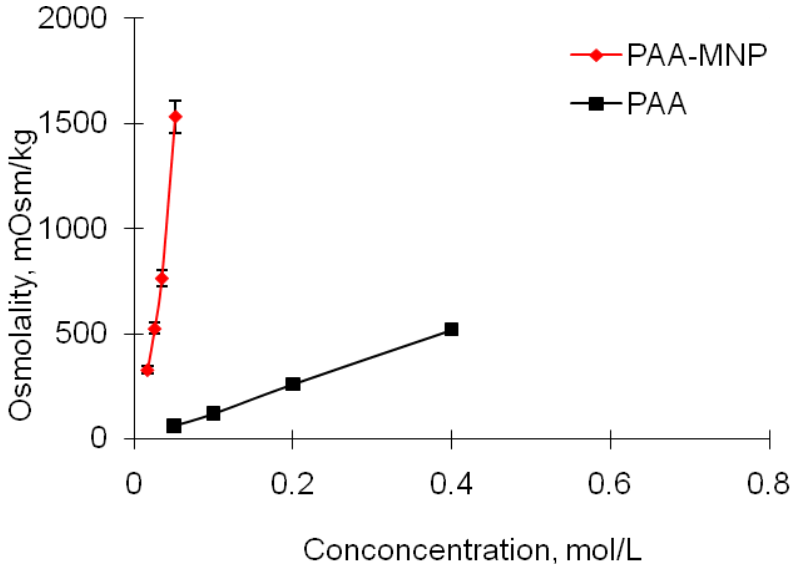

Figure 3.8 Osmolality of surface capping groups and magnetic nanoparticles in water

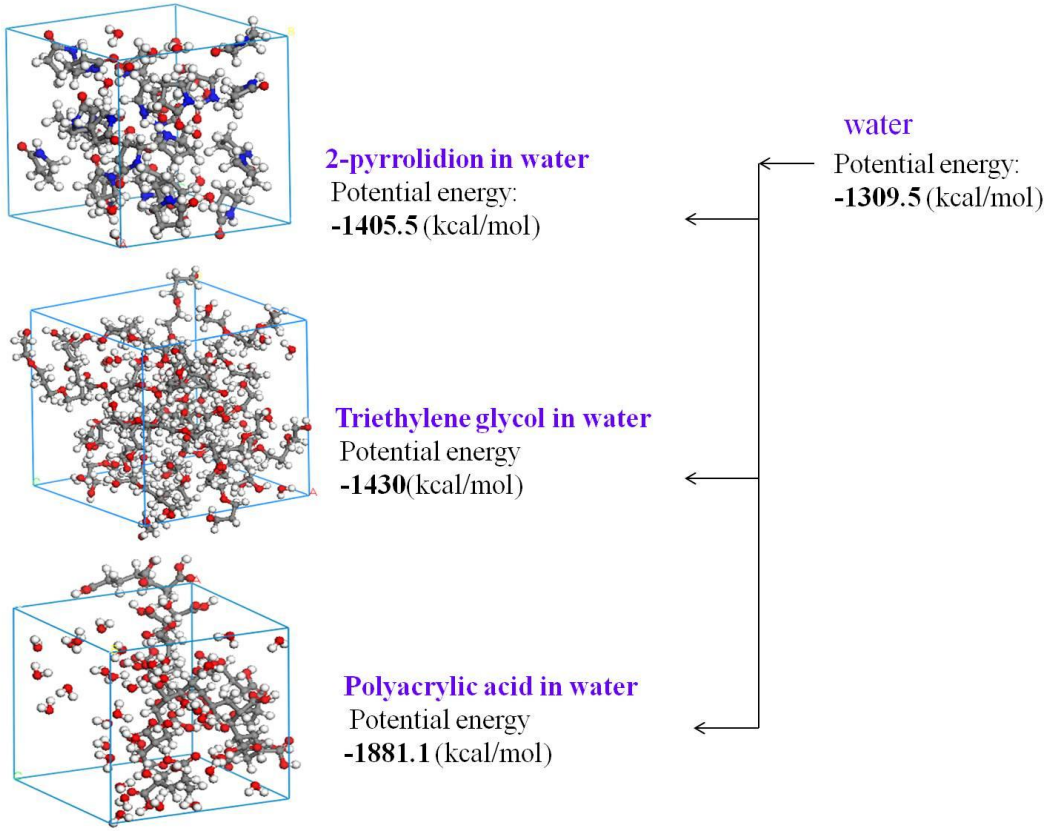

Figure 3.9 Potential energy to explain water flux differences

The theoretical predication is consistent with the experimental results from surface capping groups. As shown in Figure 3.7, water flux at 0.05 mol/L exactly follows the order of polyacrylic acid (PAA) > triethylene glycol (TREG) > 2-pyrrolidone (Pyrol). At high draw solute concentrations, the flux induced by triethylene glycol is still relatively higher than that of 2-pyrrolidone. The flux profile induced by polyacrylic acid is different from others. Even though it results in a high flux at 0.05mol/L, it keeps nearly constant with an increase in polyacrylic acid concentration. One of possible reasons is due to the strong hydrogen bonding between abundant carboxylate groups along polyacrylic acid chains and hydroxyl groups of the HTI FO membrane surface. As a result, the polyacrylic acid may closely adhere to the membrane surface or possibly partially block the pore and retard the flux enhancement. In addition, viscosity may play an important role because the viscosity of polyacrylic acid in water is found to rapidly increase with increasing polymer concentration. Thus the water transport resistance in the system increases and retards any enhancement in water flux.

Figure 3.10 tabulates and compares the flux and osmolality when magnetic nanoparticles are employed as draw solutes. As expected, PAA-MNPs can yield the highest water flux of 10.4~7.7 LMH; followed by TREG-MNPs 8.1~5.9LMH and then 2-Pyrol-MNPs 6.3~4.5LMH, which is in line with our potential energy calculations and the osmolality measurements. The water flux induced by PAA-MNPs is far superior to that of pure

polyacrylic acid, implying that PAA-MNPs can overcome the hydrogen bonding near membrane surface and realize the mobility of polyacrylic acid. This is due to the fact that polyacrylic acid has been evenly dispersed in the solution and closely attached on the extremely fine and high mass-density magnetic nanoparticles. Not only do the nano-size iron oxide cores result in significant contact surfaces between polyacrylic acid and water, but also the covalence bond between polyacrylic acid and magnetic nanoparticles provide the sufficient strength for the integrity of magnetic nanoparticles.

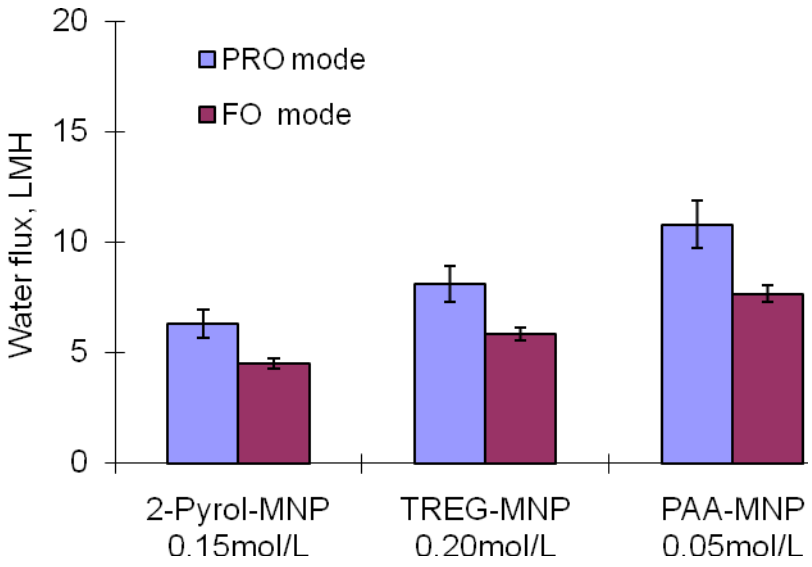

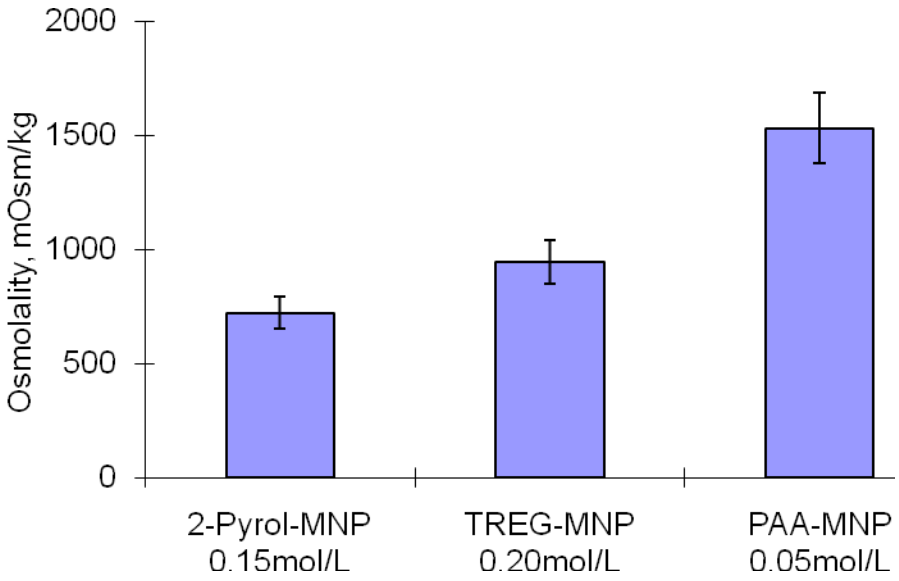

Figure 3.10 Summary of (a) highest water flux and (b) osmolality of magnetic nanoparticles of different surface chemistries

3.3.4 Facile Recovery of Magnetic Nanoparticles by Magnetic Field Capture

To fulfill the application of highly hydrophilic magnetic nanoparticles as draw solutes in FO for water reuse, the drawn water and magnetic nanoparticles in the permeate side must be easily separated and the magnetic nanoparticles must be easily recycled. A High Gradient Magnetic Separator (HGMS, model L-1CN, Frantz canister separator, from S. G. Frantz Co., Inc. Trenton, NJ) was employed to provide the magnetic field and test this concept. It was found that the magnetic nanoparticles can be readily captured by HGMS and the other product is water. Each kind of magnetic nanoparticles was then retested in the FO system as draw solutes. Figure 3.11 displays the water flux of magnetic

nanoparticles before and after recycle. Flux drops slightly possibly due to the strong strength of HGMS that causes slightly aggregation of magnetic nanoparticles; the size distribution of recycled magnetic nanoparticles is shown in Figure 3.12. Yet the recycled magnetic nanoparticles are still dispersed in water promptly, which confirmed surface functional groups have been firmly anchored onto iron oxide cores. Future works will be aimed to overcome the nanoparticle aggregation induced by HGMS.

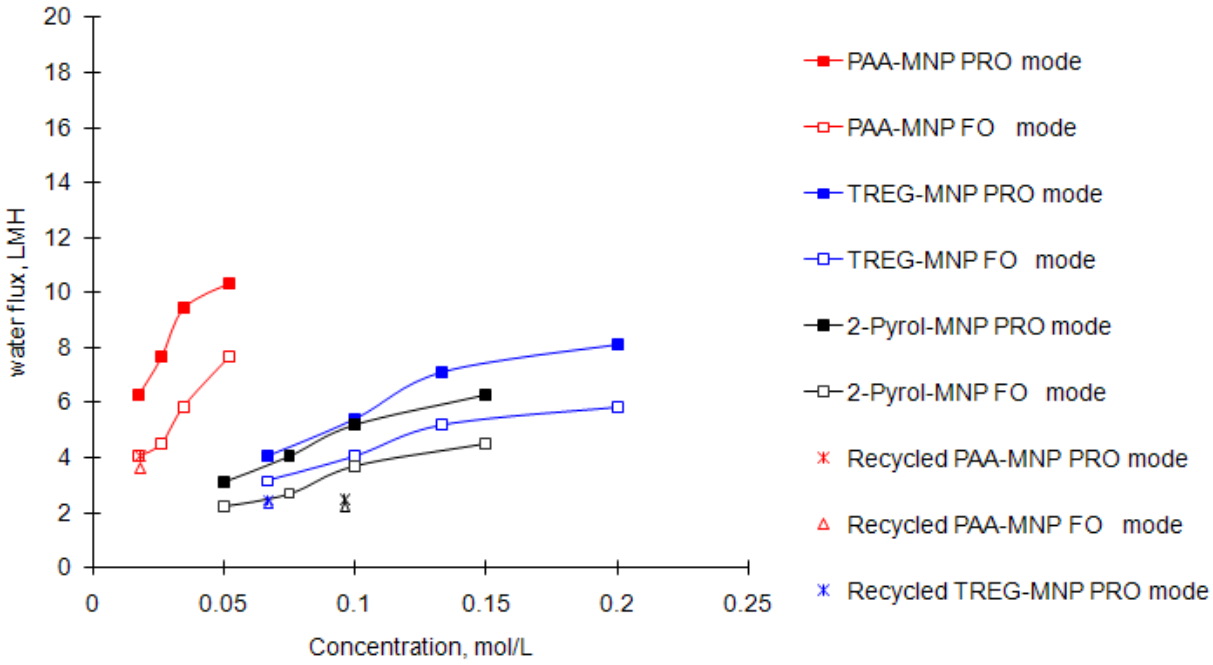

Figure 3.11 Water flux of magnetic nanoparticles before and after recycle

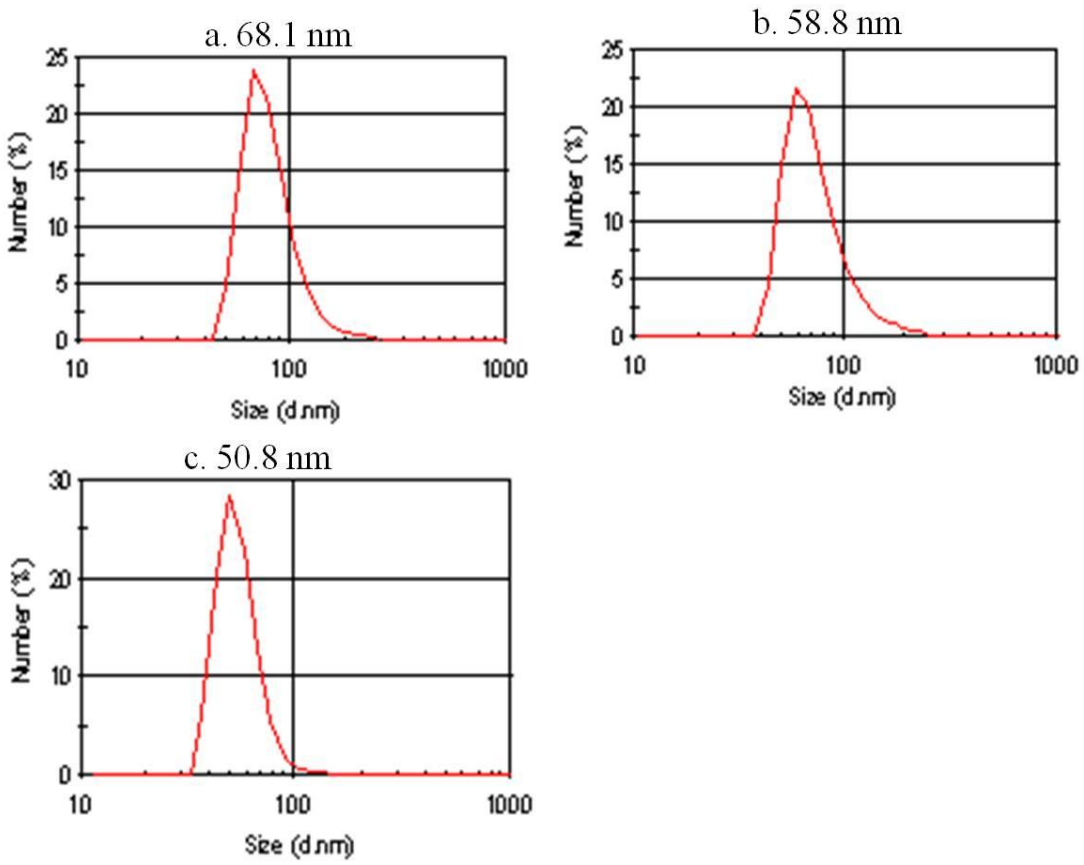

Figure 3.12 Size distribution of recycled magnetic nanoparticles (a) 2-Pyrol-MNPs (b) TREG-MNPs (c) PAA-MNPs

3.3.5 Forward osmosis performance using PAA-MNPs of Different Diameters as Draw Solute

In order to utilize magnetic nanoparticles more effectively for water reuse, PAA-MNPs, which exhibited highest water flux among the three kinds, were chosen to further explore the effect of magnetic nanoparticle diameters on water flux. The diameter of magnetic nanoparticles is tunable by adding 2.5g, 2.0g, 1.5g and 1.0g of polyacrylic acid in 25.0 ml

solvent respectively in reactions, wherein PAA-MNPs of 4 nm, 5 nm, 7 nm and 20 nm average diameters can be obtained. Figure 3.13 illustrates the diameter distributions of the resultant PAA-MNPs, while Figure 3.14 shows their corresponding water flux and osmolality. The highest driving force is achieved in the draw solution of 4 nm PAA-MNPs since more magnetic nanoparticles of smaller diameters can be located per unit volume and it has the highest osmolality. This clearly demonstrates that water flux of PAA-MNPs as draw solute increases with a decrease in MNPs diameter. However, the use of smaller PAA-MNPs in FO has some drawbacks. The magnetic property becomes smaller as a result of higher content of polyacrylic acid wrapping each particle. In addition, the recovery of smaller PAA-MNPs was unsatisfactory because their diameters jump out of the range that HGSM can capture. Thus, a compromised size of MNPs should be used between the choices of high water flux and readily recovery by the magnetic field.

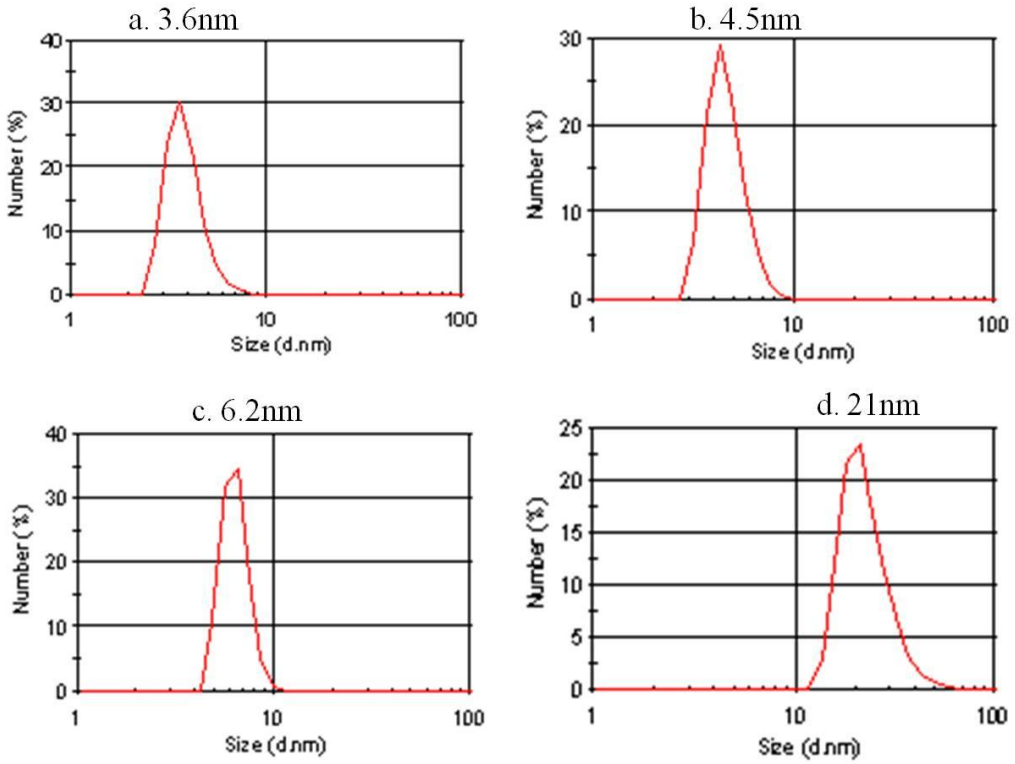

Figure 3.13 Size distribution of PAA-MNPs synthesized by adding (a) 2.5g (b) 2.0g (c) 1.5g and (d) 1.0g of polyacrylic acid in 25.0 ml solvent

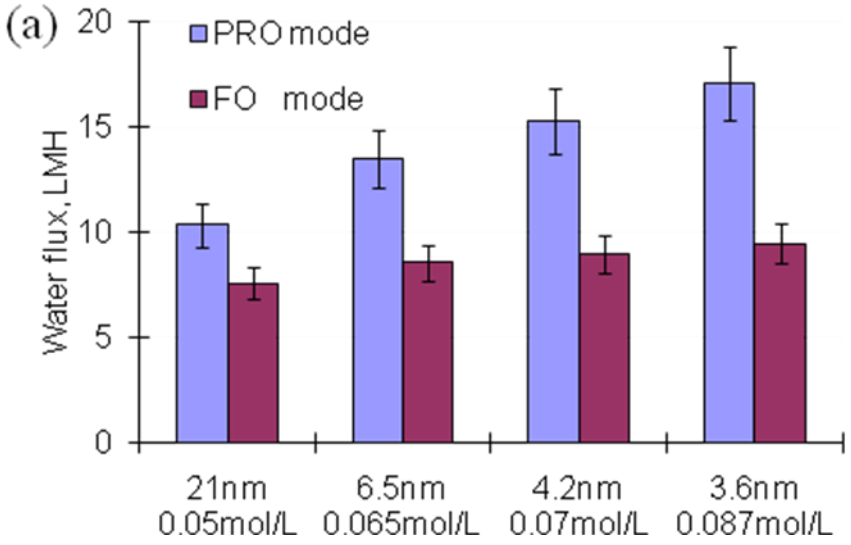

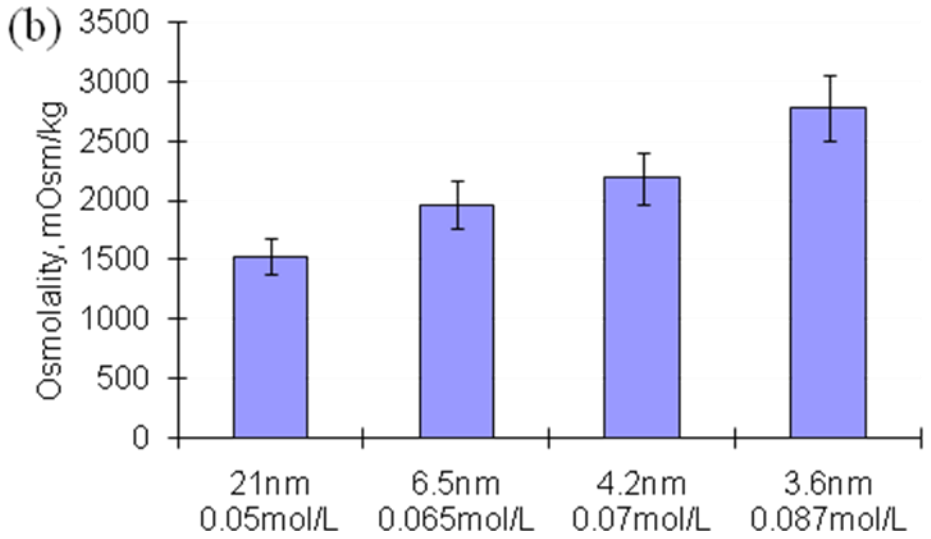

Figure 3.14 Effect of PAA-MNP particle sizes on (a) water flux and (b) osmolality

3.4 Conclusion

We have synthesized highly water-soluble magnetic nanoparticles and demonstrated them as novel robust draw solute in forward osmosis for the first time. Draw solutions of magnetic nanoparticles capped with polyacrylic acid exhibit the highest water flux among the three different surface functionalized magnetic nanoparticles. PAA-MNPs draw solution had lowest potential energy compared to other nanoparticles suspensions and the largest potential energy gap was generated between PAA-MNPs draw solution and feed solution across the membrane. Therefore, PAA-MNPs draw solution yielded superior FO performance with highest osmotic driving force in this work. It is believed that water flux can be further increased by modifying the surface chemistry. Magnetic nanoparticles after using in the FO process are readily captured in the magnetic field. HGMS provides a

facile and fast way to facilitate the recovery of magnetic nanoparticles in a continuous process. In addition, water flux can be enhanced by decreasing the diameters of magnetic nanoparticles. Future studies will be focused on (1) the optimization of surface chemistry and diameter selection of magnetic nanoparticles, (2) the investigation of their performance in forward osmosis for seawater desalination, and (3) the investigation of their sustainability in forward osmosis processes.

3.5 References

1. L. Robert, M. Elimelech, Global challenges in energy and water supply: the promise of engineered osmosis, Environ. Sci. Tech., 42(2008)8625.

2. M. A. Shannon, P. W. Bohn, M.Elimelech, J. G. Georgiadis, B. J. Marias, A. M. Mayes, Science and technology for water purification in the coming decades, Nature, 452(2008)301.

3. O.J. Morin, Design and operating comparison of MSF and MED systems, Desalination, 93(1993)69.

4. N. M. Wade, Distillation plant development in dual–purpose power and desalination plants. Desalination, 123(1999)115.

5. S. Sourirajan, Reverse Osmosis, Academic Press, Inc. New York, NY, 1970.

6. S. Loeb, Osmotic power plants. Science, 189(1974)350

7. T. Y.Cath, A. E. Childress, M. Elimelech, Forward osmosis: principles, applications, and recent developments, J. Membr. Sci. 281(2006)70.

8. J. C. Wright, R. M. Johnson, S. I. Yun, DUROS® osmotic pharmarceutical systems for parenteral & site-directed therapy. Drug Delivery Technol. 3(2003) 64.

9. Q.Yang, K. Y.Wang, T. S. Chung, A novel dual-layer forward osmosis membrane for protein enrichment and concentration. Sep. Purif. Technol., 69(2009) 269.

10. K. Y. Wang, T. S. Chung, J. J. Qin, Polybenzimidazole (PBI) nanofiltration hollow fiber membranes applied in forward osmosis process. J. Membr. Sci., 300(2007)6.

11. Q. Yang, K. Y. Wang, T. S. Chung, Dual-layer hollow fibers with enhanced flux as novel forward osmosis membranes for water reuse. Environ. Sci. Technol. 43(2009)2800.

12. E. G. Beaudry, L.A. Lampi, Membrane technology for direct osmosis concentration of fruit juice. Food Technol. 44(1990)121.

13. J. R. McCutcheon, R. L. McGinnis, M. Elimelech, A novel ammonia-carbon dioxide forward (direct) osmosis desalination process. Desalination. 174(2005)1.

14. A. H. Lu, E. L. Salabas, F. Schüth, Magnetic nanoparticles: synthesis, protection, functionalization, and application. Angew. Chem. Int. Ed. 46(2007)1222.

15. W. Wang, Y. Xu, D. C. Wang, Z. Li, Recyclable nanobiocatalyst for enantioselective sulfoxidation: facile fabrication and high performance of chloroperoxidase-coated magnetic nanoparticles with iron oxide core and polymer shell. J. AM. CHEM. SOC. 131(2009)12892.

16. G. C. Kim,; Y. Y. Li,; Y. F. Chu, S. X. Cheng, R. X. Zhuo, X. Z. Zhang, Nanosized temperature-responsive Fe3O4-UA-g-P(UA-co-NIPAAm) magnetomicelles for controlled drug release. European Polymer Journal. 44(2008)2761.

17. NanoMagnetics, Water purification, 2005. Electronic Source: http://www.nanomagnetics.com/water purification.asp.

18. S. Adham, J. Oppenheimer, L. Liu, M. Kumar, Dewatering reverse osmosis concentrate from water reuse using forward osmosis. WateReuse Foundation: Alexandria, VA 2007.

19. J. D. Hearn, A. J. Lovett, G. D. Smith. Ozonolysis of oleic acid particles: evidence for a surface reaction and secondary reactions involving criegee intermediates. Phys. Chem. Chem. Phys. 7(2005)501.

20. Z. Li,; L. Chen,; H. B. Bao,; M. Y. Gao, One-pot reaction to synthesize water-soluble magnetite nanocrystals. Chem. Mater. 16(2004)1391.

21. W. Cai, J. Q. Wan, Facile synthsis of superparamagnetic magnetite nanoparticles in liquid polyols. J. Colloid Interface Sci. 305(2007)366.

22. J. P. Ge, . X.Hu, Y; M. Biasini, C.L. Dong, J. H. Guo, W. P. Beyermann,; Y. D. Yin, One-step synthesis of highly water-soluble magnetite colloidal nanocrystals. Chem. Eur. J. 13(2007)7153

23. T. R. Zhang, J. P. Ge, Y. X.Hu, Y. D. Yin, A general approach for transferring hydrophobic nanocrystals into water. Nano Lett. 7(2007)3203.

24. Q. Zhang, S. X. Cheng , X. Z. Zhang, R. X. Zhuo, Water-soluble Polymer Protected Lipofectamine 2000/DNA Complexes for Solid-Phase Transfection. Macromolecular Bioscience. 9(2009)1262.

25. S. H. Sun, H. Zeng, D. B. Robinson, G. X. Li, Monodisperse MFe2O4 (M=Fe, Co, Mn) nanoparticles. J. AM. CHEM. SOC. 126(2004)273.

26. C. Qin,; C.Li, Y. Z. Hu, J. F. Shen, M. X. Ye, Facile synthesis of magnetic iron oxide nanoparticles using 1-methyl-2-pyrrolidone as a functional solvent. Colloids and Surfaces A: Physicochem. Eng. Aspects. 336(2009)130.

27. R. D.Palma, S.Peeters, M. V.Bael, H. V.Rul, K.Bonroy, W.Laureyn, J.Mullens, G.Borghs, G.Maes, Silane ligand exchange to make hydrophobic superparamagnetic nanoparticles water-dispersible. Chem. Mater. 19(2007)1821

28. B.X. Mi, M. Elimelech, Chemical and physical aspects of organic fouling of forward osmosis membranes. J. Membr. Sci. 320(2008)292.

29. A. L. Zydney, Stagnant film model for concentration polarization in membrane systems. J. Membr. Sci. 23(1997)275.

30. Y.Wang, T. S.Chung, H.Wang, S. H. Goh, Butanol isomer separation using polyamide–imide/CD mixed matrix membranes via pervaporation. Chemical Engineering Science.2009, 64, 5198-5209

CHAPTER 4

DESALINATION PROCESS USING SUPER HYDROPHILIC NANOPARTICLES VIA FORWARD OSMOSIS INTEGRATED WITH ULTRAFILTRATION REGENERATION

4.1 Introduction

Forward Osmosis (FO) has received worldwide attention because it is an emerging technology for water reuse [1-4], seawater desalination [5-8] and power generation [9-12] based on salinity gradients. Besides these applications, FO has been used in food processing [13], protein concentration [14] and alcohols dehydration [15]. Utilizing one powerful intrinsic energy source among molecules, the osmotic pressure difference across a semi-permeable membrane of two solutions is the driving force distinguishing FO itself with a low energy operation from traditional pressure-driven and energy-intensive processes, such as, reverse osmosis (RO) and nanofiltration (NF) [16]. Furthermore, the low membrane fouling propensity of the osmotically driven process makes FO more economically favorable [2-3]. Owing to the predictable exponential increase in worldwide energy consumption and the limited energy resources, more

studies should be emphasized in FO to advance the process, promote cost effectiveness and speed-up the adoption of industrial applications.

Many researchers have focused their works on the FO membrane development [17-22], while less attention is given to discovering new draw solutes and their regeneration methods, which are also essential to developing FO processes. Desirable draw solutes are supposed to possess high osmotic pressure and therefore can draw water from feed solutions during FO processes, after which, draw solutes must be easily separated from water and readily recycled with the aid of a suitable process. Researchers have proposed to use water-soluble gases, such as sulfur dioxide, as draw solutes in water and then the draw solutes were removed by heating [23]. Different salts and a variety of sugars were also used as draw solutes and reported [24, 25]. Thermally unstable ammonium salts, composed of ammonia and carbon dioxide, were employed as draw solutes in recent years [26]. Highly water soluble magnetic nanoparticles coated with polyacrylic acid (referred as PAA-NPs), which were separable from water in a magnetic field, were newly discovered draw solutes in FO [27]. Hydrophilic polymers can exhibit specific properties in water as tested in biomedical applications and thus be used to modify the surface of magnetic nanoparticles to induce high osmotic pressures [28-31]. It was found that the functionalized surfaces of magnetic nanoparticles have high affinity with water molecules and the smaller nanoparticles exhibit the better performance in FO. The recovery of 50 ml magnetic nanoparticle draw solution could be processed in 30 min via a magnetic separator (HGMS, model L-1CN, Frantz canister separator, from S. G. Frantz Co., Inc.

Trenton, NJ) at a power of 187 W, 110V & 1.7A. However, magnetic fields were unable to fully capture the smaller nanoparticles because the magnetic force was not dominant among diffusion force and gravity with decreasing particle sizes [32]. In addition, sizes of recycled magnetic nanoparticles increased due to the agglomeration in the magnetic field and the FO performances deteriorated accordingly.

Ultrasonication is widely utilized as a common tool to process nanomaterials. Besides sonication-assisted synthesis of nanoparticles, ultrasonication is also particularly useful in breaking and dispersing particle agglomerates in liquids [33, 34]. Membrane technology has proven to be an effectual and yet modest process for a variety of applications [35-39]. Considering the sizes of nanoparticle in FO, ultrafiltration (UF) is referred to as a suitable post-treatment to concentrate nanoparticle draw solutes because the pore size of UF membrane may be small enough to capture nanoparticles without creating much adverse effects compared to NF and RO, which are commonly used to intercept salts and organic chemicals. Therefore, the aim of this work is to explore the feasibility of developing a sustainable desalination process using super hydrophilic nanoparticles as draw solute in FO. To meet our objective, we conduct two novel approaches: (1) to investigate if ultrasonication can effectively restore agglomerated magnetic nanoparticles recycled by means of magnetic separators and to examine their FO performance. Magnetic nanoparticles capped with Triethylene glycol (TREG-NPs) were used in this study since TREG-NPs possess the highest saturation magnetization among other hydrophilic magnetic nanoparticles [27]. And (2) to study if integrated FO – UF processes can be

potentially used for seawater desalination and the regeneration of nanoparticle draw solutions. A commercially available HTI membrane is used as the FO membrane, through which to extract water from model seawater using super hydrophilic nanoparticle draw solution. UF membranes of different pore diameters were used and compared to achieve high recycle efficiency. Five continuous runs of desalination and nanoparticle regeneration through the FO-UF system were conducted.

4.2 Experimental

Materials

Iron (III) acetylacetonate ($Fe(acac)_3$, 99.9%), triethylene glycol (98%), and polyacrylic acid (PAA, M_w=1800, 98%) were purchased from Sigma-Aldrich. Ethanol (99%) and ethyl acetate (99%) were obtained from Tedia. NaCl (99.5%) was supplied by Merck. All the chemicals above were used as received. Uncharged neutral solutes of glucose, raffinose, PEG 400, PEG600, PEG1000 and PEG 2000 were supplied from Aldrich, USA. UF-PES-004H membrane (MWCO 4K) from Nadia, Germany; and UF membrane (MWCO 1K) from Millipore, USA were employed for nanoparticle draw solutes UF regeneration processes. The deionized (DI) water used in experiments was produced by a Milli-Q unit (Millipore, USA) with the resistivity of 18 MΩ cm.

4.2.1 Preparation and Characterization of Highly Water-Soluble Nanoparticles

Nanoparticles coated with different surface agents, polyacrylic acid and triethylene glycol, were synthesized by the thermal decomposition method. The details can be found in this thesis 2.1. The measurements of size distribution of nanoparticles were conducted by a Nanoparticle Size Analyzer (Nano ZS, ZEN3600). Nanoparticles were imaged using a Transmission Electron Microscope (TEM, JEOL: JEM-2010 model) by drying a dispersion of magnetic nanoparticles on amorphous carbon coated copper grids. The magnetic properties of functionalized magnetic nanoparticles were recorded in a vibrating sample magnetometer (VSM, LakeShore 450-10) with a saturating field of 1 T. Fourier transform infrared spectroscopy (FTIR) of magnetic nanoparticles, pressed into KBr pellets, were obtained on a Bio-Rad Spectrometer of FTS 135. The osmolality of nanoparticle draw solutions was obtained from an osmometer (3250, Advanced Instrument, USA) by measuring the solution freezing point depression, which can be converted to the osmotic pressure using the following equations [40, 41]:

$$-\ln a = \frac{\Delta H_f^0}{\mathrm{RT_f^2}}\Delta T \tag{1}$$

$$\ln a = -\frac{\pi V_w}{\mathrm{RT}} \tag{2}$$

Where a is the water activity; ΔH_f is the molar heat of water, 80 cal g^{-1}; R is the ideal gas constant; T_f is the freezing temperature of water, 273k; ΔT (k) is the freezing point

depression; π (atm) is the osmotic pressure; V_w is the molar volume of water, $1 cm^3 g^{-1}$; and T is room temperature, 298k.

4.2.2 Ultrasonication Process to agglomerated magnetic nanoparticles

Ultrasonic treatments were conducted using an ultrasonic probe with a diameter of 10mm and a 500W high-intensity ultrasonic processor (VCX500, Sonics and Materials Inc., USA). The converter was made of piezoelectric lead zirconate crystals. Solutions of agglomerated TREG-NPs in glass universal bottles were ultrasonicated in an ice water bath over different durations (30 mins & 60 mins), operating at 20 kHz. The probe was immersed in the center of the samples. After ultrasonication, TREG-NPs solutions were characterized and tested in a FO system.

4.2.3 Forward Osmosis Process Integrated With Ultrafiltration for Desalination

A forward osmosis process integrated with ultrafiltration was built on a lab-scale bench. In the FO process, the commercially available HTI membrane (Hydration Technologies Inc. previously Osmotek Inc.) was employed as the FO membrane; Both DI water and synthetic seawater (3.5% w/w sodium chloride solution) were used as feed solution . The

details of FO process can be found in this thesis 2.3. The water permeation flux (J_v, $L \cdot m^{-2} \cdot h^{-1}$, abbreviated as LMH) was calculated from the volume change of the feed solution.

$$J_v = \Delta V/(A\Delta t) \quad (3)$$

Where ΔV (L) is the permeation water collected over a predetermined time Δt (h) in the FO process duration; A is the effective membrane surface area (m^2).

The concentration of surface capping groups surrounding each nanoparticle was calculated using the formula below:

$$C = \frac{(\rho - 1000) \cdot w}{M_w} \quad (4)$$

Where C is the molar concentration of surface capping groups on magnetic nanoparticles in water (mol/L); ρ is the density of magnetic nanoparticles solution (g/L) while the water density is assumed to be 1000 g/L; w is the mass percentage of the surface capping groups upon magnetic nanoparticles obtained by TGA via weight percentage change before and after burning magnetic nanoparticles at high temperatures; M_w is the molecular weight of the surface capping groups (g/mol).

After water was extracted from the feed solution in the FO process, the diluted draw solution of super hydrophilic nanoparticles was concentrated by an ultrafiltration process, as illustrated in Figure 4.1. The flat sheet membrane module made from stainless steel was employed to house the UF membrane, with effective membrane area 9.6 cm^2 (3.5cm in diameter). A magnetic stirring bar was put inside the cell so that the effect of

concentration polarization was minimized. Two UF membranes of different molecule weight cut off (MWCO) were used for investigation of nanoparticles draw solution re-concentration. Before any experimental work, each membrane was rinsed with DI water according to the standard procedures to remove preservatives. The UF processes operated under the trans-membrane pressure of at least 5 bar and stopped when permeate water was weighted the same as water drawn in each FO process.

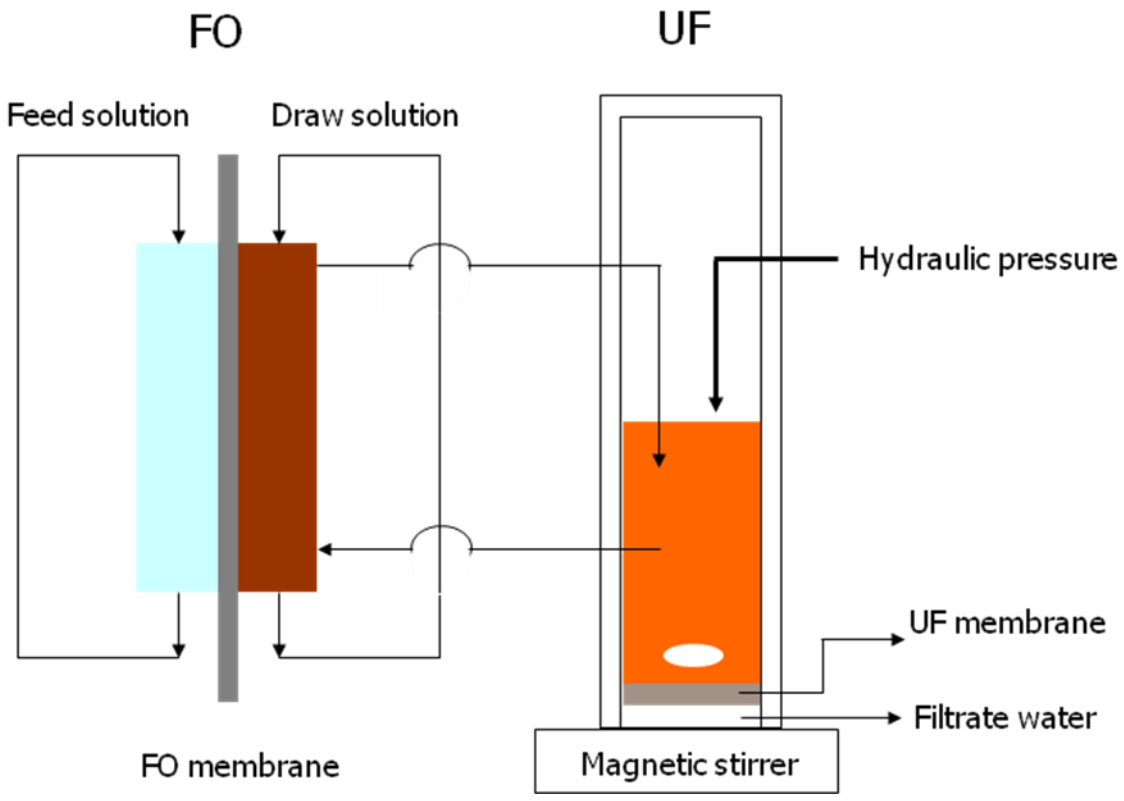

Figure 4.1 Schematic diagram of the laboratory-scale integrated FO-UF system

4.2.4 Characterization of Pore Size Distribution of UF Membranes

UF membranes were subjected to separation tests of 200 ppm solutions containing neutral solutes of different molecule weights. The concentrations of each solute in the feed solution and in the permeation were detected using a Total Organic Carbon Analyzer (TOC ASI-5000A, Shimadzu, Japan). The apparent solute separation coefficient R_E was calculated using the equation:

$$R_E = (1 - \frac{C_p}{C_f}) \times 100\% \quad (5)$$

Where C_p and C_f are the solute concentrations in permeate and feed solutions, respectively.

The relationship between the Stokes radius, r_s, nm, and the molecular weight (Mw, g/mol) of the neutral solutes used can be represented as [42]:

$$\log r_s = -1.3363 + 0.395 \log Mw \quad (6)$$

The radius, r_s, of a hypothetical solute at a given MW can be estimated using Eq. (4). The mean pore radius and the pore size distribution of the UF membranes were then obtained based on the traditional solute transport approach [43-45]. A straight line is obtained when the solute rejection, R_E, is plotted against the solute radius r_s:

$$F(R_E) = A + B(\ln r_s) \quad (7)$$

By ignoring the influences of the steric and hydrodynamic interaction between the solute and the membrane pores on the solute rejection, the mean effective pore radius, μ_p, and the geometric standard deviation, σ_p, can be assumed to be the same as μ_s (the geometric

mean radius of the solute at R_E = 50%) and σ_s (the geometric standard deviation defined as the ratio of the r_s at R_E = 84.13% over that at R_E = 50%). The pore size distribution of membrane can be expressed as the following probability density function [44]:

$$\frac{dR_E}{dr_p} = \frac{1}{r_p \ln \sigma_p \sqrt{2\pi}} \exp\left[-\frac{\left(\ln r_p - \ln \mu_p\right)^2}{2\left(\ln \sigma_p\right)^2} \right] \tag{8}$$

4.3 Results and Discussion

4.3.1 Nanoparticles Characterization

Nanoparticles prepared in this work followed the procedure in our precious study [27]. For the FO-magnetic separation system, TREG-NPs were synthesized around 20 nm in diameter to meet the required particle size range of recovery by the magnetic separator. For the FO-UF system, PAA-NPs were synthesized around 5 nm in diameter so that larger surface-area-to-volume ratio of nanoparticles provides more sites for polyacrylic acid to anchor on, which can induce a higher osmotic pressure and therefore enhance the performance of desalination process. TEM images in Figure 4.2a show that the particle size is approximately 5 nm in diameter. The lattices in Figure 4.2b correspond to a group of atomic planes within the particle, indicating that the particle is a single crystal [46].

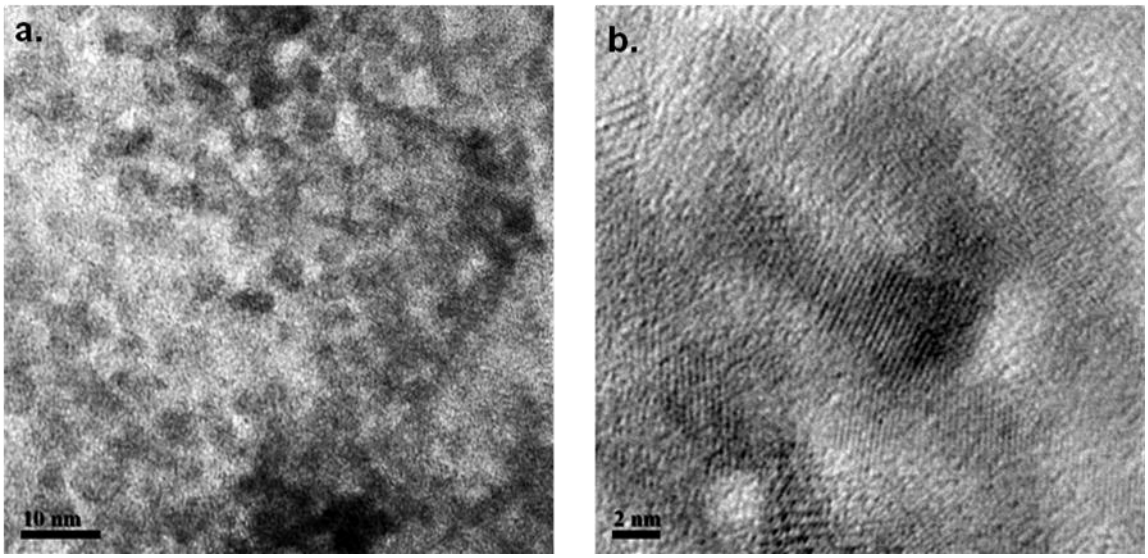

Figure 4.2 TEM images of regenerated PAA-NPs.

4.3.2 Evaluation of Ultrasonication to Agglomerated Magnetic Nanoparticles

Fresh TREG-NPs were very stable and showed no precipitation in water for months. However, after TREG-NPs is used as draw solutes in the FO system and then recycled by a magnetic separator, their particle sizes tend to increase due to the agglomeration as shown in Figure 4.3a. Ultrasonication of TREG-NPs aims to break agglomerates, increase surface area and recover their FO performance. Size distributions of TREG-NPs in Figure 3a show that after ultrasonication, the average diameter of TREG-NPs can be reduced from 58 nm, 48nm to 40 nm. Figure 4.3b compares FTIR spectra of the original; agglomerated and ultrasonicated TREG-NPs under different time durations. No obvious changes of absorption were observed. Clearly, ultrasonication seems to be an effectively method to lower magnetic nanoparticle sizes without modifying the surface chemistry.

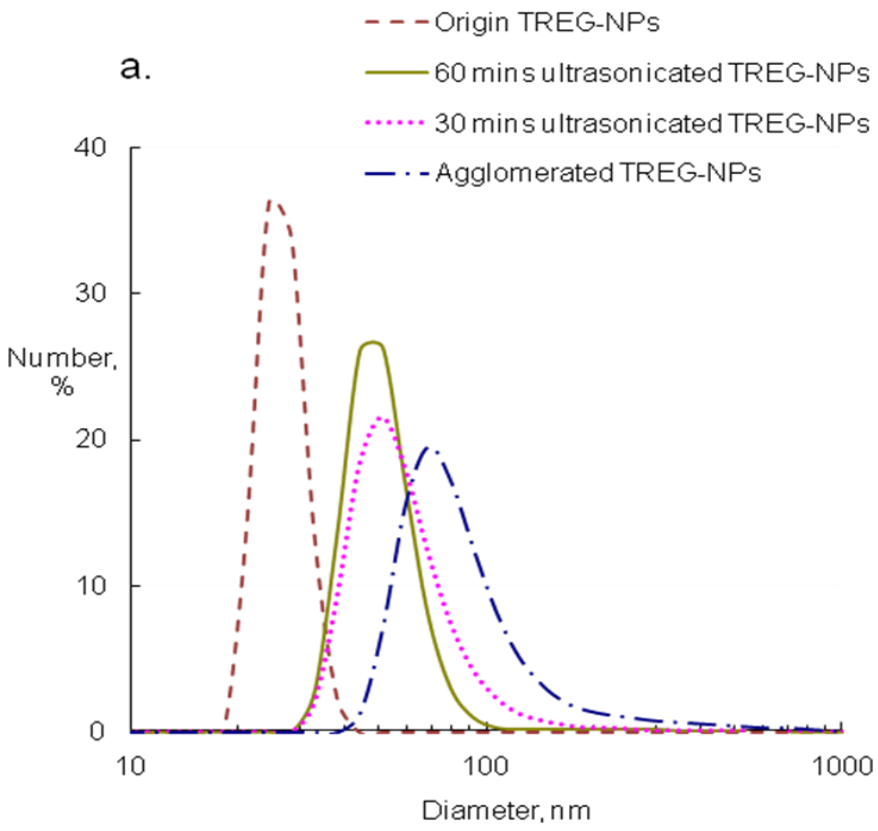
a.
Origin TREG-NPs
60 mins ultrasonicated TREG-NPs
30 mins ultrasonicated TREG-NPs
Agglomerated TREG-NPs
40
30
20
10
0
Number, %
10
100
1000
Diameter, nm

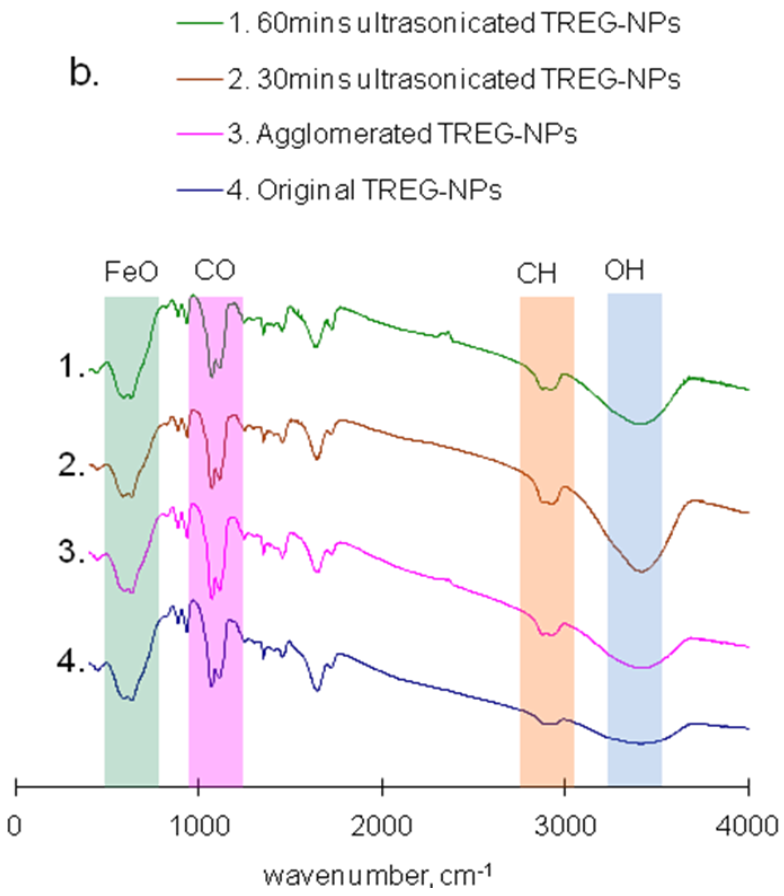

Figure 4.3 Size distributions (a) and FTIR spectra (b) of TRGE-NPs

Figure 4.4a illustrates the magnetic properties of TREG-NPs before and after ultrasonication. Magnetization of a material is derived from dividing its magnetic moments directly measured in VSM by the sample mass. Saturation magnetization indicates the maximum possible magnetization the material can exhibit in the magnetic field. The saturation magnetization of agglomerated TREG-NPs almost doubles the value of the original TREG-NPs. This is attributed to the fact that saturation magnetization is proportional to particle size [47]. However, it is surprising to note that ultrasonicated

TREG-NPs of much bigger diameters exhibit even lower saturation magnetization than the original TREG-NPs, which is contradictory to the usual size-dependent property. For magnetic nanomaterials, the saturation magnetization is a function of chemical composition and particle size. Larger particles possess a higher saturation magnetization with the same composition. Magnetite Fe_3O_4 possesses a higher inherent saturation magnetization than hematite Fe_3O_4. It is believed that more Fe_2O_3 were converted from Fe_3O_4 as the composition of magnetic nanoparticle core during the ultrasonication processes, resulting in the decreased saturation magnetization. The intensity of the ultrasonication process accelerates the oxidization of the nanoparticle core from Fe_3O_4 to Fe_2O. Nevertheless, improvements in water flux in FO tests are obtained with ultrasonicated TREG-NPs because of small particle sizes, as depicted in Figure 4.4b. If we want to match the water flux of the original TREG-NPs, ultrasonication operation must be operated with a longer time and higher intensity to break agglomerates into smaller particles. By doing so, the magnetic property of TREG-NPs will deteriorate and lower the recovery efficiency of nanoparticles by means of the current magnetic separators. Hence, ultrasonication may not be the ideal method to restore agglomerated magnetic nanoparticle draw solutes in FO processes. Alternative method for nanoparticle draw solute regeneration shall be explored.

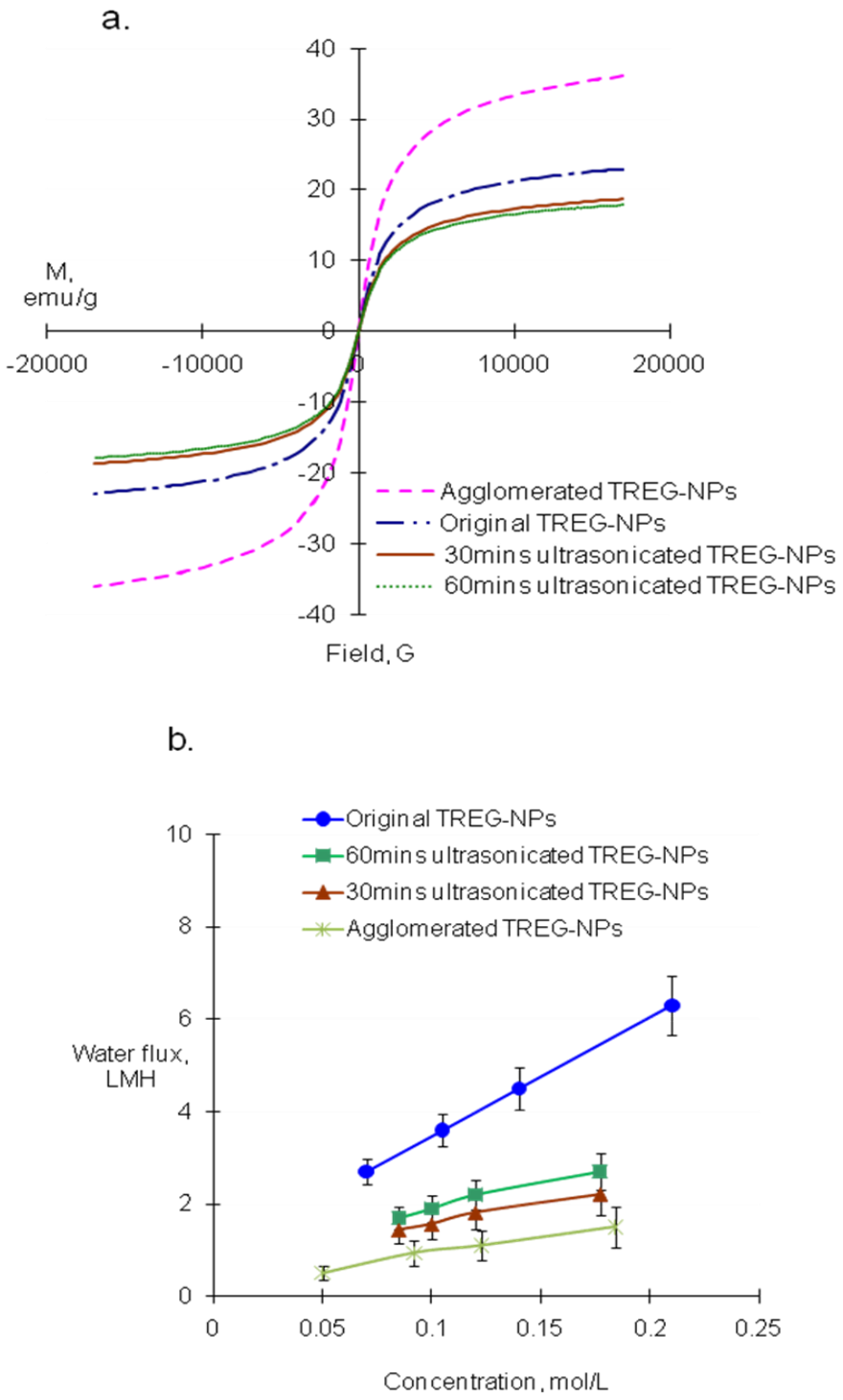

Figure 4.4 Hysteresis loops (a) and water flux (b) of TREG-NPs

4.3.3 Integrated FO-UF System using Super Hydrophilic Nanoparticles as Draw Solutes

Inorganic salts and organic compounds can easily induce high osmotic pressures but their recovery via RO or heat is relatively energy intensive. It is difficult for nanoparticles to generate high osmotic pressure owing to their large size compared to salts or organic molecules. Nevertheless, one of the superiorities of hydrophilic nanoparticles is their extremely high surface-area-to-volume ratio that minimizes drawback of large particle sizes. In addition, the snag of big size may become positive for their recovery because they can be caught easily by magnetic and electrical fields, ultrafiltration, or other means.

Following our previous work [27], PAA-NPs of high osmotic pressures were employed in this work as draw solutes to investigate the integrated FO – UF process for water reuse and seawater desalination. The initial draw solution of PAA-NPs, with a concentration of PAA on nanoparticles surface 0.08mol/L, possessed an osmotic pressure of around 70 atm, which was much higher than the model seawater of 26 atm (3.5% w/w sodium chloride solution). Two types of UF membranes were studied; namely, MWCO 1K and 4K. Figure 4.5a shows that the osmotic pressure of PAA-NPs draw solution as a function of the number of regeneration through different UF membranes, after which PAA-NPs were recycled to FO process using DI water as the feed solution, as illustrated in Figure 4.1. The osmotic pressure of the recycled PAA-NPs solution decreases much severer with UF membranes with a MWCO value of 4K than those with 1K. This phenomenon arises from the fact that PAA-NPs with smaller diameters than the pore size of UF membranes

of MWCO 4K may pass through the membrane pores together with the filtrate water, which leads to the loss of draw solutes and thus decreases the effective osmotic pressure. Figure 4.6a.confirms our hypothesis and shows the sizes of leaked nanoparitcles in each run are around 1 nm. As a result, water flux of the regenerated nanoparticle draw solution tested in the PRO mode (i.e., the draw solution against the dense selective layer of the FO membrane) decreases with the number of recycle, as shown in Figure 4.5b.

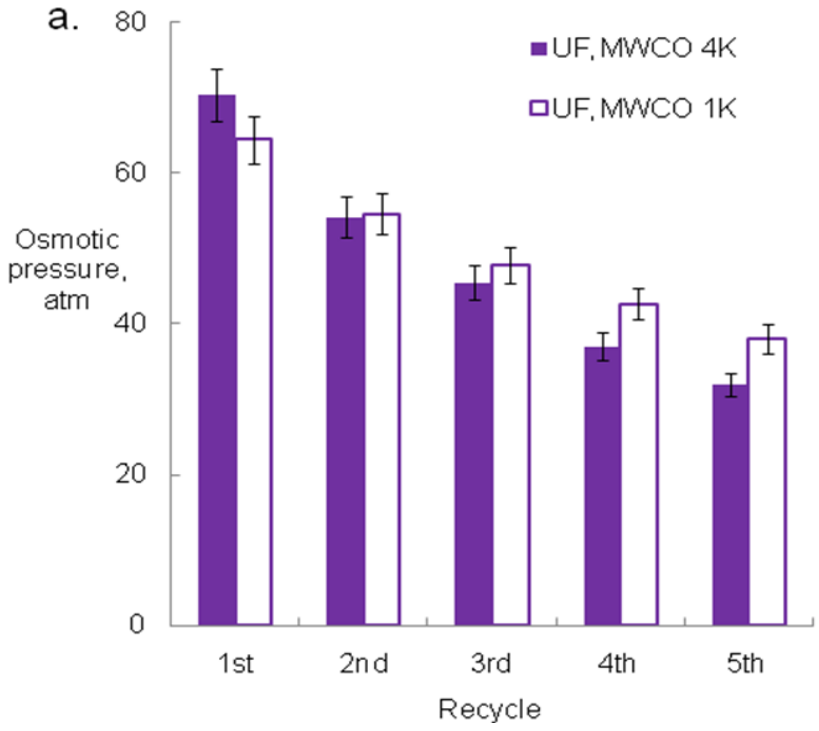

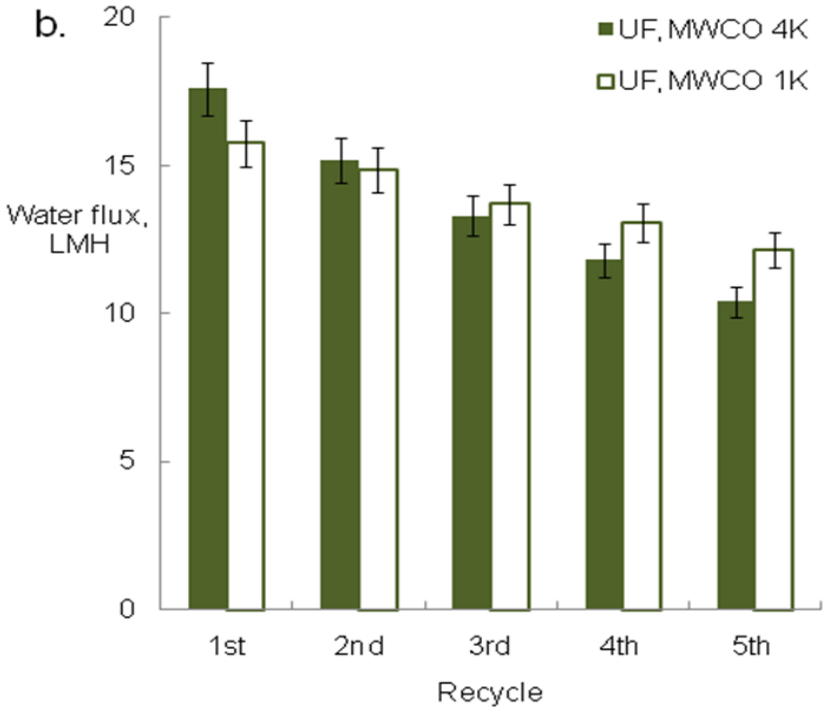

Figure 4.5 Osmotic pressure (a) and water flux of FO process (b) comparisons of PAA-NPs draw solutions regenerated by UF membranes (MWCO 1K & 4K), DI water as feed solution in FO, PRO mode

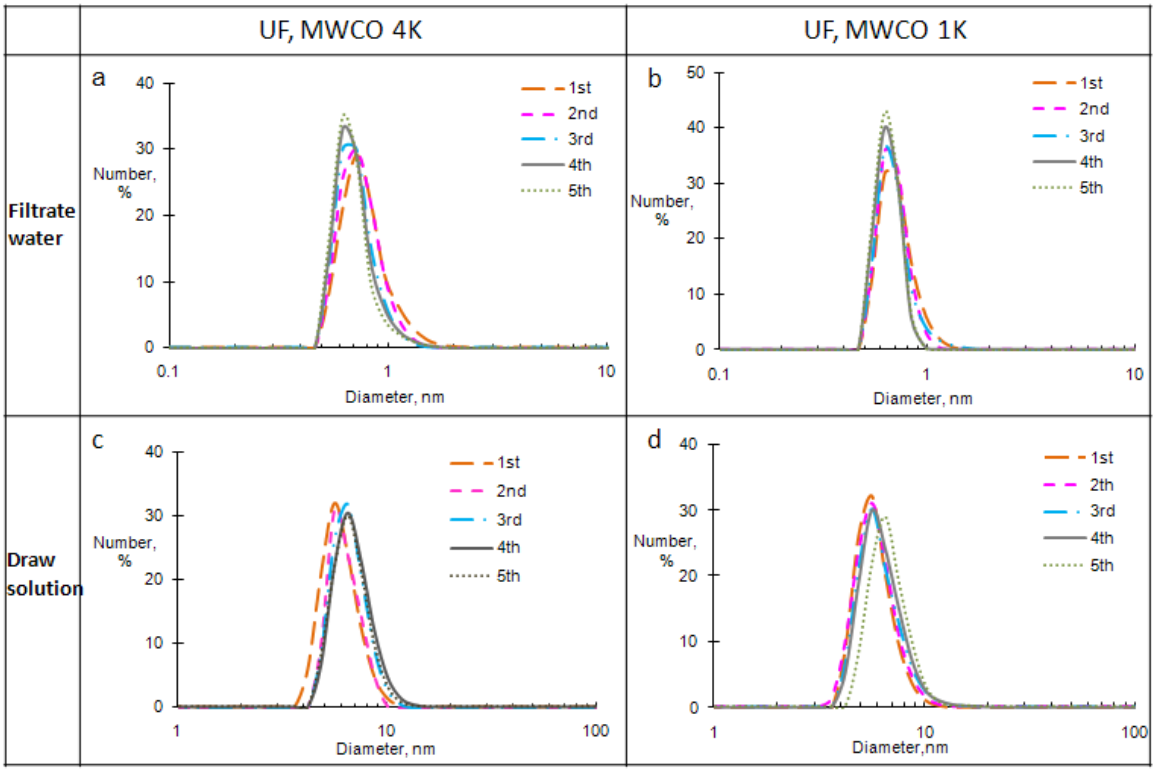

Figure 4.6 Size distributions of PAA-NPs in draw solutions and filtrate water

The UF process of nanoparticles can be complicated due to the concentration polarization and the potential formation of a cake layer on membrane surface, which are governed by interparticle electrostatic double layer interactions and hydrodynamic filtration conditions [48-49]. In this work, the nanoparticles are particularly small and exhibit extreme hydrophilicity in water, thus the effect of concentration polarization plays an important role in flux declination [48-49]. A magnetic stirrer bar was therefore placed above the UF membrane and it was vigorously stirred to eliminate the possible particles accumulation on membrane surface. The water flux across the UF membrane during the regeneration of the nanoparticle solution was about 0.42 LMH/bar.

On the other hand, UF membranes of smaller pore diameter (MWCO 1K) show much better performance in terms of osmotic pressure (Figure 4.5a) and water flux (Figure 4.5b). The pore diameters of UF membranes (MWCO 1K & 4K) were therefore characterized to give a comprehensive elucidation of membrane structure. Figure 4.7a, b & c illustrate their rejections, cumulative pore size distributions, and probability density functions. The mean pore diameters are about 1 nm and 1.5 nm for UF membranes (MWCO 1K & 4K), respectively. These pore size values are consistent with the observation of leaked nanoparticle sizes in filtrate water, as displayed in Figure 4.6a and 6b. The filtrate water has more nanoparticles larger than 1 nm when using UF membranes of MWCO 4K than MWCO 1K. In addition, the UF membrane of MWCO 1K regenerates draw solutions with more uniform nanoparticle sizes. The evident improvement of water flux decline demonstrates that UF membranes (MWCO 1K) can potentially retain PAA-NPs draw solutes during recovery processes. Since the nanoparticle size is in the range of 1-10 nm, the UF membrane exhibits different rejections to the nanoparticles of different sizes. For UF membranes of MWCO 4K & 1K, the rejections were about 90.5 % and 92.7%. A high rejection more than 98-99% can be obtained if a UF membrane of tighter pore size is used and the data will be revealed in future. The amount of nanoparticles adsorbed on the UF membrane is trivial compared to the nanoparticles in the draw solution even though it may contribute to a minor loss of nanoparticles.

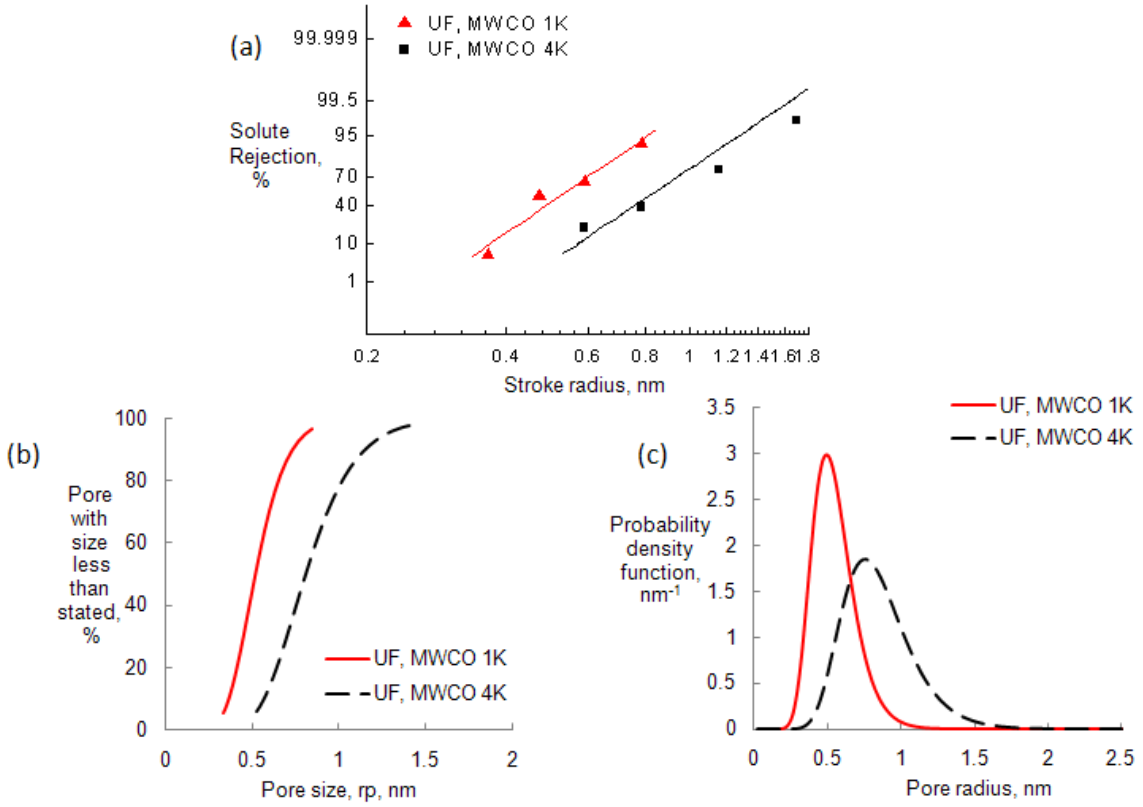

Figure 4.7 (a) Solute rejection plotted on the log-normal probability co-ordinate system, (b) cumulative pore size distribution curves, and (c) pore size distribution density curves

Images of product water through the FO-UF process using different UF membranes (MWCO 1K & 4K) are presented in Figure 4.8. The filtrate water through UF membranes of MWCO 4K is quite dark due to the existence of leaked nanoparticles. In order to reduce the amount of leaked nanoparticles in filtrate water and improve the water quality, two stage UF processes using the membrane of MWCO 4K were conducted. As seen in Figure 4.8c, the color of this filtrate water is much clearer with fewer nanoparticles in

water. However, a more clear and transparent water vision can be obtained by the UF recovery process using membranes of MWCO 1K, as displayed in Figure 4.8d. For the purpose of portable water use, designing nanoparticles with a narrow size distribution or employing a NF or other integrated filtration process are essential to facilitate the removal of residual nanoparticles in the water. The energy to regenerate NPs through the UF step may take a certain percentage in the overall energy consumption. However, compared to RO to regenerate draw solute, its energy consumption is expected considerably lowered in terms of the pressures applied. The improvement of water flux in UF processes can effectively reduce the system energy consumption, which redeems FO-UF more economically favorable.

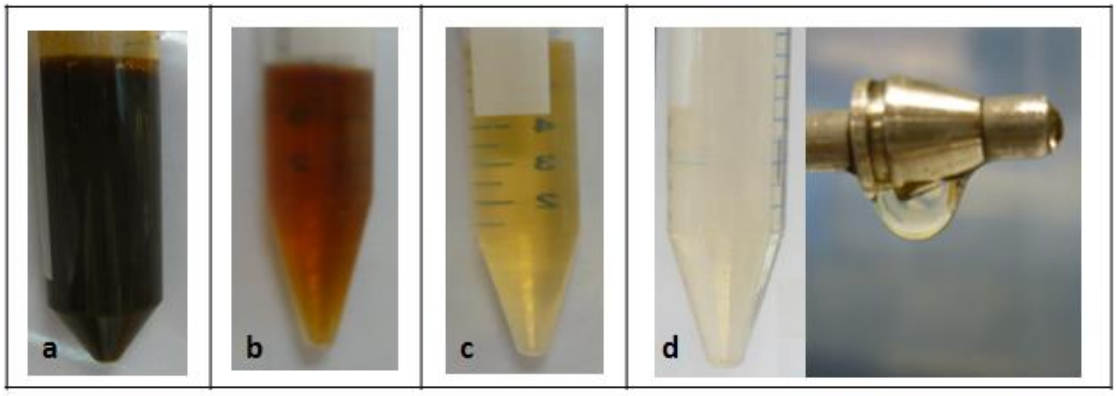

Figure 4.8 Images of PAA-NPs draw solutions and filtrate water. a. Draw solute; b. Filtrate water by UF, MWCO 4K, one stage; c. Filtrate water by UF, MWCO 4K, two stages; d. Filtrate water by UF, MWCO1K, one stage

Size distributions of PAA-NPs regenerated by UF processes using membranes (MWCO 1K & 4K) were also measured in each recycle and shown in Figure 4.6c & 6d. There was

no much change of particle sizes even after 5 runs, which confirmed the integrity of nanoparticle draw solutes and the full extension of hydrophilic groups on nanoparticle surface contacting with water sufficiently.

4.3.4 Desalination Process of Integrated FO-UF System with Super Hydrophilic Nanoparticles

The integrated FO-UF system with the aid of super hydrophilic nanoparticles as draw solute was tested for desalination, using a UF membrane of MWCO 1K in the UF process and synthetic seawater (3.5% w/w sodium chloride solution) as the feed solution in the FO process. Figure 4.9 compares the overall FO performance using DI water and seawater as feed solutions in both PRO mode and FO mode (the draw solution against the porous layer). The water fluxes in the PRO mode are higher than that in the FO mode for both DI water and seawater as feed solutions, due to the effect of internal concentration polarization [4]. Super hydrophilic nanoparticle draw solution itself possesses high osmotic pressure, thereby extracting water from synthetic seawater. For each recycle, water from the feed solution is fully recovered through the novel FO-UF process. The salt (NaCl) content in the finish water through FO-UF is dependent on the salt rejection of FO membrane. In the current system, the salt (NaCl) content in finish water was about 0.12g/L by measuring its conductivity without interference from the nanoparticle draw solutes.

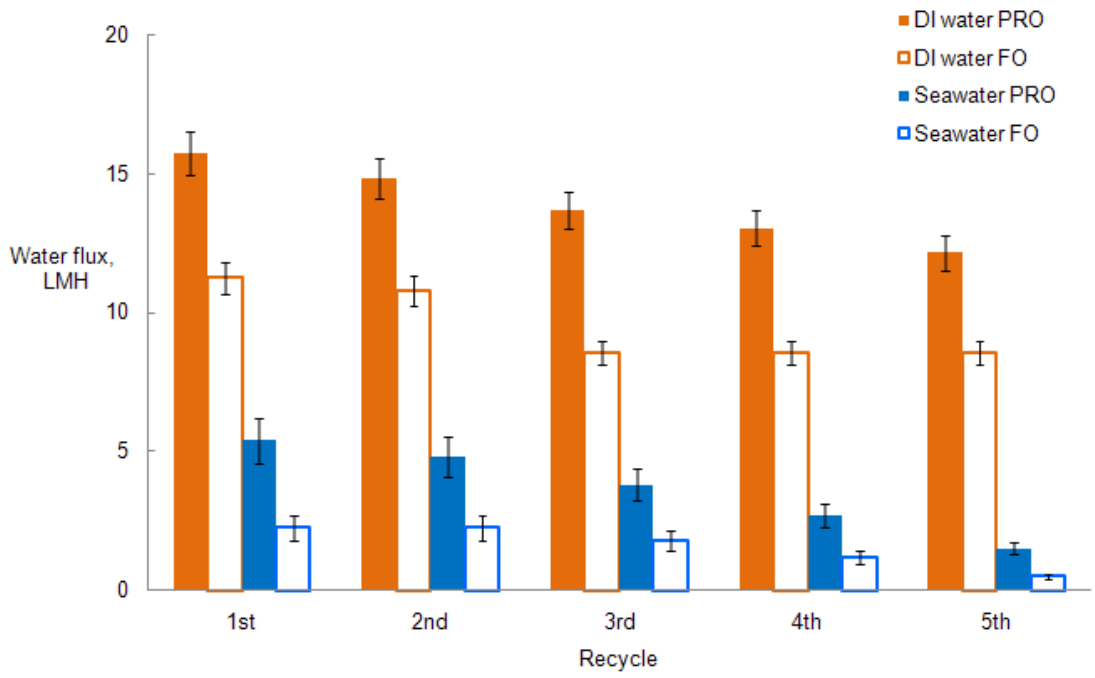

Figure 4.9 FO performance using PAA-NPs as draw solutes, DI water and model seawater as feed solution

Figure 4.10 shows the normalized water flux of regenerated PAA-NPs draw solutions by means of UF membrane MWCO 1K against DI water and model seawater as the feed solutions. The normalized water flux is defined as water flux divided by the concentration of surface functional groups on nanoparticles. It is important to note that the normalized water flux is almost constant, which indicates that the water flux drop in each run is mainly ascribed to the concentration decrease caused by the loss of smaller PAA-NPs draw solutes leaking through UF membranes. In other words, the FO performance is sustainable in the FO-UF system if the leaked PAA-NPs draw solutes can

be reduced or recycled and the basic osmotic characteristics of the PAA-NPs draw solutes remain the same after 5 recycle runs.

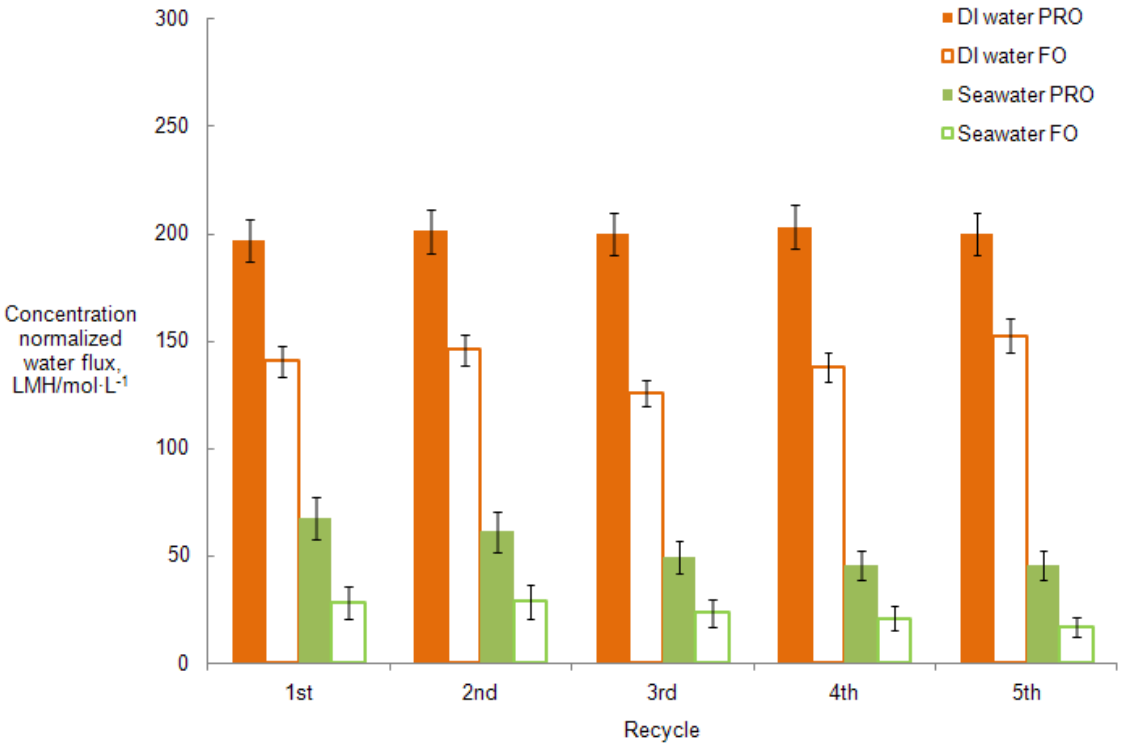

Figure 4.10 Normalized water flux comparison of PAA-NPs draw solutions, DI water and model seawater as feed solution in FO.

4.4 Conclusion

We have conceptually demonstrated, for the first time, a potentially sustainable integrated FO-UF system for water reuse and desalination with super hydrophilic nanoparticles as draw solutes. Experimental results indicate that the agglomeration of magnetic nanoparticles recovered by magnetic fields can be solved by ultrasonication, but the magnetic properties of nanoparticles may deteriorate. The integrated FO-UF process may

be better than the FO-magnetic separation process when using super hydrophilic nanoparticles as draw solutes. A novel FO-UF process has been demonstrated and investigated. PAA-NPs draw solutions can be recycled in FO-UF for 5 times to desalinate synthetic seawater without increasing their sizes or reducing its osmotic functionality. UF membranes of small pore diameter and narrow pore size distribution are preferred to enhance recovery efficiency of nanoparticle draw solution. Our future work will aim to further design and engineer the nanoparticle draw solutes with high osmotic pressures and narrow particle distributions in order to improve the FO performance especially in desalination and make the draw solutes more compatible in the FO-UF system to achieve higher recovery efficiency. In addition, integrated systems to produce pure water and together with the energy/economic analyses will be investigated. It is believed the proposed FO-UF integrated system using super hydrophilic nanoparticles as draw solutes is a promising technology to desalinate both seawater and brackish water and to reclaim water from wastewater.

4.5 References

1. T.S. Chung, S. Zhang, K.Y. Wang, J.C. Su, M.M. Ling, Forward osmosis processes: Yesterday, today and tomorrow, Desalination, doi:10.1016/j.desal.2010.12.019

2. B.X. Mi, M. Elimelech, Chemical and physical aspects of organic fouling of forward osmosis membranes, J. Membr. Sci. 320(2008)292.

3. B.X. Mi, M. Elimelech, Gypsum scaling and cleaning in forward osmosis: measurementsand mechanisms, Environ. Sci. Technol. 44 (2010) 2022.

4. L. Robert, M. Elimelech, Global challenges in energy and water supply: the promise of engineered osmosis. Environ. Sci. Tech., 42(2008) 8625.

5. J.R. McChtcheon, R.L. McGinnis, M. Elimelech, A novel ammonia--carbon dioxide forward (direct) osmosis desalination process. Desalination, 174(2005)1.

6. Q. C. Ge, J.C. Su, T.S. Chung, G. Amy, Hydrophilic superparamagnetic nanoparticles: synthesis, characterization, and performance in forward osmosis processes. Ind. Eng. Chem. Res. 50(2011) 382.

7. J.C. Su, Q. Yang, J.F. Teo, T.S. Chung, Cellulose acetate nanofiltration hollow fiber membranes for forward osmosis processes. J. Membr. Sci. 355(2010)36.

8. N. Y. Yip, A. Tiraferri, W. A. Phillip, J. D. Schiffman, M. Elimelech, High performance thin-film composite forward osmosis membrane, Environ. Sci. Tech., 44(2010)3812.

9. N. Y. Yip, A. Tiraferri, W. A. Phillip, L. A. Hoover, J. D. Schiffman, Y. C. Kim, M. Elimelech, Thin-film composite pressure retarded osmosis membranes for sustainable power generation from salinity gradients, . Environ. Sci. Tech., in press

10. K. L. Lee, R.W. Baker, H.K. Lonsdale, Membranes for power generation by pressure-retarded osmosis. J. Membr. Sci. 8(1981)141.

11. R.J. Aaberg, Osmotic power: A new and powerful renewable energy source? Refocus, 4(200) 48.

12. S.E. Skilhagen, J.E. Dugstad, R.J. Aaberg, Osmotic power—power production based on the osmotic pressure difference between waters with varying salt gradients. Desalination, 220(2008) 476.

13. K.B. Petrotos, P.C.Quantick, H. Petroparkis, Direct osmotic concentration of tomato juice in tubular membrane – module configuration. II. The effect of using clarified tomato juice on the process performance. J. Membr. Sci. 160(1999)171.

14. Q. Yang, K.Y. Wang, T.S. Chung, A novel dual-layer forward osmosis membrane for protein enrichment and concentration. Sep. Purif. Technol. 69(2009)269.

15. S.S. Madaeni, A. Khodabahkshi, Dehydration of alcohols using osmotic concentration-dehydration of aqueous glycerol solution. J. Food Eng. 86(2008)49.

16. R.L. McGinnis, M. Elimelech, Energy requirements of ammoinia-carbon dioxide forward osmosis desalination. Desalination, 207(2007)370.

17. J. Herron, Asymmetric forward osmosis membranes, World Intellectual Property Organization, WO 2006/110497.

18. K.Y. Wang, T.S. Chung, J.J. Qin, Polybenzimidazole (PBI) nanofiltration hollow fiber membranes applied in forward osmosis process. J. Membr. Sci. 300(2007)6.

19. Q. Yang, K.Y. Wang, T.S. Chung, Dual-layer hollow fibers with enhanced flux as novel forward osmosis membranes for water reuses and protein enrichment. US Patent, WO 2010/045430.

20. T. Thorsen, T. Holt, Semi-permeable membrane for use in osmosis, and method and plant for providing elevated pressure by osmosis to create power. US Patent 7,566,402.

21. K.Y.Wang, R.C. Ong, Double-selectivel forward osmosis membranes for the elimination of internal concentration polarization within the porous sublayer. Ind. Eng. Chem. Res. 49(2010)4824.

22. S. Zhang, K.Y. Wang, T.S. Chung, H.M. Chen, Y.C. Jean, G. Amy, Well-constructed cellulose acetate membranes for forward osmosis: minimized internal concentration polarization with an ultra-thin selective layer. J. Membr. Sci. 360(2010)522.

23. G.W. Batchelder, Process for the demineralization of water, US Patent, 3,117,799 (1965)

24. B.S. Frank, Desalination of sea water, US Patent 3,670, 897 (1972)

25. J.O.Kessler, C.D. Moody, Drinking water from sea water by forward osmosis. Desalination, 18(1976)297.

26. J.R. McChtcheon, R.L. McGinnis, M. Elimelech, A novel ammonia--carbon dioxide forward (direct) osmosis desalination process. Desalination, 174(2005)1.

27. M.M. Ling, K.Y. Wang, T.S. Chung, Highly water-soluble magnetic nanoparticles as novel draw solutes in forward osmosis for water reuse. Ind. Eng. Chem. Res. 49(2010)5869.

28. Q. Zhang, S.X. Cheng, X.Z.nZhang, R.X. Zhuo, Water-soluble Polymer Protected Lipofectamine 2000/DNA Complexes for Solid-Phase Transfection. Macromolecular Bioscience. 9(2009)1262.

29. L. Zhang, C.H. Hu, S. X. Cheng, R.X. Zhuo, Hyperbranched amphiphilic polymer with folate mediated targeting property, Colloids Surf., B, 79(2010) 427.

30. X.Z. Zhang, D.Q. Wu, G.M. Sun, C.C. Chu, Novel biodegradable and thermalsensitive Dex-AI/PNIPAAm hydrogel, Macromol Biosci, 3(2003) 87.

31. Z.M. Miao, S.X. Cheng, X.Z. Zhang, R.X. Zhuo, Study on drug release behaviors of poly-α,β-[N-(2-hydroxyethyl)-L-aspartamide]-g-poly(ε-caprolactone) nano- and microparticles, Biomacromolecules, 7(2006)2020.

32. G.D. Moeser, K.A. Roach, W.H. Green, T.A. Hatton, High-gradient magnetic separation of coated magnetic nanoparticles. AIChE.50 (2004)2835.

33. http://www.hielscher.com/ultrasonics/nano_01.htm

34. E.S.K. Tang, M. Huang, L.Y. Lim, Ultrasonication of chitosan and chiosan nanoparticles. Int J Pharm. 265(2003)103.

35. Y. Wang, S.H. Goh, T.S. Chung, N. Peng, Polyamide-imide/polyetherimide dual-layer hollow fiber membranes for pervaporation dehydration of C1–C4 alcohols. J. Membr. Sci. 326(2009)222.

36. J. Xu, D. Bhattacharyya, Membrane-based bimetallic nanoparticles for environmental remediation: Synthesis and reactive properties, Environ. Prog. 24(2005)358.

37. D.E. Meyer, D. Bhattacharyya, Impact of membrane immobilization on particle formation and trichloroethylene dechlorination for bimetallic Fe/Ni nanoparticles in cellulose acetate membranes, J. Phys. Chem. B. 111(2007)7142.

38. S. Lewis, V. Smuleac, A. Montague, L. Bachas, D. Bhattacharyya, Iron-Functionalized Membranes for Nanoparticle Synthesis and Reactions. Sep. Sci. Technol. 44(2009)3289.

39 R. Hausman, B. Digman, I.C. Escobar, M. Coleman, T.S. Chung, Functionalization of polybenzimidizole membranes to impart negative charge and hydrophilicity, J. Membr. Sci. 363(2010)195.

40. R.H. Boyd, P.J. Phillips, The science of polymer molecules. Combridge University Press, 1996

41. P.R. Bergethon, The physical basis of biochemistry: the foundations of molecular. Springer, 2010

42. W.R. Bowen, A.W. Mohamad, Characterization and prediction of nanofiltration membrane performance-a general assessment. Trans. IChemE: Part A. 76(1998)885.

43. A.S. Michaels, Analysis and prediction of sieving curves for ultrafiltration membrane: a universal correclation. Sep. Sci. Technol. 15(1980)1305.

44. K.H. Youm, W.S. Kim, Prediction of intrinsic pore properties of ultrafiltration membrane by solute rejectioni curves-effects of operating conditions on pore properties. J. Chem. Eng. Jpn. 24(1991)1.

45. S. Singh, K.C. Khulbe, T. Matsuura, P. Ramamurthy, Membrane characterization by solute transport and atomic force microscopy. J. Membr. Sci. 142(1998)111.

46. S.H. Sun, H. Zeng, D.B. Robinson, G.X. Li, Monodisperse MFe2O4 (M=Fe, Co, Mn) nanoparticles. J. AM. CHEM. SOC. 126(2004)273.

47. H.M. Lu, W.T. Zheng, Q. Jiang, Saturation magnetization of ferromagnetic and ferrimagnetic nanocrystals at room temperature. J. Phys. D: Appl. Phys. 40(2007)320.

48. R.S. Faibish, M. Elimelech, Y. Cohen, Effect of Interparticle electrostatic double layer interactions on permeate flux decline in crossflow membrane filtration of colloidal suspensions: an experimental investigation, J. Colloid Interface Sci., 204(1998)77.

49. M. Elimelech, S. Bhattacharjee, A novel approach for modeling concentration polarization in crossflow membrane filtration based on the equivalence of osmotic pressure model and filtration theory, J. Membr. Sci. 145 (1998) 223.

CHAPTER 5

NOVEL DUAL-STAGE FORWARD OSMOSIS SYSTEM FOR SUSTAINABLE ENRICHEMENT USING NANOPARTICLES AS INTERMEDIATE DRAW SOLUTE

5.1 Introduction

Proteins, as the most important biopolymer in nature, have a wide range of commercial applications in nutraceutical, medical and pharmaceutical markets [1]. The global protein market is booming with a solid growth rate and expected worth of 77 billion by 2011 [2]. The production of proteins with high resolution and high productivity has been considered as technically and economically challenging [3]. In protein production, the process of protein enrichment plays an important role and is companied with protein separations. Most proteins are labile and heat sensitive, athermal separations are preferred. Therefore, searching for innovative athermal enrichment processes provides strong incentives for protein industries because not only can it protect protein quality but also lower the production cost [3]. In addition, proteins have gradually expanded their applications as sensors for the analyses of complicated biological samples in modern analytic instruments. There is a market demand for high purity proteins [4].

Membrane technologies have received attention as alternative protein enrichment processes in the last decade. In addition to separating proteins based on their sizes, membranes have the advantage of conducting separation without the addition of chemicals or heat that may denature proteins [5-10]. Among the current membrane technologies, ultrafiltration (UF) prevails in concentrating protein solutions, especially in food processing, with advantages of minimal protein denatured and well preserved microfactions [3,11]. Water and smaller molecules are permeated out through UF membranes under pressures; proteins are retained and thereby concentrated. However, the retentate protein can easily cause membrane fouling and decrease the output. Backwash and membrane replacement are commonly used to maintain the high production, which increase the production cost and prolong the production cycle.

Forward Osmosis (FO), as an emerging technology to alleviate global water shortage in the coming decennia, is now intensely studied by researchers [12-22]. In FO, the osmotic pressure difference across the semi-permeable membrane acts as the driving force to extract water from the solution of the higher chemical potential to the lower, which is molecularly triggered without any external help. Traditionally, a hydraulic pressure is necessarily applied in nearly all other membrane processes to force water and other permeates through the membrane. Comparing to pressure-driven membrane separation processes, FO is unique by utilizing osmotic pressure gradients as the driving force with

potentially lower energy consumption and less membrane fouling propensity, which makes the osmotically driven FO process more economically favorable.

With the advances in FO technology, a batch protein enrichment process has been conceptually demonstrated in a single FO system using magnesium chloride as the draw solute in our group [8]. To further expand batch FO technologies to a continuous mode, the choice of draw solution as well as its regeneration and disposal can be an issue, considering the economic and environmental impacts. A self sustainable FO process must be developed with easily recyclable draw solutions without causing protein denature. In principle, using small molecules, salts and electrolytes as draw solutes for protein dehydration may be achievable but not be economic and practical. One may have difficulties of recovering these draw solutes as well as preventing the leakage of these solutes across the FO membrane to denature proteins, in addition to inducing clogging in the supporting layer and resulting in severe fouling and internal concentration polarization.

In this work, it is to demonstrate, for the first time, a self-sustainable dual-stage FO system for protein enrichment using (1) highly hydrophilic nanoparticles as draw solute to concentrate protein solutions in the up-stage FO, and (2) reverse osmosis (RO) retentate of RO plants as the draw solute to re-concentrate nanoparticle solutions in the down-stage FO, operated in a continuous mode. Highly hydrophilic nanoparticles capped

with polyacrylic acid (PAA-NPs) were chosen as draw solutes in this work for the protein enrichment because of their high osmotic pressure; and they could be recycled by either magnetic field [23-24] or ultrafiltration process [25]. Moreover, their reverse flux (i.e., back diffusion to the protein solution) is minimal as they are too large to pass FO membrane pores [23]. Protein molecules are sensitive to ionic strengths in solutions. Their conformation and stability could be influenced thereby [26-27]. Hence, using nanoparticles as draw solute can greatly lower the risk of denaturing proteins during the enrichment process.

In the down-stage FO, a RO retentate was employed to regenerate hydrophilic nanoparticle solution because the sodium chloride retentate emitted from RO plants possesses extremely high osmotic pressures. A 14 wt% NaCl solution, assuming 75% recovery from the RO process of seawater (3.5% NaCl solution), was used as the model RO retentate in this work. The RO retentate solution has an osmotic pressure of 90 atm that can effectively dehydrate the diluting PAA-NPs solution and renew the osmotic driving force of the PAA-NPs draw solution for continuous protein enrichment. Besides, it would be a waste if it is discharged by drilling underground or piping into seawater [28]. The reuse of RO retentate may be a better strategy to solve or avert disposal problem. Utilizing the FO process to recover the PAA-NPs intermediate draw solution is facile and spontaneous; likewise it is more energy-efficient in contrast with the ordinary nanoparticle regeneration methods, such as magnetic separation and ultrafiltration.

To explore the universal applicability of the newly proposed dual-stage FO process for protein enrichments, 3 types of proteins with different molecular weights, charge characteristics and interactions with membrane surfaces were tested. The fundamental science and process engineering of the integrated dual-stage FO system were also investigated. It is believed that this dual-stage FO system will have significant contributions to future protein enrichment and other chemical and pharmaceutical processes in the years to come.

5.2 Experimental

Materials:

Iron (III) acetylacetonate ($Fe(acac)_3$, 99.9%), triethylene glycol (98%), and polyacrylic acid (PAA, M_w=1800, 98%) were purchased from Sigma-Aldrich. Ethanol (99%) and ethyl acetate (99%) were obtained from Tedia. NaCl (99.5%) was supplied by Merck. Uncharged neutral solutes of glycerol, glucose, saccharose and raffinose were supplied from Aldrich, USA. Molecular weights, diffusivities and Stokes radii of neutral solute were referred to from [16]. Bovine Serum Album (BSA), Lysozyme (LYZ) and Soybean Trypsin Inhibitor (STI) were supplied by Sigma-Aldrich. All the chemicals above were used as received. The commercially available HTI FO membrane (Batch No. 090128-NW-1; Hydration Technologies Inc. previously Osmotek Inc.) was employed in FO systems. The deionized (DI) water used in experiments was produced by a Milli-Q unit (Millipore, USA) with the resistivity of 18 MΩ cm.

5.2.1 Preparation of Highly Hydrophilic Nanoparticle Draw Solutes

Highly hydrophilic nanoparticles of 6 nm in diameter were synthesized by the thermal decomposition method in the presence of Iron (III) acetylacetonate, using polyacrylic acid as capping agent and triethylene glycol as solvent. The synthesized PAA-NPs have proven to be very hydrophilic and super stable in water. Dialysis of PAA-NPs solution against DI water was conducted for 48 hours to remove any impurities prior to application. Size distribution of nanoparticles was measured by a Nanoparticle Size Analyzer (Nano ZS, ZEN3600). The detailed synthetic procedures and other characterizations can be found in this thesis 2.1 & 2.2. The osmolality of nanoparticle draw solutions was obtained from an osmometer (3250, Advanced Instrument, USA) by measuring the solution freezing point depression, which can be converted to the osmotic pressure .

5.2.2 Characterization of Pore Size Distribution of FO Membranes

The FO membrane was subjected to separation tests of 200 ppm solutions containing neutral solutes of different molecule weights. The concentrations of each solute in the feed solution and in the permeation were detected using a Total Organic Carbon Analyzer (TOC ASI-5000A, Shimadzu, Japan). The apparent solute separation coefficient R_E was calculated using the equation:

$$R_E = (1 - \frac{C_p}{C_f}) \times 100\% \quad (1)$$

Where C_p and C_f are the solute concentrations in permeate and feed solutions, respectively. The relationship between the Stokes radius, r_s, nm, and the molecular weight (Mw, g/mol) of the neutral solutes including glycerol, glucose, saccharose or raffinose can be represented as [31]:

$$\log r_s = -1.3363 + 0.395 \log Mw \quad (2)$$

The radius, r_s, of a hypothetical solute at a given Mw can be estimated using Eq. (4). The mean pore radius and the pore size distribution of the membrane were then obtained based on the traditional solute transport approach [31-34]. By ignoring the influences of the steric and hydrodynamic interaction between the solute and the membrane pores on the solute rejection, the mean effective pore radius, μ_p, and the geometric standard deviation, σ_p, can be assumed to be the same as μ_s (the geometric mean radius of the solute at R_E = 50%) and σ_s (the geometric standard deviation defined as the ratio of the r_s at R_E = 84.13% over that at R_E = 50%). The pore size distribution of the membrane can be expressed as the following probability density function [33]:

$$\frac{dR_E}{dr_p} = \frac{1}{r_p \ln \sigma_p \sqrt{2\pi}} \exp\left[-\frac{(\ln r_p - \ln \mu_p)^2}{2(\ln \sigma_p)^2} \right] \quad (3)$$

5.2.3 Forward Osmosis based on the HTI FO Membrane

FO experiments were carried out on a lab-scale circulating filtration unit, as depicted in this thesis 2.3. NaCl solutions of different concentrations and DI water were employed as draw and feed solutions, respectively. The velocities of both draw and feed solutions were maintained at 12.8 cm/s through permeation cell with rectangular channels (8.0 cm in length, 1.0 cm in width and 0.25 cm in height). The temperatures of the FO system were kept at 22 ± 0.5ºC. The water permeation flux (J_v, $L \cdot m^{-2} \cdot hr^{-1}$, abbreviated as LMH) was calculated from the volume change of feed solution.

$$J_v = \frac{\Delta V}{A \cdot \Delta t} \qquad (4)$$

where ΔV (L) is the permeation water collected over a predetermined time Δt (hr) in the FO process duration; A is the effective membrane surface area (m^2).

The salt leakage (i.e., reverse diffusion) of NaCl draw solution was deduced from the increase of conductivity of the feed, using a calibration curve for the NaCl solution. The salt reverse diffusion flux (J_s in $gm^{-2}\ h^{-1}$, abbreviated as gMH) was therefore calculated as below:

$$J_s = \frac{C_t \cdot V_t}{A \cdot \Delta t} \qquad (5)$$

where C_t and V_t are the salt concentration and the volume of the feed in the end of FO tests, respectively.

5.2.4 Protein Enrichment via Dual-Stage FO system

The experimental set-up of the overall protein enrichment process consists of two interconnecting FO subsystems, as shown in Figure 5.1. In the up-stage FO process, the protein solution was set as the feed; and the water within was automatically extracted by the PAA-NPs draw solution in the other side of the membrane. In the down-stage FO process, the PAA-NPs solution was referred to as the feed, while the model RO retentate was used as the draw solution. In a continuous operation mode, the PAA-NPs solution was circulated along two FO permeation cells, applied as feed and draw solutions, separately. The water drawn from the protein solution was expected to accumulate in the downstream RO retentate solution ultimately. An ultraviolet (UV) visible spectrophotometer (BIOCHROM LIBRA S32) with a kinetic function was introduced to indicate the protein enrichment trend. The absorbance of 280 nm wavelength was measured for all protein solutions to record the protein concentration profile on-line.

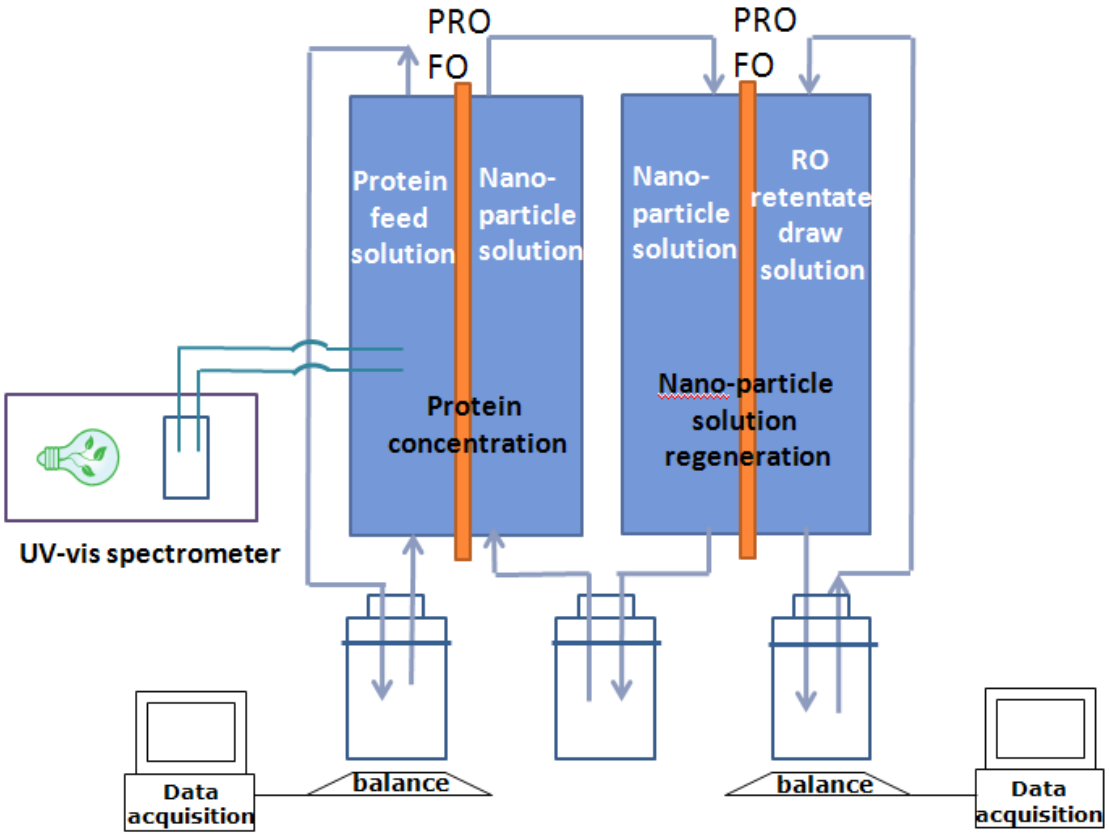

Figure 5.1 Schematic diagram of the laboratory-scale dual FO system for protein enrichment

The structure of proteins in experiments was investigated by both SDS-gel electrophoresis (Biorad vertical gel electrophoresis) and Circular Dichroism (CD) spectra. In CD measurements, the protein conformational change was quantified with α-helix content as estimated below [26].

$$\%\alpha - Helix content = \frac{\theta_{mrd}^{208} - 4000}{33000 - 4000} \qquad (6)$$

where θ_{mrd}^{208} ($\circ$ cm^2/dmol) is the mean molar ellipticity per residue at a wavelength of 208 nm. The enrichment percentage is defined as the ratio of protein concentration enriched during the process, $(C_t - C_0)$, to the initial feed protein concentration C_0.

5.3 Results and Discussion

5.3.1 Protein Enrichment in the Dual FO System

Figure 5.2 displays the FO performance of a single-stage FO system consisting of HTI FO membranes, DI water and NaCl as feed and draw solutions, respectively. The pressure retarded osmosis (PRO) mode is defined when the draw solution faces against the dense layer, while the forward osmosis (FO) mode is when the draw solution faces against the porous layer. It shows that the PRO mode has a higher water flux than the FO mode. However, the reverse salt leakage into the feed solution exists for both operation modes because salt molecules cannot be perfectly rejected by the FO membrane. Therefore, in the case of using salts as draw solute to enrich protein solutions, the protein structure cannot be kept intact because of the inevitable salt leakage that alters protein intrinsic characteristics. Figure 5.3 shows a comparison between pore size distribution of the HTI FO membrane and diameter distribution of PAA-NPs used in this work. The average pore diameter of the HTI FO membrane is about 0.5 nm, which is in the same scale as H_2O and NaCl molecules, but significantly smaller than the PAA-NPs diameter.

As a result, PAA-NPs cannot diffuse into the protein solution and denature proteins. This phenomenon will be discussed in the late section.

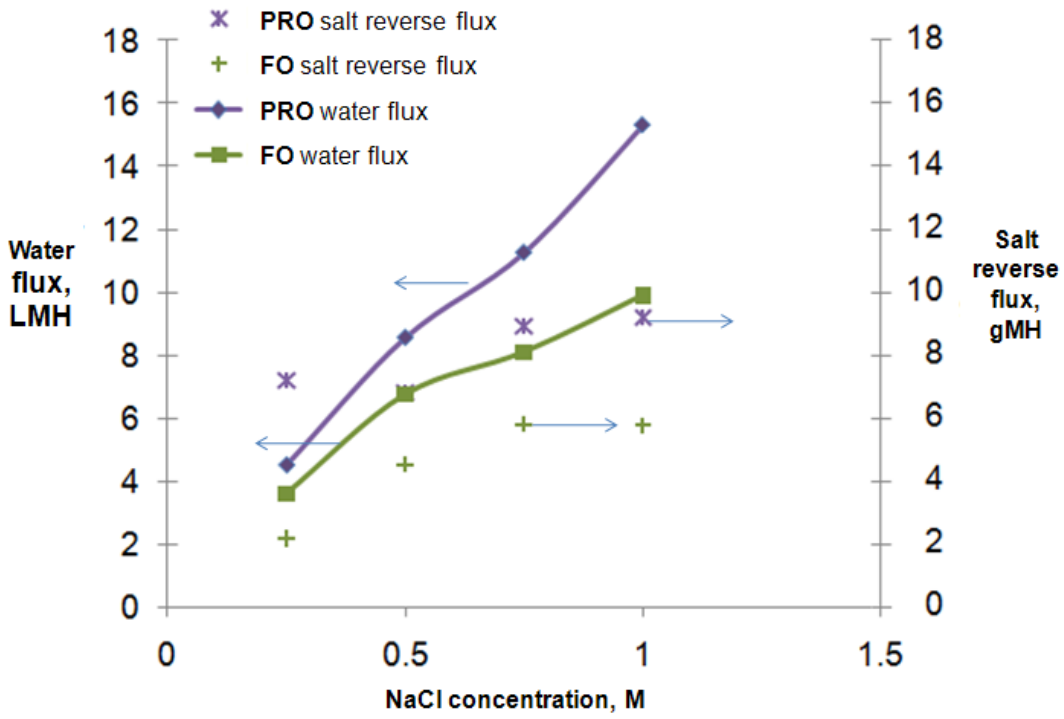

Figure 5.2 Water flux and salt flux of HTI FO memebrane, using NaCl as draw solute

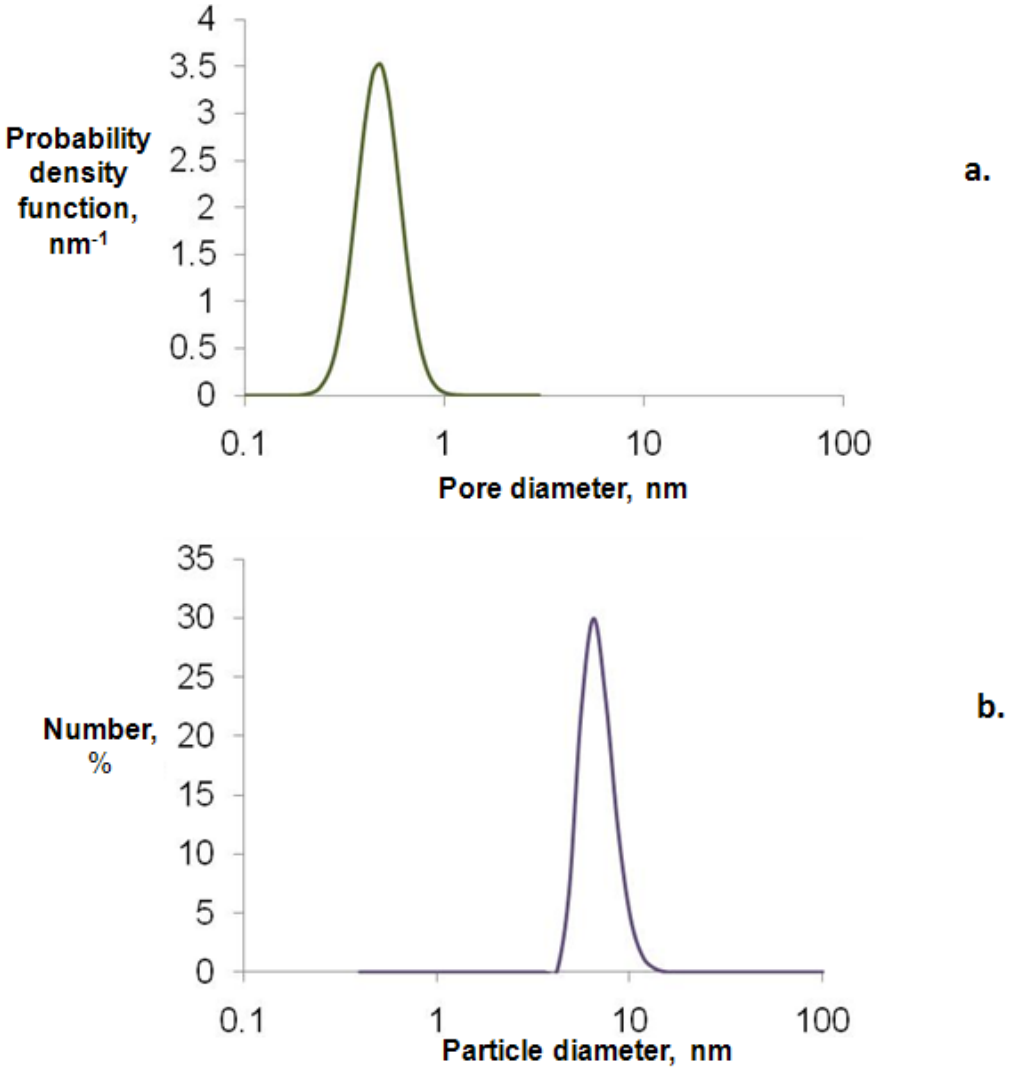

Figure 5.3 a. pore size distribution of HTI FO membrane; b. diameter distribution of PAA-NPs

BSA dissolved in DI water was studied as the model protein solution. The pH value of solution was not further adjusted since PI value of BSA was around 4.9. To investigate protein enrichment via FO, both single- and dual-stage FO processes were conducted. In the single-stage FO, both RO retentate and PAA-NPs were used to concentrate BSA

solutions, while in the dual-stage FO, 4 different operation modes; namely, PRO PRO, PRO FO, FO PRO and FO FO were carried out. Figure 5.4 compares the BSA concentration as a function of operation modes in both single- and dual-stage FO processes. The highest BSA concentration is achieved using RO retentate as the draw solution in the single-stage FO. Since the PAA-NPs draw solution has a lower osmotic pressure compared to the model RO retentate, it extracts less water from BSA solutions and results in lower BSA concentrations during the enrichment. However, with the aid of RO retentate in the down-stage FO, the dual-stage FO has better protein enrichment than the single-stage FO using PAA-NPs as the draw solute.

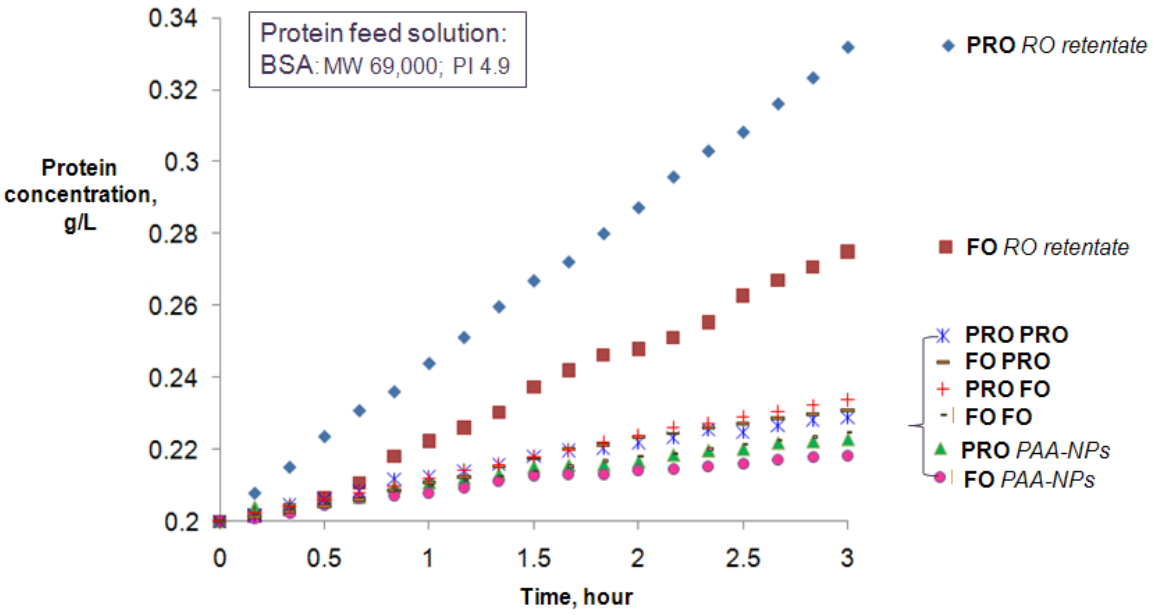

Figure 5.4 Kinetics of protein enrichment in single and dual FO systems

Gel track of all the BSA solutions were performed to assess the integrity of protein before and after enrichment. As displayed in Figure 5.5, no changes were found between the original and the concentrated BSA in solutions, which implies FO causes no protein precipitations. BSA conformational structure was further tested via CD measurements. As exhibited in Figure 5.6, CD spectra reveal that there is a considerable detour between the original BSA and the BSA concentrated by the RO retentate, which indicates that the structure of BSA enriched by the RO retentate has been changed. In the contrary, for BSA concentrated by the PAA-NPs solution in both single and dual-stage FO, no obvious changes were observed compared to the original BSA, which verifies that the BSA was kept intact. From CD spectra analyses shown in Table 5.1, it is also found that using PAA-NPs as draw solutes to enrich BSA results in a slight loss of the alpha-helix content and thus the BSA structures have been well preserved. On the other hand, the secondary structure of BSA is severely damaged using RO retentate as the draw solute. The comparison of salt reverse flux in Figure 5.7 elucidates the causes for BSA structural changes. The high salt reverse flux from the RO retentate solution could result in a large amount of NaCl dwelling in the BSA feed solution and therefore affect the protein conformational stability. A more moderate solution environment can be provided using PAA-NPs as intermediate draw solutes in the dual-stage FO with a much lower salt reverse flux.

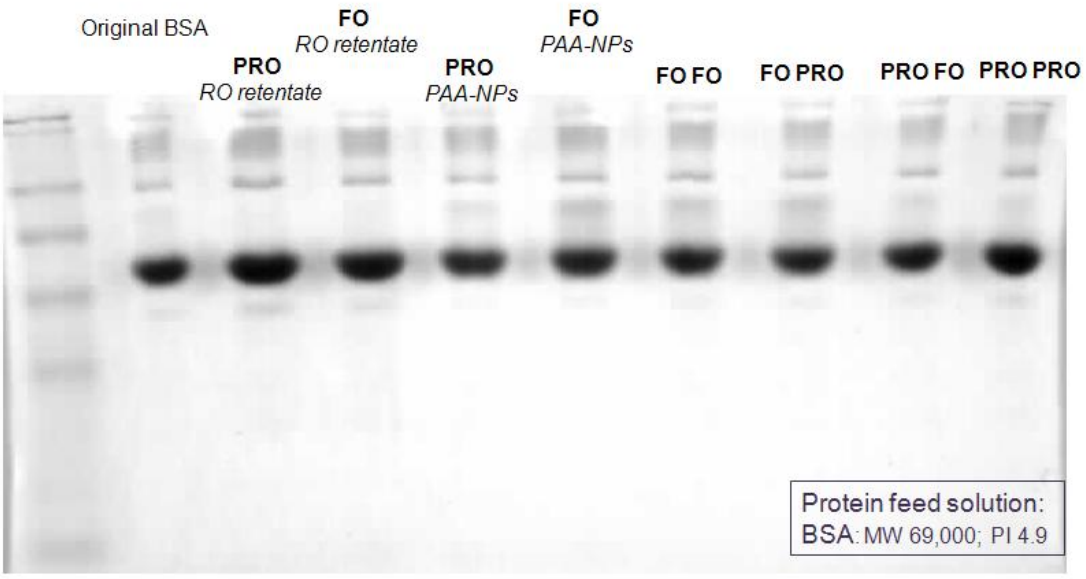

Figure 5.5 Gel track of BSA of original and concentrated

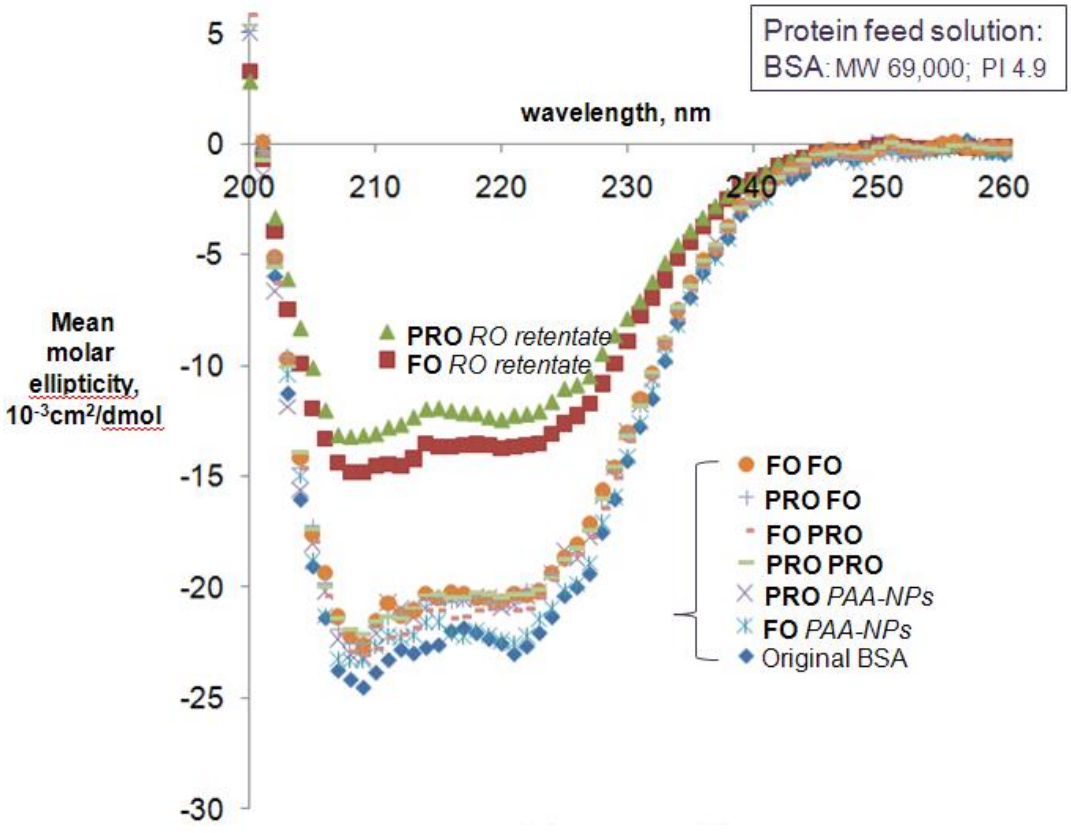

Figure 5.6 CD spectra of BSA of original and concentrated

		% α-Helix
Single FO System	Original BSA	69.7%
	PRO *RO retentate*	31.7%
	FO *RO retentate*	37.4%
	PRO *PAA-NPs*	65.6%
	FO *PAA-NPs*	66.6%
Dual FO System	**PRO PRO**	61.7%
	PRO FO	64.1%
	FO PRO	62.9%
	FO FO	65.3%

Table 5.1 Secondary structure of original BSA and concentrated BSA

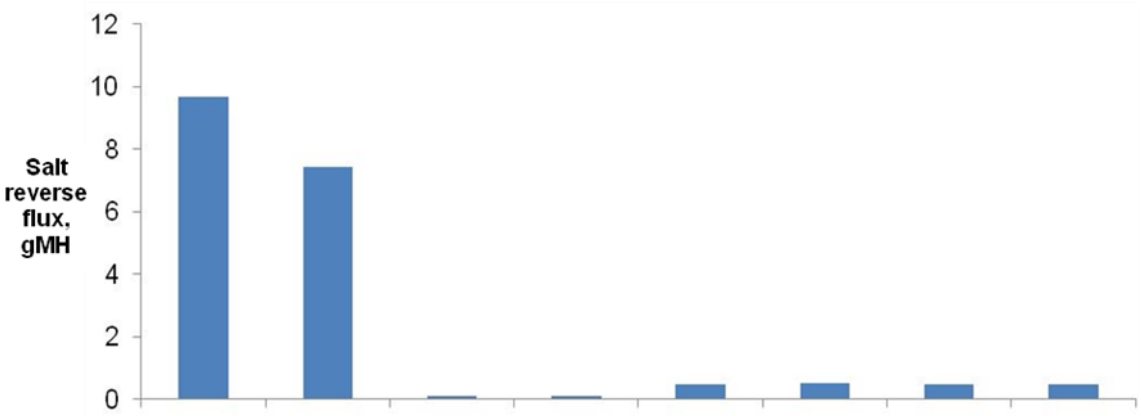

Figure 5.7 Salt flux of single and dual FO system during protein enrichment

The enlarged concentration profiles of BSA enriched by PAA-NPs in both single and dual-stage FO are presented in Figure 5.8. The concentrations of BSA generally increase linearly with operation time in the dual-stage FO, while the enrichment gradually slows down in the single-stage FO. This is due to the fact that the osmotic driving force of draw solution is reduced in the single-stage FO system as the concentration of draw solute is diluted with water accumulated. In the dual-stage FO, the RO retentate draw solution in the down-stage regenerates the PAA-NPs solution onsite so that the osmotic driving force of nanoparticle draw solution is maintained with an almost constant concentration. Therefore, BSA could be enriched steadily in the dual-stage FO systems with a stable osmotic driving force.

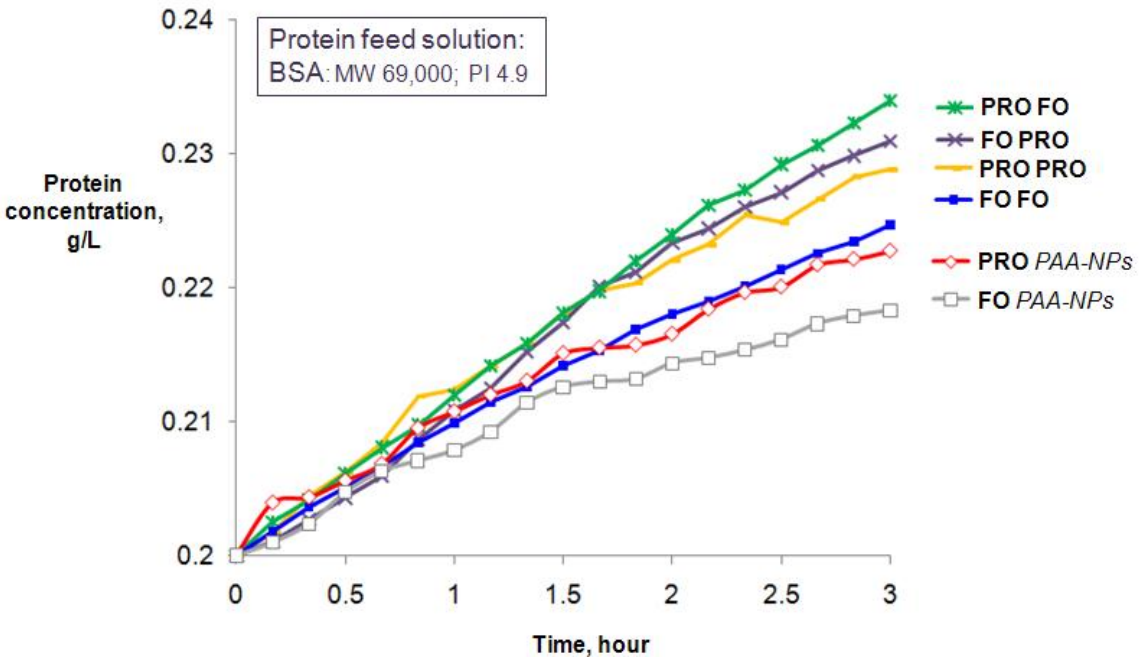

Figure 5.8 Comparison of enlarged kinetics using PAA-NPs in single and dual FO systems

5.3.2 Size Effect in Protein Enrichment via Dual-Stage FO System

Protein STI and BSA were applied in the dual-stage FO system respectively to study the protein size effect during the enrichment. STI and BSA possess similar isoelectric point (PI) values (STI, 4.5; BSA, 4.9) but very different molecular weights and sizes (STI, MW 21,500, and radius 1.9nm; BSA, MW 69,000, and radius 3.2nm). With the same initial mass concentration of 0.2g/L of either protein, much more numbers of STI molecules could be located in the solution per unit volume; thus a higher osmotic pressure of the STI feed solution could be generated. The osmotic pressures of protein feed solutions are practically low and undetectable by the osmometer (3250, Advanced Instrument, USA).

In order to exaggerate the impact of different protein sizes through the enrichment, a PAA-NPs solution of a relatively low osmotic pressure 6 atm was set here as the intermediate draw solution. Figure 5.9 shows a comparison of enrichment performance. Clearly, the dual-stage FO is applicable for both proteins. However, BSA feed solutions can be enriched faster than STI feed solutions in all operations modes. In addition to their difference in osmotic pressure, another possible reason for better enrichment performance of BSA than STI is that, smaller STI molecules could be more easily stuck in membrane pores and decrease water flow, thus resulting in lower enrichment efficiency.

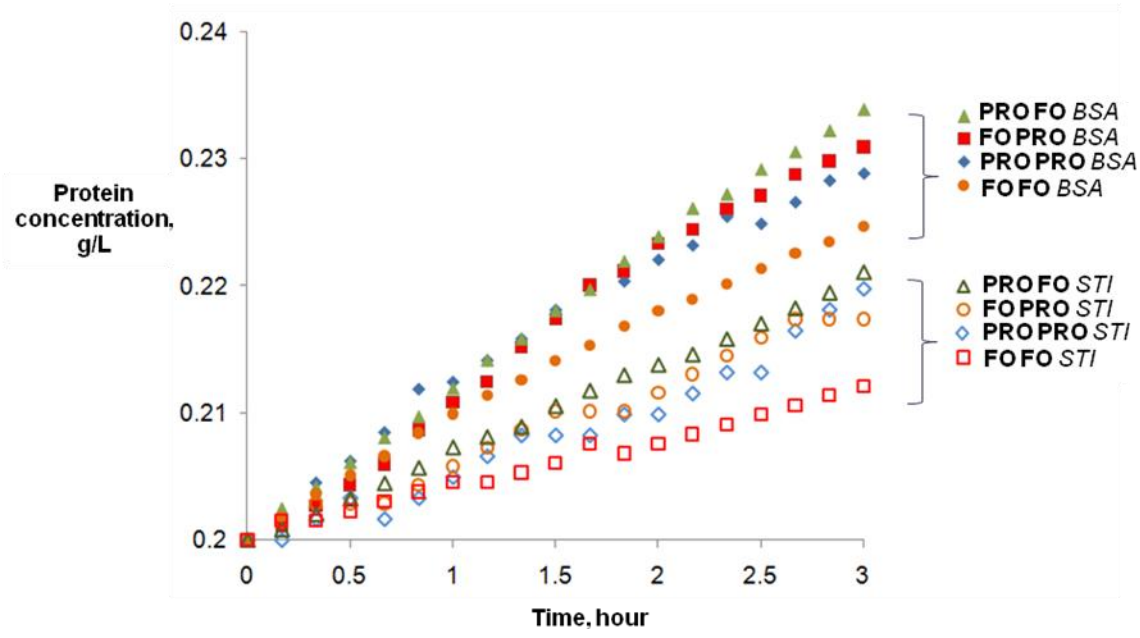

Figure 5.9 Comparison of protein enrichment kinetics for proteins of different sizes

5.3.3 Charge Effect in Protein Enrichment via Dual-stage FO System

To study charge effects of proteins and their interactions with FO membranes in the dual-stage FO system, proteins STI and LYZ of completely opposite charges in DI water but with similar molecular weights (STI, PI 4.5, negatively charged in water, MW 21,500; LYZ, PI 11, positively charged in water, MW 18,000) were selected to compare. BSA was not chosen to compare together with LYZ and STI, because BSA possesses very similar charge characteristics as STI and also a much larger size than both STI and LYZ. Figure 5.10 shows the concentration kinetics of proteins. The concentration of STI is a little higher than LYZ in feed solutions after 3-hour enrichment. However, the LYZ concentration of the PRO FO mode increases faster than the STI concentration of the same mode in the beginning but levels off after 1.5-2 hour test. Many factors affect the transit and overall enrichment process. The HTI FO membrane applied in this work is made of cellulose triacetate (CTA) and possesses slightly negatively charge on surface. As depicted in Figure 5.11a, an exclusive repulsion could be generated between negatively charged STI molecules and membrane surface, which could alleviate the chances of STI fouling on the CTA membrane surface. For LYZ of positive charge in water, the phenomenon of membrane fouling could be aggravated since LYZ molecules were more likely to attach on the CTA membrane surface with the electrostatic attraction in between, as illustrated in Figure 5.11b. The resultant fouling would retard water transport through membrane pores and thus decline the enrichment performance as compared to STI.

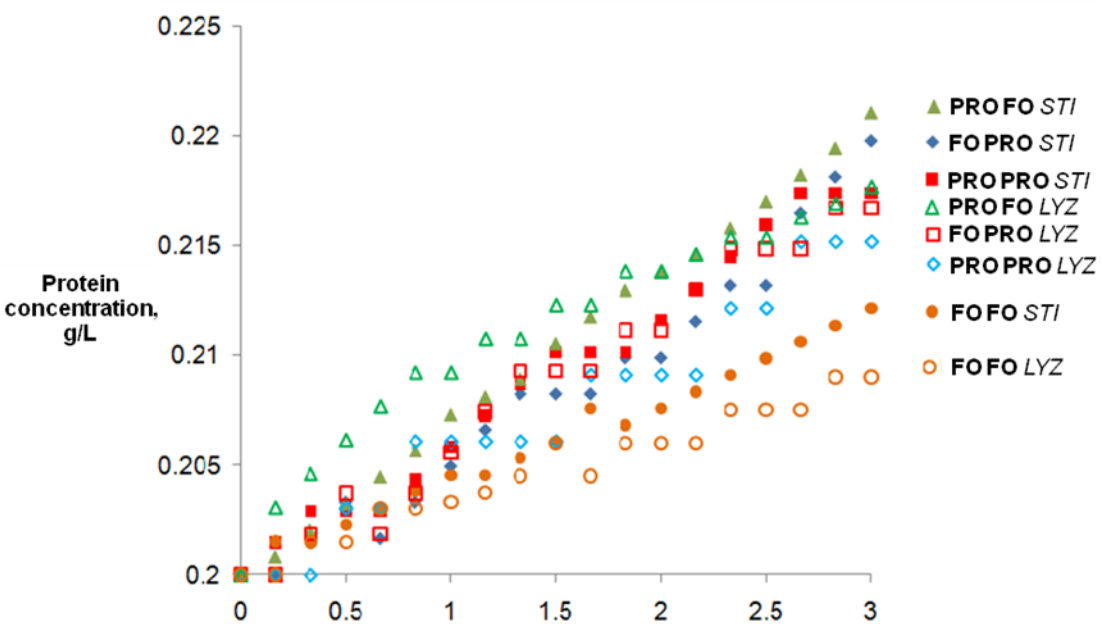

Figure 5.10 Comparison of protein enrichment kinetics for proteins of different charges

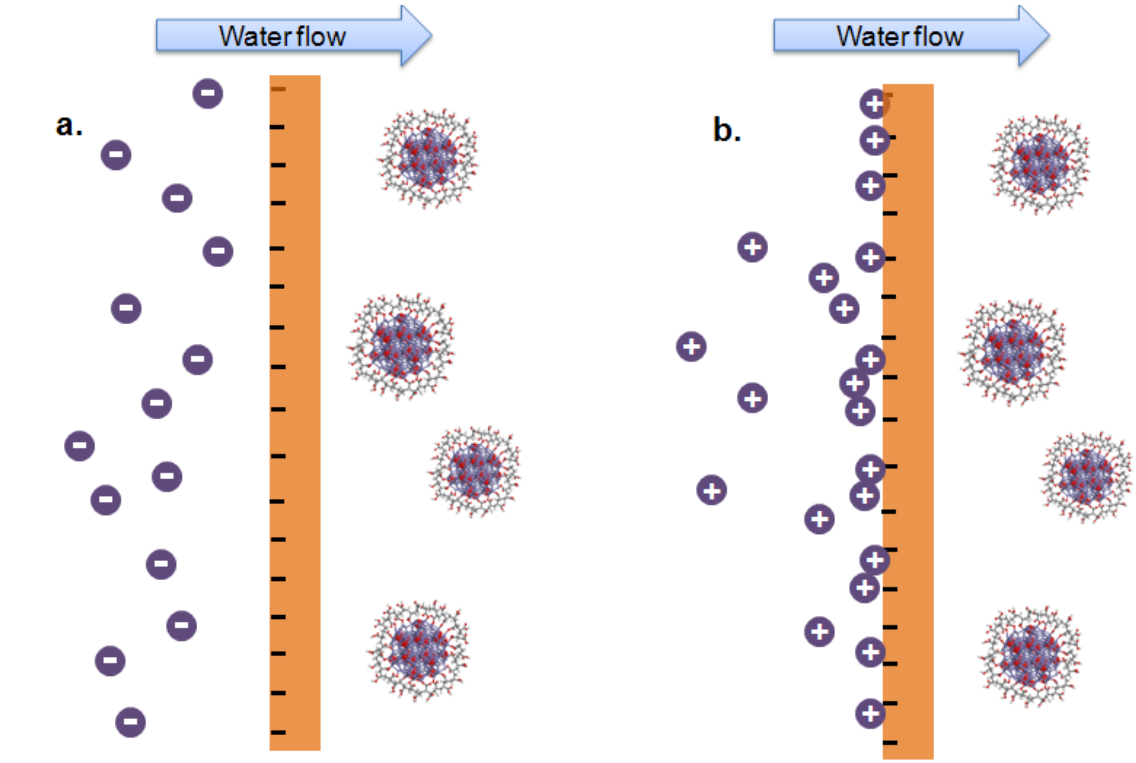

a: negatively charged STI ⊖ in water. b: positively charged LYZ ⊕ in water.
: PAA-NPs as draw solute to enrich protein solutions

Figure 5.11 Illustration of interactions between charged proteins and negatively charged membrane surface

5.3.4 Comparison of BSA enrichment kinetics with improved performance

To pursue high enrichment efficiency in the dual-stage FO system using nanoparticles as draw solutes, several operational parameters were altered accordingly. Effects of PAA-NPs concentration and membrane area have been studied. As displayed in Figure 5.12, by utilizing a double concentration of PAA-NPs draw solutions alone (i.e., the osmotic pressure increases from 6 atm to 13 atm), the enrichment percentage is improved from 15% to 23% because the PAA-NPs draw solution of doubled concentration can draw water molecules from the BSA feed solution faster under a larger potential energy gap. A similar phenomenon can be found when increasing membrane area from the original 8 cm^3 to 18 cm^3, the enriched percentage is increased from 15% to 28% as shown in Figure 5.13. Figure 5.14 shows the evolution of protein concentration by utilizing a combination of both PAA-NPs draw solution of higher osmotic pressure (16.7 atm) and enlarged membrane surface area (18 cm^2) in the dual-stage FO system for 7-hour operation. The enrichment percentage could be easily raised to nearly 100% because the BAS increases from 0.2 g/L up to about 0.4 g/L. Therefore, adequate adjustments of process parameters in the dual-stage FO system can improve the enrichment performance.

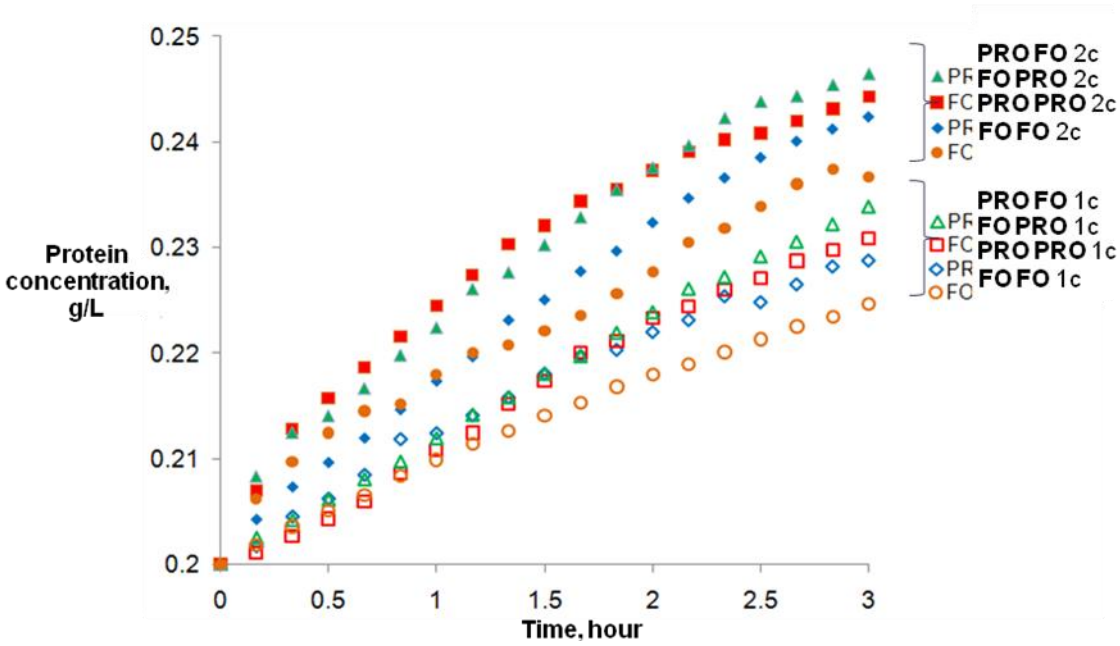

Figure 5.12 Comparison of protein enrichment kinetics with increased PAA-NPs concentration. (Ic: initial PAA-NPs solution of 6 atm osmotic pressure; 2c: double-concentrationed PAA-NPs solution of 13 atm)

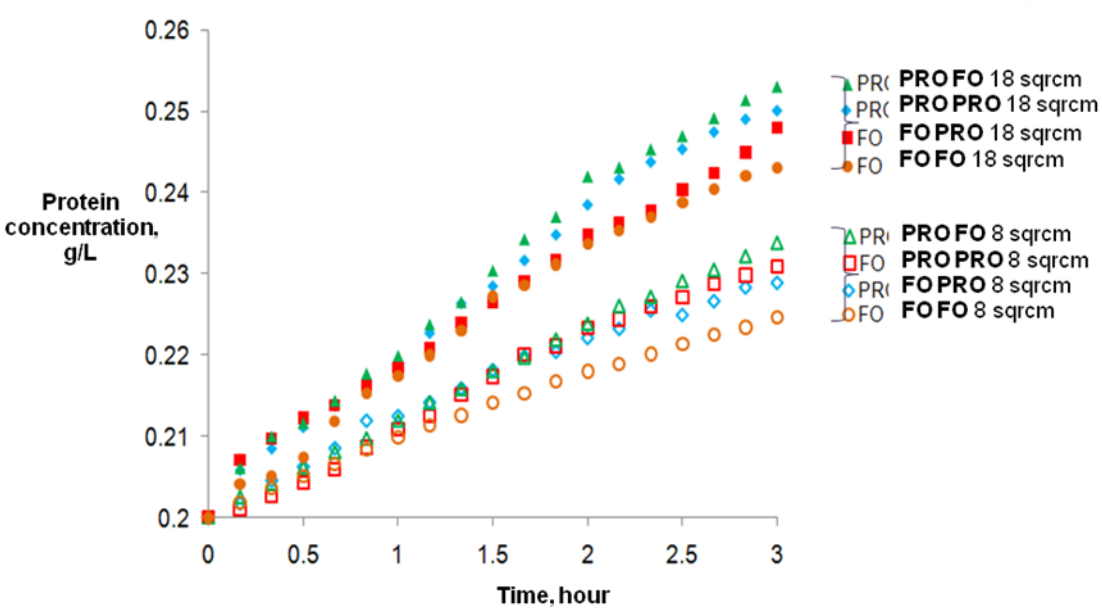

Figure 5.13 Comparison of protein enrichment kinetics with increased membrane area

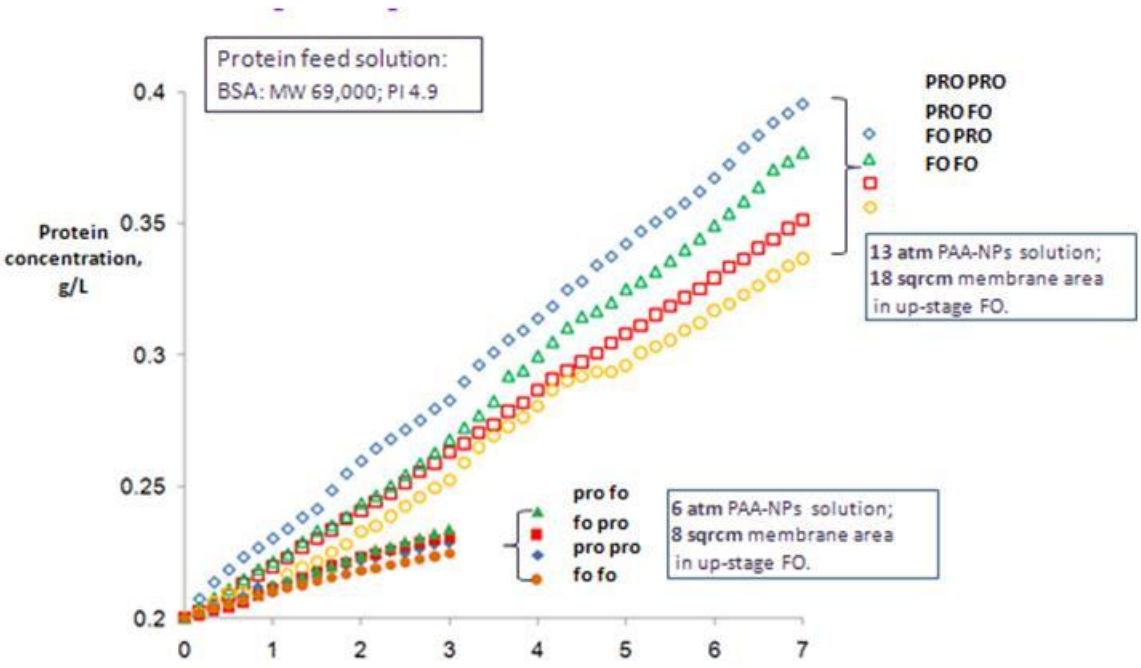

Figure 5.14 Improved protein enrichment kinetics with increased PAA-NPs concentration and membrane area

5.3.5 Effects of FO Membrane Orientation on Protein Enrichment Performance

Concentration polarization (CP), including external concentration polarization (ECP) and internal concentration polarization (ICP), is usually inevitable in FO processes. Four types of membrane orientations in dual-stage FO systems along with CP phenomena are illustrated in Figure 5.15. ECP can be alleviated by increasing the flow rate and turbulence. Although neither protein molecules nor PAA-NPs can pass through FO

membranes owing to the much larger sizes than membrane pores, they may cause either concentrative or dilutive ICP when they are facing the porous layer of FO membranes depending on (1) protein and draw solute sizes and their osmotic pressures, (2) porosity and pore size of the porous layer, (3) charge characteristics of proteins and draw solutes, (4) system's pH value and membrane charge characteristics, and (5) the degree of fouling in the porous layer. Sodium chloride from the RO retentate draw solution in the down-stage FO can easily penetrate FO membranes and propagate in the porous layer of the asymmetric membrane, resulting in ICP in the down-stage FO, as depicted in Figure 5.15. Therefore, the water transport in the dual-stage FO is very complicated and is a delicate balance of many factors.

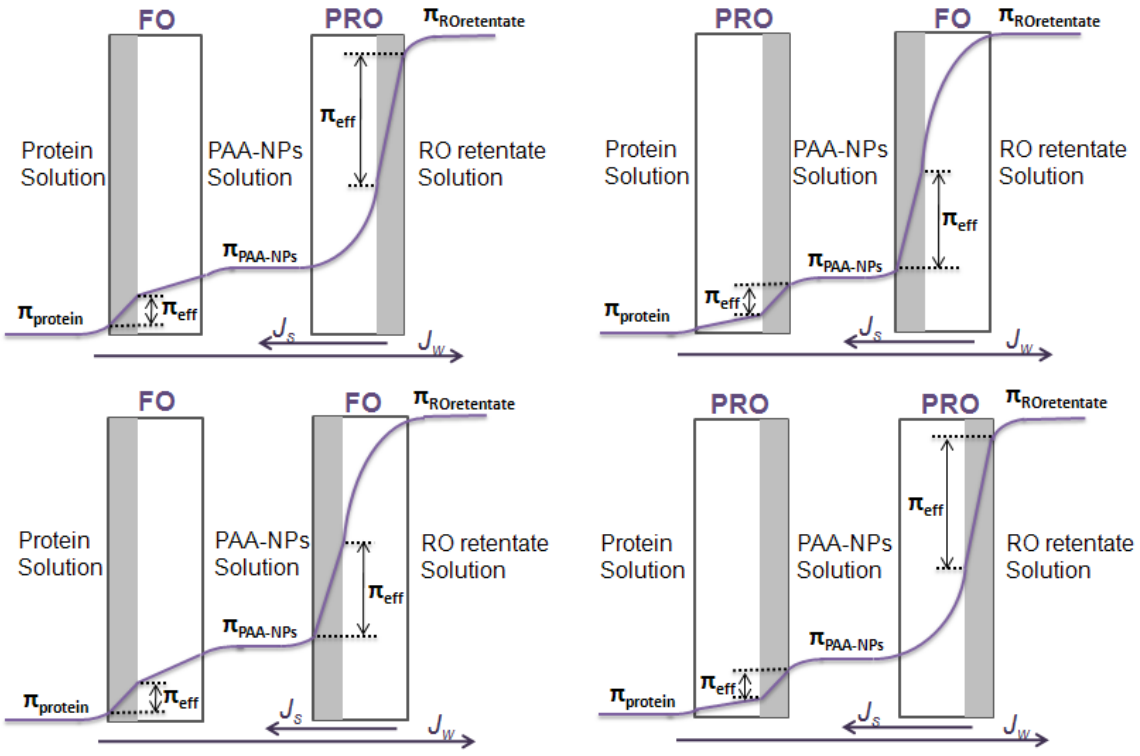

Figure 5.15 Illustrations of CPs in dual-stage FO in all membrane orientations

Using the initial experimental conditions as an example where PAA-NPs with an osmotic pressure of 6 atm and a membrane area of 8 cm^2 were used. The highest concentration through the dual-stage FO was achieved in the PRO FO mode, followed by FO PRO, PRO PRO and FO FO modes, as seen in Figures 5.9, 5.10 and 5.11. In the PRO FO mode, a dynamic balance was well obtained between up-stage FO and down-stage FO systems. Water extracted from the protein solution to the PAA-NPs solution was adequately further drawn to the RO retentate solution. The dilution of RO retentate could be ignored since the osmotic pressure was extremely high. Thus the osmotic driving force of PAA-NPs intermediate solution was better maintained and the protein solution was enriched at an almost constant rate. When the down-stage FO system was operated in the PRO mode (i.e., the system was in the PRO PRO mode), a higher osmotic driving force was generated and overwhelmed the one in the up-stage FO. As a result, the PAA-NPs solution was more concentrated to enrich protein solutions with a higher osmotic driving force. Therefore, concentrative ECP in the protein feed solution side in the up-stage FO was gradually aggravated and the proteins were more likely to foul on the membrane surface, which could block more channels of water flow through the membrane and deteriorate the protein enrichment efficiency, as compared to the FO mode in the down-stage FO system. A comparison of protein concentration profiles between 0.5–1 hr of Figure 5.8 confirms our hypothesis. The PRO PRO mode has a higher flux but gradually levels off after 1 hour. If protein fouling in the up-stage FO can be minimized and the

water drawn from the two stages is balanced, the PRO PRO mode may have the highest efficiency for protein enrichment as shown in Figure 5.14.

For the FO PRO mode takes the advantage of less protein fouling in the up-stage FO system and a higher osmotic driving force in the down-stage FO system to dehydrate the immediate PAA-NPs solution by means of the PRO mode. The FO FO mode usually has the slowest dehydration rate mainly because of inadequate water drawn to the RO rententation solution as operated in the FO mode.

With an increase in osmotic driving force of PAA-NPs solutions, the enrichment process becomes fast. Thus the double concentrated PAA-NPs solution can generally improve the enrichment performance and yet has no influence on the order of the effects of membrane orientations, as seen in Figure 5.12. When the membrane area in the up-stage FO was increased from 8 cm^2 to 18 cm^2, it was found that the concentration enriched in the PRO PRO mode exceeded the FO PRO mode, as shown in Figure 5.13. This may be due to the effect of less fouling because of a large membrane surface area.

When dual-stage FO was operated with increased both osmotic pressure of PAA-NPs solution and membrane area of the up-stage, the highest protein concentration was achieved in the PRO PRO mode, superior to the PRO FO mode as displayed in Figure 5.14. Under the improved experimental conditions, more water could be drawn from the protein solution to the PAA-NPs solution with the increased osmotic driving force and

more water flow channels in the up-stage FO system. Since the dual-stage FO is a complex system, future works will focus on mathematical modeling of its separation performance as a function of membrane orientation, osmotic pressure of solutions applied, membrane surface area, type of solutes added, charge characteristics and other parameters as well. It is crucial to combine experimental conditions, results and mathematic simulation for dual-stage FO systems in order to identify the optimal enrichment conditions.

5.4 Conclusion

We have demonstrated dual-stage FO systems, for the first time, for protein enrichment using nanoparticles as intermediate draw solutes. The newly developed system can be applicable to various proteins of different sizes and charges. The dual-stage FO system consisting of a large membrane surface and highly osmotic draw solutes can effectively dehydrate protein solutions under athermal conditions. In addition, experimental results show that (1) The PAA-NPs intermediate draw solution is efficacious to keep protein intact and stable during the enrichment, while concentrated salts as draw solutes may denature proteins; (2) The steady osmotic driving force of PAA-NPs solution can be maintained in the continuous dual-stage FO; (3) The model RO retentate can regenerate PAA-NPs solutions effectively, (4) the PRO PRO model may enrich proteins fast if protein fouling is minimal and (5) Dual-stage FO integrated with nanoparticles exhibits superiority than one-stage FO to enrich protein solutions, considering the aspects of

reverse salt flux as well as expense and disposal of draw solutions. The proposal system can be used for the application of other pharmaceutical and bio-molecule enrichments.

5.5 References

1. S. Jones, J. M. Thornton, Principles of protein-protein interactions. Proc.Natl.Acad.Sci. 93(1996) 13.

2. http://www.activery.com/pharmaceutical-market-news/168-the-global-protein-therapeutics-market-will-be-worth-77bn-by-2011-with-biogenerics-playing-an-increasingly-important-rol

3. R. Gosh, Protein Bioseparation Using Ultrafiltration: Theory, Applications and New Developments. Imperial College Press, 2003

4. A. Wang, C. J. Wu, S. H. Chen, Gold nanoparticle-assisted protein enrichment and electroelution for biological samples containing low protein concentrations- a Prelupe of gel electrophoresis. J.Proteome.Res. 5(2006)1488

5. Y. Li, T.S. Chung, S.Y. Chan, High-affinity sulfonated materials with transition metal counterions for enhanced protein separation in dual-layer hollow fiber membrane chromatography. J. Chromatogr. A. 1187(2008) 285

6. S.P. Sun, K.Y. Wang, N. Peng, T.A. Hatton, T.S. Chung, Novel polyamide-imide/cellulose acetate dual-layer hollow fiber membranes for nanofiltration. J. Membr. Sci. 363(2010)232.

7. Z.Z. Zhou, Y.C. Xiao, T.A. Hatton, T.S. Chung, Novel membrane processes for the enantiomeric resolution of tryptophan by selective permeation enhancements, J. Membr. Sci., 339(2009)21.

8. Q. Yang, K.Y. Wang, T.S. Chung, A novel dual-layer forward osmosis membrane for protein enrichment and concentration. Sep. Purif. Technol. 69(2009)269.

9. A. L. Zydney, Protein separations using membrane filtration: new opportunities for whey Fractionation, Int. Dairy J. 8(1998)243.

10. M.M. Rohani, A.L. Zydney, Role of electrostatic interactions during protein ultrafiltration, Adv. Colloid Interface Sci. 160(2010)40.

11. http://chemelab.ucsd.edu/ultra/background.html

12. L. Robert, M. Elimelech, Global challenges in energy and water supply: The promise of engineered osmosis. Environ. Sci. Tech. 42(2008)8625.

13. J. R. McCutcheon, R. L. McGinnis, M. Elimelech, A novel ammonia-carbon dioxide forward (direct) osmosis desalination process. Desalination. 174(2005)1.

14. B.X. Mi, M. Elimelech, Chemical and physical aspects of organic fouling of forward osmosis membranes. J. Membr. Sci. 320(2008)292.

15. B.X. Mi, M. Elimelech, Gypsum scaling and cleaning in forward osmosis: measurementsand mechanisms, Environ. Sci. Technol. 44 (2010) 2022.

16. K.Y. Wang, T.S. Chung, J.J. Qin, Polybenzimidazole (PBI) nanofiltration hollow fiber membranes applied in forward osmosis process. J. Membr. Sci. 300(2007)6.

17. K.Y. Wang, R.C. Ong, Double-selective Layer Forward Osmosis Membranes for the Elimination of Internal Concentration Polarization within the Porous Sublayer. Ind. Eng. Chem. Res. 49(2010)4824.

18. S. Zhang, K.Y. Wang, T.S. Chung, H.M. Chen, Y.C. Jean, G. Amy, Well-constructed Cellulose Acetate Membranes for Forward Osmosis: Minimized Internal Concentration Polarization with an Ultra-thin Selective Layer. J. Membr. Sci. 360(2010)522.

19. J.J. Qin, S.J. Chen, M.H. Oo, K.A. Kekre, E. R. Cornelissen, C. J. Ruiken, Experimental studies and modeling on concentration polarization in forward osmosis, Water. Sci. Technol.61 (2010) 2897.

20. J.J. Qin, M.H. Oo, G. Tao, E.R. Cornelissen, C.J. Ruiken, K.F. de Korte, L.P. Wessels, K. A. Kekre, Optimization of operating conditions in forward osmosis for osmotic membrane bioreactor, Open Chem. Eng. J. 3 (2009) 27.

21. J.C. Su, Q. Yang, J.F. Teo, T.S. Chung, Cellulose acetate nanofiltration hollow fiber membranes for forward osmosis processes. J. Membr. Sci. 355(2010)36.

22. R. Hausman, B. Digman, I.C. Escobar, M. Coleman, T.S. Chung, Functionalization of polybenzimidizole membranes to impart negative charge and hydrophilicity, J. Membr. Sci. 363(2010)195.

23. M.M. Ling, K.Y. Wang, T.S. Chung, Highly water-soluble magnetic nanoparticles as novel draw solutes in forward osmosis for water reuse. Ind. Eng. Chem. Res. 49(2010)5869.

24. Q. C. Ge, J.C. Su, T.S. Chung, G. Amy, Hydrophilic superparamagnetic nanoparticles: synthesis, characterization, and performance in forward osmosis processes. Ind. Eng. Chem. Res. In press.

25. M.M. Ling, T.S. Chung, Desalination process using super hydrophilic nanoparticles via forward osmosis integrated with ultrafiltration regeneration, 278 (2011) 194

26. N. Greenfield, G.D. Fasman, Biochemistry, 1969, 8, 4108–4116.

27. B.N. Dominy, D. Perl, F.X. Schmid, C.L. Brooks, The effects of ionic strength on protein stability: the cold shock protein family. J. Mol. Biol. 319(2002)541.

28. S. Adham, Oppenheimer, J.; Liu, L.; Kumar, M. Dewatering reverse osmosis concentrate from water reuse using forward osmosis. WateReuse Foundation: Alexandria, VA 2007

29. R.H. Boyd, P.J. Phillips, The science of polymer molecules. Combridge University Press, 1996

30. P.R. Bergethon, The physical basis of biochemistry: the foundations of molecular. Springer, 2010

31. W.R. Bowen, A.W. Mohamad, Characterization and prediction of nanofiltration membrane performance-a general assessment. Chem. Eng. Res. Des.76 (1998)885.

32. A.S. Michaels, Analysis and prediction of sieving curves for ultrafiltration membrane: a universal correclation. sep. sci. technol. 15(1980)1305.

33. K.H. Youm, W.S. Kim, Prediction of intrinsic pore properties of ultrafiltration membrane by solute rejection curves: effects of operating conditions on pore properties. Journal of Chemical Engineering of Japan.24 (1991) 1.

34. S. Singh, K.C. Khulbe, T. Matsuura, P. Ramamurthy, Membrane characterization by solute transport and atomic force microscopy. J. Membr. Sci.142(1998) 111.

CHAPTER 6

FACILE SYNTHESIS OF THERMOSENSITIVE MANGETIC NANOPARTICLES AS 'SMART' DRAW SOLUTE IN FORWARD OSMOSIS

6.1 Introduction

Osmotically driven processes stand at the forefront to meet our ever-increasing global demand for clean water. Forward Osmosis (FO) is broadly acknowledged as the key technology to integrate future sea water desalination and waste water reclamation processes to solve global water scarcity problem [1-2]. In recent years, FO technology has been intensively studied for its use in desalination, water reuse, as well as protein enrichment processes [3] and power generation [4]. Forward osmosis utilizes the osmotic pressure difference of two solutions separated by a semi-permeable membrane to induce spontaneous movement of water molecules from the less concentrated solution (feed solution) to the other solution (draw solution) while most solutes are rejected by the FO membrane [1-2]. Contrary to reverse osmosis and other water production processes, FO discloses an innovative scenario to obtain water from concentrated solutions without any external aid including hydraulic pressure or heat. Since energy consumption is increasing exponentially as energy sources become scarcer and natural disasters affect the supply of water to millions of people each year, FO provides a versatile technology which minimizes energy consumption while maintaining high rejection of solutes and low

membrane fouling propensity [5].

Eligible FO membranes of high water permeate and low reverse salt flux play an important role in FO processes [6-11]. Likewise, the selection of suitable draw solute can greatly influence the efficiency of FO. In general, entitled draw solutes in FO for water production possess the qualities of being able to generate high osmotic pressures and easy recovery of the water obtained. A variety of chemical compounds have been attempted as draw solutes in FO applications but the progress is well behind the development of FO membranes [2, 12-17]. Ammonium bicarbonate induces reasonable FO fluxes and the water product must be obtained via thermal decomposition of the ammonium salt at about 60 ^{o}C [12]. Highly water-soluble superparamagnetic nanoparticles were recently discovered as a new type of draw solutes and exhibit the advantages of extreme low reverse flux compared to traditional chemicals [15-16]. Nanoparticles with hydrophilic surface functionality and high surface-area-to-volume ratio may generate high osmotic pressures for desalination and water reclamation purposes. Moreover, the nanoparticles can be readily regenerated using more efficient and conventional methods, such as magnetic fields. However, magnetic nanoparticles were found to aggregate to much larger sizes under high-strength magnetic field, causing a significant decrease in efficiency. Stimuli-responsive polymer hydrogels have been explored as a draw agent [17], but their FO performance is poor at room temperature and the dewatering process needs a hydraulic pressure of 30 bar at elevated temperatures.

Therefore, the objectives of this part of the thesis are, for the first time, (1) to overcome aforementioned hurdles of magnetic nanoparticles and stimuli-responsive polymer hydrogels, and (2) conceptually demonstrate magnetic nanoparticles with thermo-responsive properties for FO processes and easy regeneration without performance deterioration. At temperatures above the Lowest Critical Solution Temperature (LCST), thermosensitive magnetic nanoparticles tend to agglomerate together resulting from the coil-to-globule transition of the thermosensitive polymer on their surface [18-19]. As such, a magnetic field of much lower strength can facilitate the separation of thermosensitive magnetic nanoparticles when the temperature is above the LCST and significantly decrease the possibility of irreversible agglomeration caused by high-strength magnetic fields. As a result, thermosensitive magnetic nanoparticles can effectively function as 'smart' draw solutes in FO without particle size changes upon magnetic separation.

6.2 Thermosensitive magnetic nanoparticles as draw solute in forward osmosis

So far, thermosensitive magnetic nanoparticles are mainly synthesized by the method of either ligand exchange of particles initially capped with oleic acid [16] or by polymerization on the surface of magnetic nanoparticles prepared from co-precipitation reaction [21]. The ligand exchange method suffers from the disadvantages of a large amount of solvent consumption and a low yield while the polymerization method is more

complicated and involves many reaction parameters. More importantly, the resultant particle size and uniformity of particles through these two methods are not satisfactory as draw solutes in FO processes.

In order to fulfil the required characteristics of draw solutes in FO, thermosensitive magnetic nanoparticles must possess both highly hydrophilic groups to induce osmotic pressures and extremely thermosensitive polymer on the surface to facilitate easy regeneration via low-strength magnetic field separation. Here we report a facile synthesis of monodisperse thermosensitive magnetic nanoparticles in a one-step thermal decomposition method with improved solubility in water and their application as 'smart' draw solute in FO. In this work, poly(N-isopropylacrylamide) is selected as the stabilizer and triethylene glycol as the organic solvent. The detailed synthesis procedures can be found in supporting information. Poly(N-isopropylacrylamide) as the basic thermosensitive polymer possesses the coordination capacity with transition metal ions owing to its amide groups [22] and hence it can be added directly as the nanoparticle surface capping agent in the thermal decomposition reaction without modification. Triethylene glycol is chosen as the solvent because of its high boiling point and modest interaction with poly(N-isopropylacrylamide) at elevated temperatures. More importantly, it can functionalize the nanoparticle surface with improved hydrophilicity. Both poly(N-isopropylacrylamide) and triethlyene glycol would compete to bind on the magnetic nanoparticle surface during the reaction to inhibit the nanoparticle growth because they both possess the available ligands to form strong chemical coordination

with iron cations on nanoparticle surface. In addition, the copious C=O groups along the chain of poly(N-isopropylacrylamide) result in multiple anchor points on the iron oxide core surface, which contribute to the robust coating of poly(N-isopropylacrylamide) on the nanoparticles. Therefore, in order to perform as 'smart' draw solute in FO, thermosensitive magnetic nanoparticles functionalized with poly(N-isopropylacrylamide) and triethlyene glycol (PNIPAM/TRI-MNP) exhibit enhanced hydrophilic properties and optimal responses to dual stimuli (heat and magnetic field) when compared to conventional thermosensitive nanoparticles.

The core material of PNIPAM/TRI-MNPs is composed of magnetite, which is verified by the X-ray diffraction (XRD) patterns as displayed in Figure 6.1 show that the position and relative intensity of the diffraction peaks match well with the standard XRD magnetite data (JCPDS file No. 19-0629). Moreover, the black colour of the dry PNIPAM/TRI-MNPs sample also indicates magnetite as the core material rather than maghemite of similar XRD patterns. Figure 6.2 shows TEM pictures of PNIPAM/TRI-MNPs dispersed in water before and after magnetic separations. The nanoparticles of sphere shape are observed and they exhibit a slight polydisperse distribution of 9 ±3 nm in diameter which is close to the crystallite size of the core metal oxide of 8.2 nm obtained from XRD data using the Scherrer's formula, indicating the single crystal of each nanoparticles [25]. However, the particle sizes determined from TEM and XRD are smaller than the size distribution (Figure 6.3) obtained from the Nanoparticle Size Analyzer, which can be ascribed to some degrees of nanoparticle aggregation and

hydration of the hydrophilic polymeric layer upon the nanoparticles in the aqueous solution. Magnetic nanoparticles synthesized in triethylene glycol alone (TRI-MNP) were also characterized to affirm the existence of poly(N-isopropylacrylamide) on the PNIPAM/TRI-MNPs. TGA measurements were conducted to determine the polymer coverage on nanoparticle surface. As shown in Figure 6.4, the major weight loss of both the nanoparticles span from 150 ^{o}C to 700 ^{o}C due to the degradation of the organic shell. It is observed that PNIPAM/TRI-MNPs exhibit a different pattern compared to TRI-MNPs, which indicates the existence of poly(N-isopropylacrylamide) on the PNIPAM/TRI-MNP surface compared to TRI-MNPs capped with only triethylene glycol. PNIPAM/TRI-MNP nanoparticles have a much greater polymeric coverage (38%) than TRI-MNP (20%) on nanoparticle surface owing to the decomposition of poly(N-isopropylacrylamide) of high molecule weight (10K). Magnetic properties of PNIPAM/TRI-MNPs and TRI-MNPs were also examined. Figure 6.5 compares the magnetization hysteresis loops of both the nanoparticles at room temperature. The magnetic nanoparticles possess superparamagnetic property as both the hysteresis loops show zero coercivity and magnetic remanence. The saturation magnetization of PNIPAM/TRI-MNPs (40 emu/g) is lower than TRI-MNPs (50 emu/g), which further confirms that poly(N-isopropylacrylamide) was successfully grafted on the nanoparticles. These experimental results also accord with the phenomenon from other researchers that the superparamagnetic property of magnetic nanoparticles is strongly dependent on the amount of polymer grafted [23]. The thermosensitive property of PNIPAM/TRI-MNPs was examined by measuring the particle size through a series of temperature changes.

Sharp and reversible changes of particle size were observed at 35 °C upon heating and cooling (Figure 6.6). The reversible thermosensitive properties in terms of particle size and osmotic pressure are essential for the regeneration of PNIPAM/TRI-MNPs with higher recovery rates in modest energy consumptions.

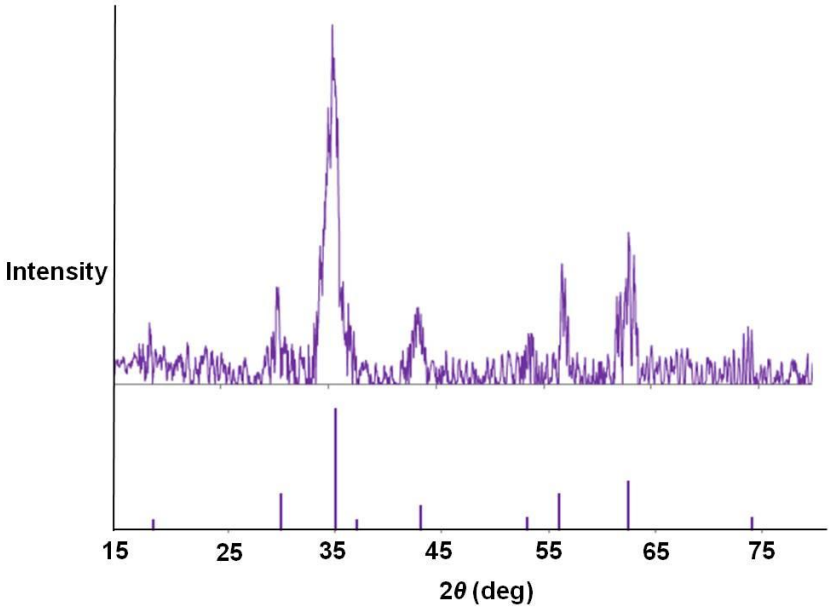

Figure 6.1 XRD patterns for PNIPAM/TRI-MNP.

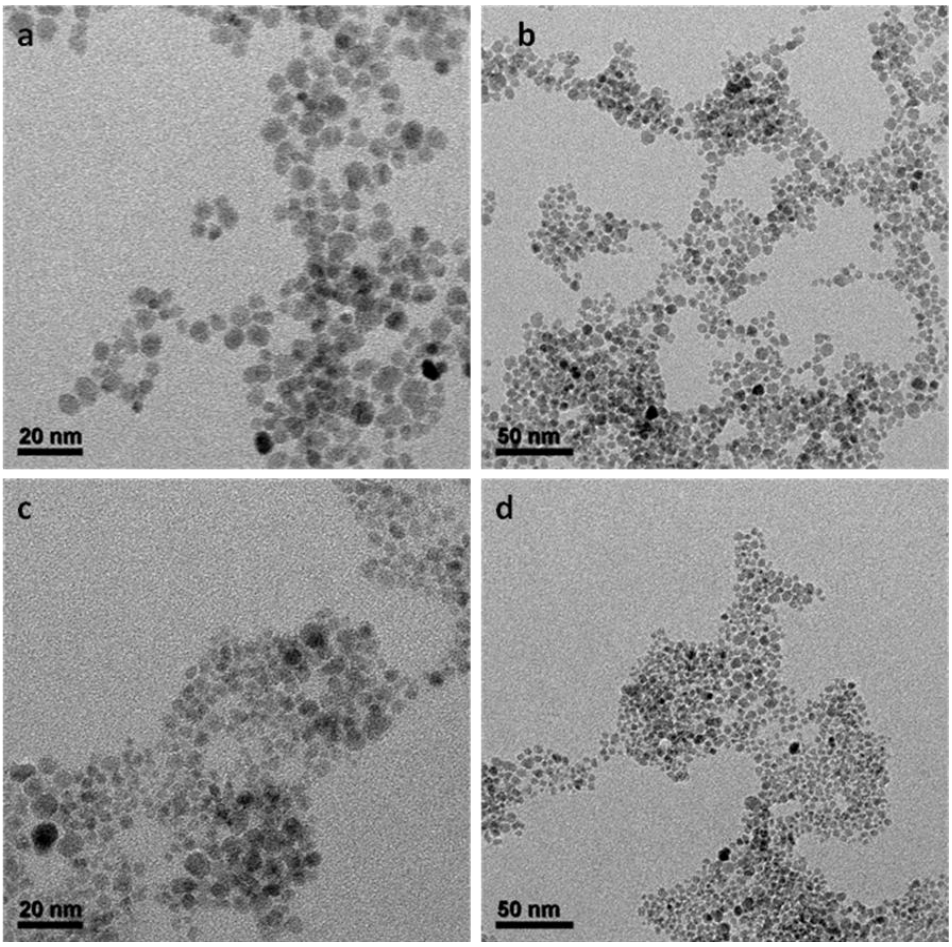

Figure 6.2 TEM images of PNIPAM/TRI-MNP before (a,b) and after magnetic separation for times (c,d)

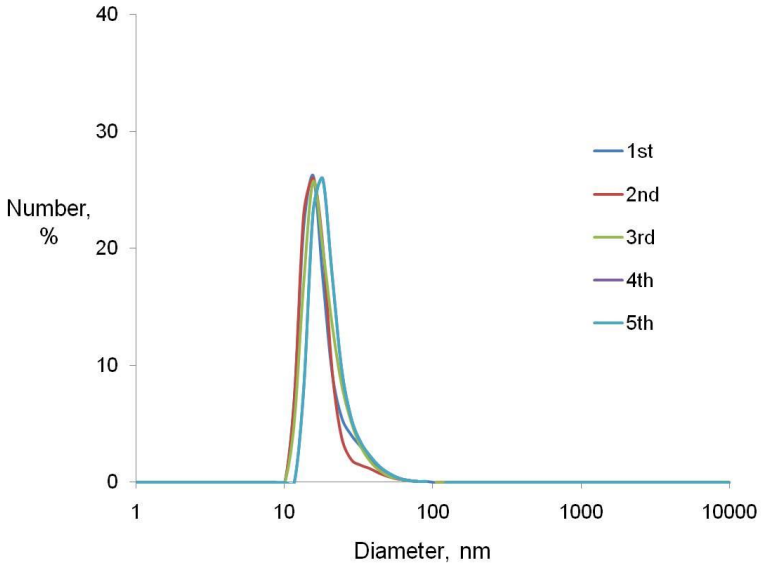

Figure 6.3 Size distributions of PNIPAM/TRI-MNP after each regeneration.

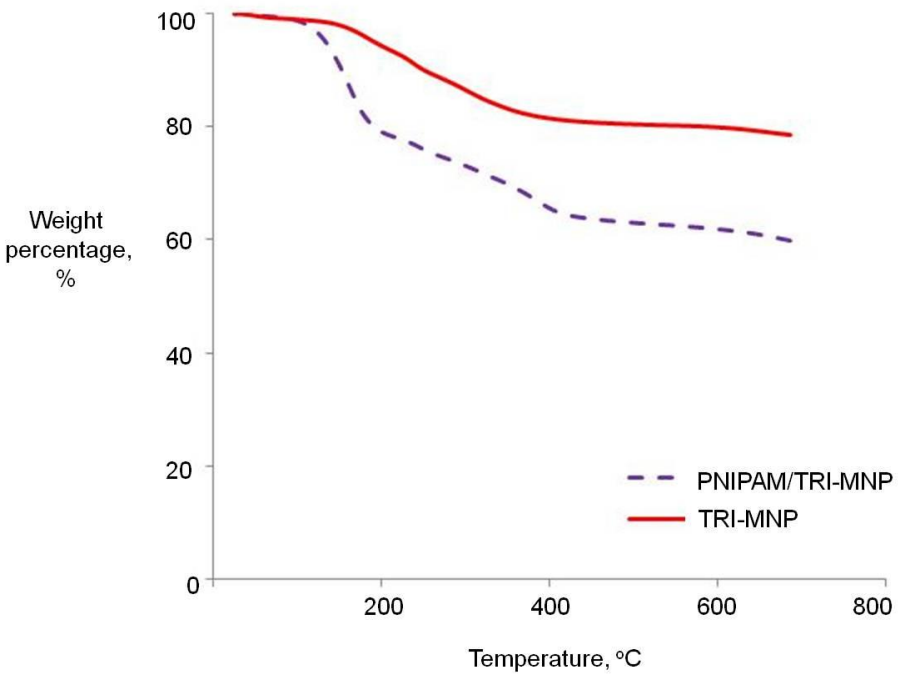

Figure 6.4 TGA profile of PNIPAM/TRI-MNP and TRI-MNP

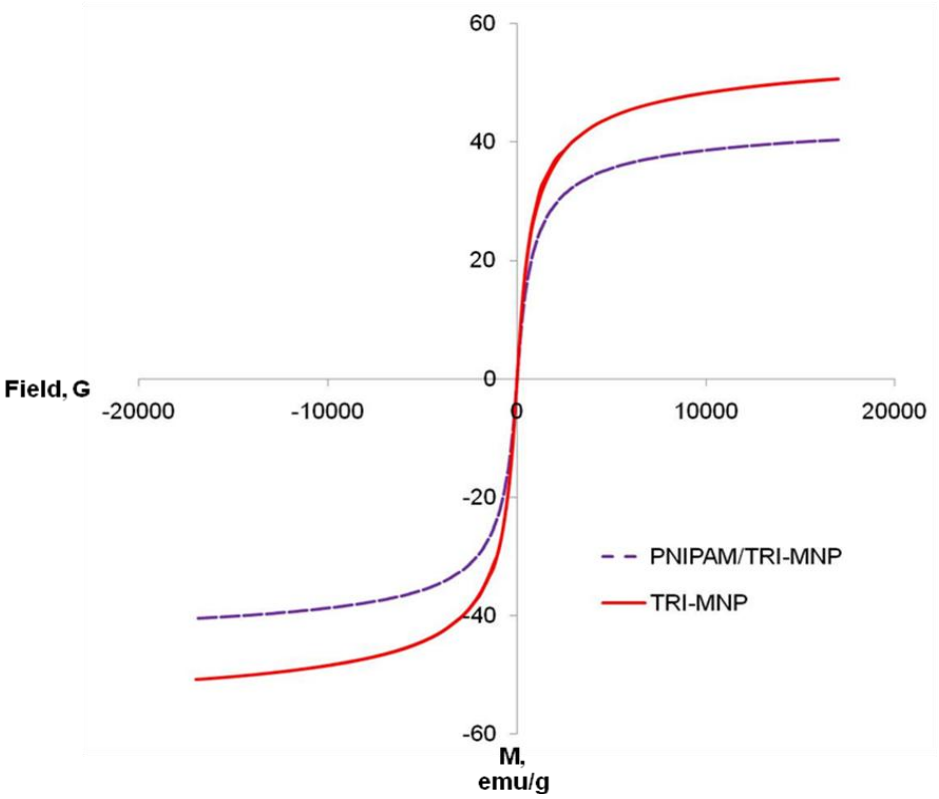

Figure 6.5 VSM loops of PNIPAM/TRI-MNP and TRI-MNP

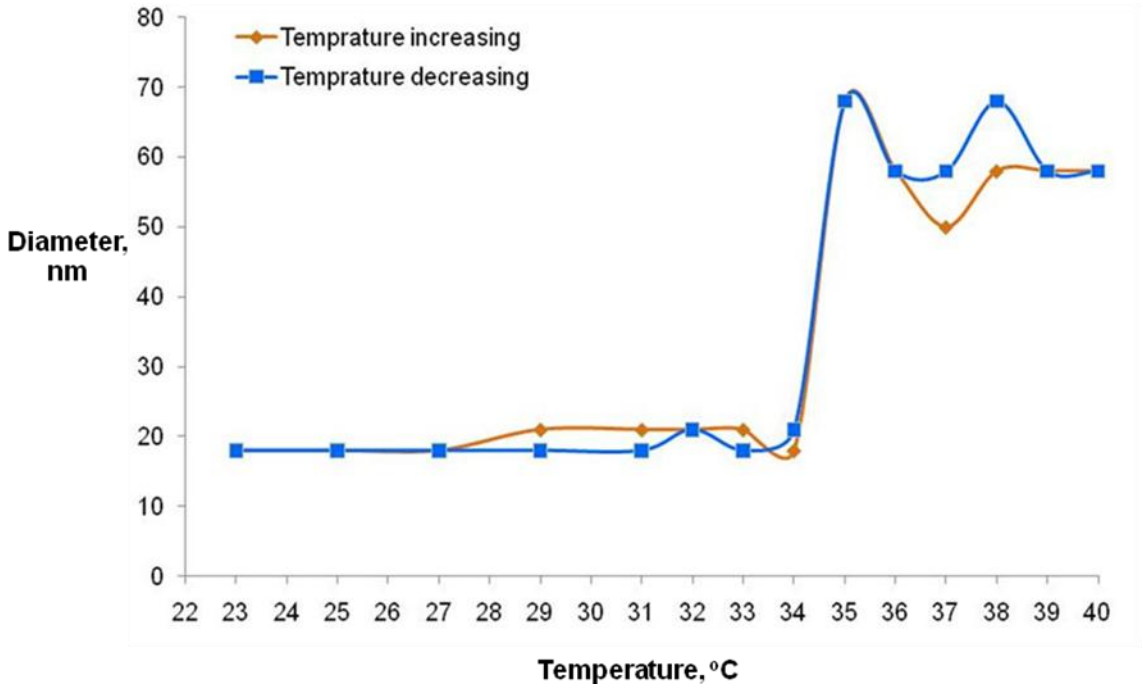

Figure 6.6 PNIPAM/TRI-MNP size changes at different temperatures

6.3 Evaluation of thermosensitive magnetic nanoparticles as draw solute in forward osmosis

To evaluate the thermosensitive magnetic nanoparticles as draw solutes in FO, PNIPAM/TRI-MNPs were tested in FO systems at room temperature and regenerated via low-strength magnetic separation at temperatures above its LCST for 5 runs. The detailed experimental setup and procedures are shown in Figure 6.7. The size measurements of PNIPAM/TRI-MNPs were conducted after regenerations and no increment in particle size was observed even after 5 runs (Figure 6.3). The TEM images in Figure 2 c & d show the recycled PNIPAM/TRI-MNPs and no obvious particle changes were found

either. The reversible thermosensitive property of the PNIPAM/TRI-MNPs synthesized in our approach and the low-strength magnetic separations contribute to the intactness and robustness of PNIPAM/TRI-MNPs as a 'smart' draw solute in FO. Thereafter, as displayed in Figure 6.8, the FO performance of PNIPAM/TRI-MNPs can be well maintained through 5 runs in both Pressure Retarded Osmosis (PRO) mode (draw solution facing the dense layer of FO membrane) and Forward Osmosis (FO) mode (feed solution facing the dense layer of FO membrane).

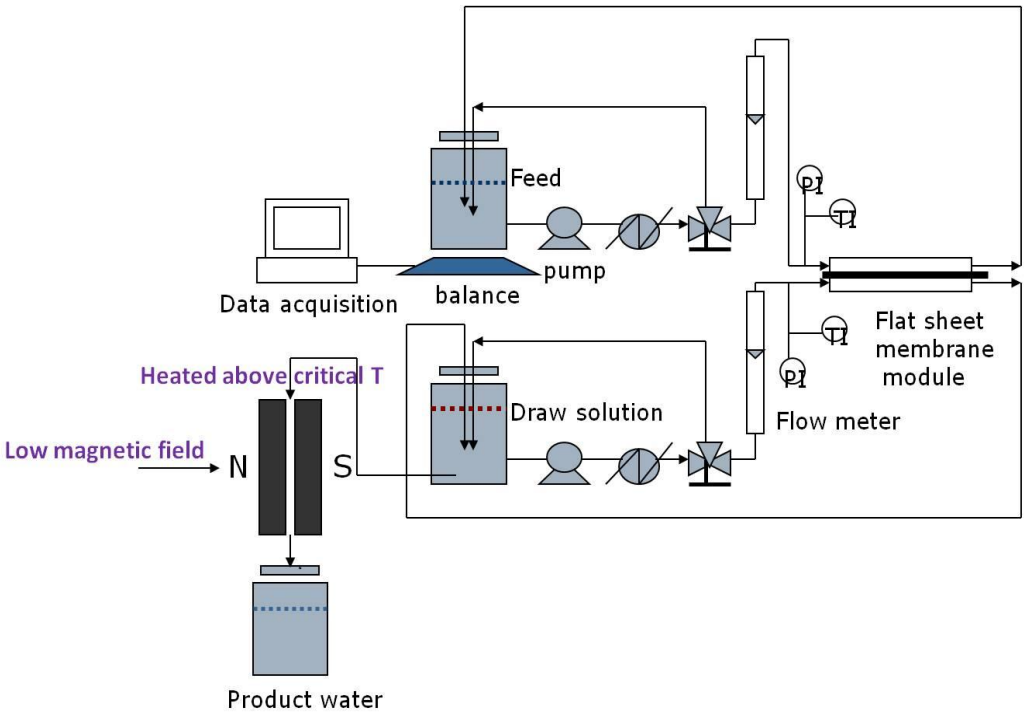

Figure 6.7 Schematic diagram of laboratory-scale FO set-up using thermosensitive magnetic nanoparticles as draw solute

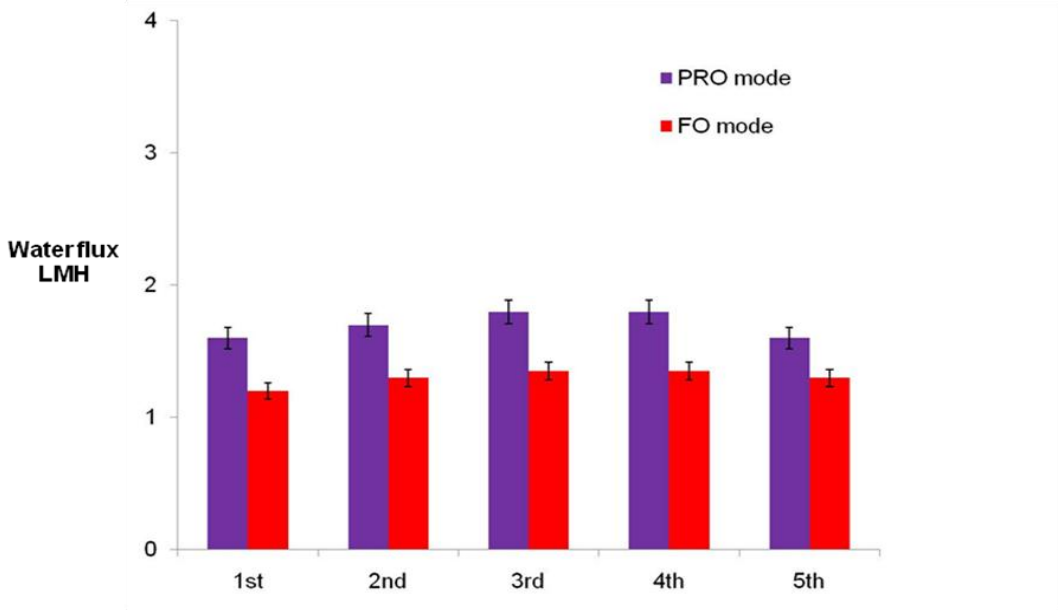

Figure 6.8 FO performance of recycled PNIPAM/TRI-MNP

6.4 Conclusion

In conclusion, thermosensitive superparamenetic nanoparticles have been successfully synthesized with improved hydrophilicity in one step. The resultant PNIPAM/TRI-MNPs exhibit uniform particle sizes of less than 20 nm and excellent stability in water. We have demonstrated that PNIPAM/TRI-MNPs can be recycled as a 'smart' draw solute in FO processes without losing performance efficiency as a result of their reversible thermosensitive property facilitating the magnetic separation of low strength to assure the integrity of nanoparticle draw solutes. The FO performance can be enhanced with nanoparticle surface engineering and decreasing particle sizes. It is believed that thermosensitive magnetic nanoparticles hold great potential as a novel draw solute in FO processes for water reuse, desalination, protein dehydration and biomedical applications.

6.5 References

1. R.L. McGinnis, M. Elimelech, Global challenges in energy and water supply: the promise of engineered osmosis, Environ. Sci. Tech., 42(2008)8625.

2. T.S. Chung, S. Zhang, J.C. Su, K.Y. Wang, M.M. Ling, Forward osmosis processes: Yesterday, today and tomorrow, doi:10.1016/j.desal.2010.12.019 .

3. M. M. Ling and T. S. Chung, Novel dual-stage FO system for sustainable protein enrichment using nanoparticles as intermediate draw solutes J. Membr. Sci.,15(2011) 201.

4. K. Gerstandt, K. V. Peinemann, S. E. Skilhagen, T. Thorsen and T. Holt, Membrane processes in energy supply for an osmotic power plant, Desalination, 224(2008)64.

5. B.X. Mi, M. Elimelech, Gypsum scaling and cleaning in forward osmosis: measurementsand mechanisms, Environ. Sci. Technol. 44 (2010) 2022.

6. K. Y. Wang, T. S. Chung and J. J. Qin, Polybenzimidazole (PBI) nanofiltration hollow fiber membranes applied in forward osmosis process, *J. Membr. Sci.* 300(2007) 6.

7. S. Zhang, K.Y. Wang, T.S. Chung, H.M. Chen, Y.C. Jean, G. Amy, Well-constructed cellulose acetate membranes for forward osmosis: minimized internal concentration polarization with an ultra-thin selective layer. J. Membr. Sci.360(2010)522.

8. J.C. Su, Q. Yang, J.F. Teo, T.S. Chung, Cellulose acetate nanofiltration hollow fiber membranes for forward osmosis processes. J. Membr. Sci. 355(2010)36.

9. J. R. McCutcheon, R. L. McGinnis, M. Elimelech, A novel ammonia-carbon dioxide forward (direct) osmosis desalination process. Desalination. 174(2005)1.

10. P. McCormicka, J. Pellegrino, F. Mantovani and G, Sarti, Water, salt, and ethanol diffusion through membranes for water recovery by forward (direct) osmosis J. Membr. Sci., 325(2008) 467.

11. M.M. Ling, K.Y. Wang, T.S. Chung, Highly water-soluble magnetic nanoparticles as novel draw solutes in forward osmosis for water reuse. Ind. Eng. Chem. Res. 49(2010)5869.

12. Q. C. Ge, J.C. Su, T.S. Chung, G. Amy, Hydrophilic superparamagnetic nanoparticles: synthesis, characterization, and performance in forward osmosis processes. Ind. Eng. Chem. Res. 50(2011)382.

13. D. Li, X. Y. Zhang, J. F. Yao, G. P. Simon and H. T. Wang, Stimuli-responsivpolymer hydrogels as a new class of draw agent for forward osmosis desalinationw Chem. Commun., 47(2011)1710.

14. X. D .Xu, C. S. Cheng, Z. C. Wang, G. R. Wang, S. X. Cheng, X. Z. Zhang and R. X. Zhuo, “Click” chemistry for in situ formation of thermoresponsive P(NIPAAm-co-HEMA)-based hydrogels J. Polym. Sci., Part A: Polym. Chem., 46(2008)5263.

15. H. Cheng, J. L. Zhu, Y. X. Sun, S. X. Cheng, X. Z. Zhang and R. X. Zhuo, Novel thermoresponsive nonviral gene vector: P(NIPAAm-co-NDAPM)-b-PEI with adjustable gene transfection efficiency Bioconjug Chem. 19(2008)1368.

16. I. Robinson, C. Alexander, L. D. Tung, D.G. Fernig, and N.T.K. Thanh, J. Magn. Magn. Mater. Fabrication of water-soluble magnetic nanoparticles using thermo-responsive polymers, 321(2009)1421.

17. S. Kalele, R. Narain and K.M.Krishnan, Probing temperature-sensitive behavior of pNIPAAm-coated iron oxide nanoparticles using frequency-dependent magnetic measurements, J. Magn. Magn. Mater. 321(2009)1377

18. C. F. Lee, C. C. Lin, C. A. Chien and W.Y.Chiu, Thermosensitive and control release behavior of poly(N-isopropylacrylamide-co-acrylic acid)/nano-Fe3O4 magnetic composite latex particle that is synthesized by a novel method, Eur Polym J, 44(2008)2768.

19. R. Narain, M. Gonzales, A. S. Hoffman, P. S. Stayton and K. M. Krishnan, Synthesis of Monodisperse Biotinylated p(NIPAAm)-Coated Iron Oxide Magnetic Nanoparticles and their Bioconjugation to StreptavidinLangmuir, 23(2007)6299.

20. I. Robinson, C. Alexander, L.T.Lu, L.D.Tung, D.G. Fernig and N.T.K. Thanh, One-step synthesis of monodisperse water-soluble 'dual-responsive' magnetic nanoparticles, Chem. Commun.,(2007) 4602

21. P. L. Golas, S. Louie, G.V. Lowry, K. Matyjaszewski and R.D.Tilton, Comparative Study of Polymeric Stabilizers for Magnetite Nanoparticles Using ATRP, Langmuir, 26(2010)16890.

22. B. Y. Du, A. X. Mei, P. J. Tao, B, Zhao, Z. Cao, J. J. Nie, J. T. Xu and Z. Q. Fan, Poly[N-isopropylacrylamide-co-3-(trimethoxysilyl)-propylmethacrylate] Coated Aqueous Dispersed Thermosensitive Fe3O4 Nanoparticles, J. Phys. Chem. C,113(2009)10090.

23. Z. Li, L. Zhao, H.B. Bao and M.Y. Gao, One-pot reaction to synthesize water-soluble magnetite nanocrystals. Chem. Mater., 16(2004)1391.

24. C. Wei and J. Wan, Facile synthsis of superparamagnetic magnetite nanoparticles in liquid polyols. J. Colloid Interface Sci., 305(2007)366.

25. H. P. Klug and L.E. Alexander, X-Ray Diffraction Procedures, Wiley, New York, 1959.

CHAPTER 7

SURFACE-DISSOCIATED NANOPARTICLE DRAW SOLUTIONS INI FORWARD OSMOSIS AND THE REGENERATION IN AN INTEGRATED ELECTRIC FIELD AND NANOFILTRATION SYSTEM

7.1 Introduction

Clean water and reliable energy are the two most valuable resources of every modern society. As populations grow and countries become more industrialized, the demand for these resources accelerates. The global demand for energy and the limitations of current resources to produce energy is leading researchers to developing low-energy separation processes for water production [1-3]. Forward osmosis (FO) technology has emerged as one of the most promising technologies being to address this global demand for clean water because it offers significant advantages over traditional water production processes [2-11]. The osmotic pressure difference generated between two solutions separated by a semi-permeable membrane serves as the driving force for the FO process. In comparison with reverse osmosis (RO) and distillation process, FO can essentially reduce the energy consumption as it operates under the osmotic driving force which is the intrinsic energy source among molecules without any external aid, such as heat or hydraulic pressure. Moreover, FO possesses a lower membrane fouling propensity than pressure-driven

processes which is preferred in prolonging membrane lifetime and cutting backwashing cost. With the aforementioned advantages of FO, not only is FO utilized in water production, but also many other important applications, such as protein enrichment [12-13], food processing [14] and osmotic power generation [15-16].

As FO attracts more attention from various disciplines, demands on high performance FO membranes and superior draw solutes are arising. So far, remarkable developments of FO membranes have been achieved by many researchers [6-12, 15-24]. On the contrary, the study of draw solutes for FO is much less found. As literally defined, eligible draw solutes should create a sufficiently high osmotic pressure in order to draw water from feed solution effectively. Considering the aspects of energy consumption and environmental impact, draw solutes must be recyclable and regenerated in an energy-friendly process.

Searching for excellent draw solutes is challenging especially for the application of water production. In order to induce a high osmotic pressure, the size of draw solutes should be as small as possible since osmotic pressure is a colligative property and draw solutes with a high surface area are important. However, draw solutes of small size cause recovery issues, salt leakage, and severe internal concentration polarization in the FO membranes. Thus, a careful and balanced consideration should be made when designing draw solutes. Ammonium bicarbonate has been explored as draw solute [25]. Upon heating to 60 ^{o}C, the compound decomposes to NH_3 and CO_2 and therefore is regenerated. Highly water-

soluble nanoparticles have been synthesized and investigated as draw solutes in FO [26-27]. Not only can these nanoparticles induce reasonable water fluxes and osmotic pressures through engineering their surface hydrophilicity and particle size, but also be recovered by various methods including magnetic field [26-27], UF [28] and FO [13] as well as combined methods. To enhance the separation efficiency and reduce nanoparticle loss during recycling, thermo-responsive magnetic nanoparticles were invented as draw solutes and recovered in a low-strength magnetic field with pre-heating above its critical temperature [29]. Recently, a series of poly(acrylic acid sodium) (PAA-Na) polyelectrolyte were discovered as draw solutes that can be easily regenerated via ultrafiltration (UF) and membrane distillation (MD) process [30-31]. Diluted fertilizer draw solutions which can be directly applied for fertigation were also reported [32].

Since electric fields have been utilized in collecting colloid particles in wastewater treatment [33] and the recovered nanoparticles do not show irreversible changes [34]. In addition, nanoparticles with increased conductivity via surface dissociation show improved responses to the electric field. These merits inspire us to explore nanoparticles of enhanced surface-dissociation as draw solutes in FO applications. Therefore, in addition to conducting fundamental science on draw solutes, the objectives of this research are (1) to molecularly design nanoparticle draw solutes of enhanced surface-dissociation for improved FO performance and (2) to develop regeneration method via an integrated electric field and nanofiltration (NF) system. Compared with unmodified nanoparticles, surface-dissociated nanoparticle draw solutes prepared with various alkalis

exhibited higher osmotic pressures. No reverse leakages of nanoparticle draw solutes can be found in vigorous FO tests. It is believed that this work may provide significant insights on draw solute design for various FO applications.

7.2 Experimental

7.2.1 Materials

Iron (III) acetylacetonate ($Fe(acac)_3$, 99.9%), triethylene glycol (98%), 2-pyrrolidone (99%), polyacrylic acid (PAA, Mw=1800, 98%), poly(N-isopropylacrylamide) (PNIPAM, Mw=10k, 98%), sodium hydroxide (99%) and calcium hydroxide (99%) were purchased from Sigma-Aldrich. Ethyl acetate (99%) was obtained from Tedia. NaCl (99.5%) was supplied by Merck. All the chemicals above were used as received. TriSep Flat Sheet Membrane TS80 purchase from Sterlitech was employed in the NF process. The deionized (DI) water used in experiments was produced by a Milli-Q unit (Millipore, USA) with a resistivity of 18 MΩ /cm.

7.2.2 Synthesis of Surface-dissociated Nanoparticles

Nanoparticles of different ligand compositions and surface-dissociated with different alkalis were prepared in this work. The nanoparticle cores were composed of iron oxide. Nanoparticles capped with PAA and PNIPAM as well as PAA alone denoted as PAA-PNIPAM@NP and PAA@NP. They were firstly synthesized by thermal decomposition

method as illustrated in the first line of Table 1. After that, COOH groups on nanoparticle surfaces were further dissociated by the addition of either NaOH or $Ca(OH)_2$. The four types of surface-dissociated nanoparticles are abbreviated as Na/PAA@NP, Na/PAA-PNIPAM@NP, Ca/PAA@NP and Ca/PAA-PNIPAM@NP, as illustrated in the second and third lines of Table 1.The synthesis details can be found in this thesis 2.1.

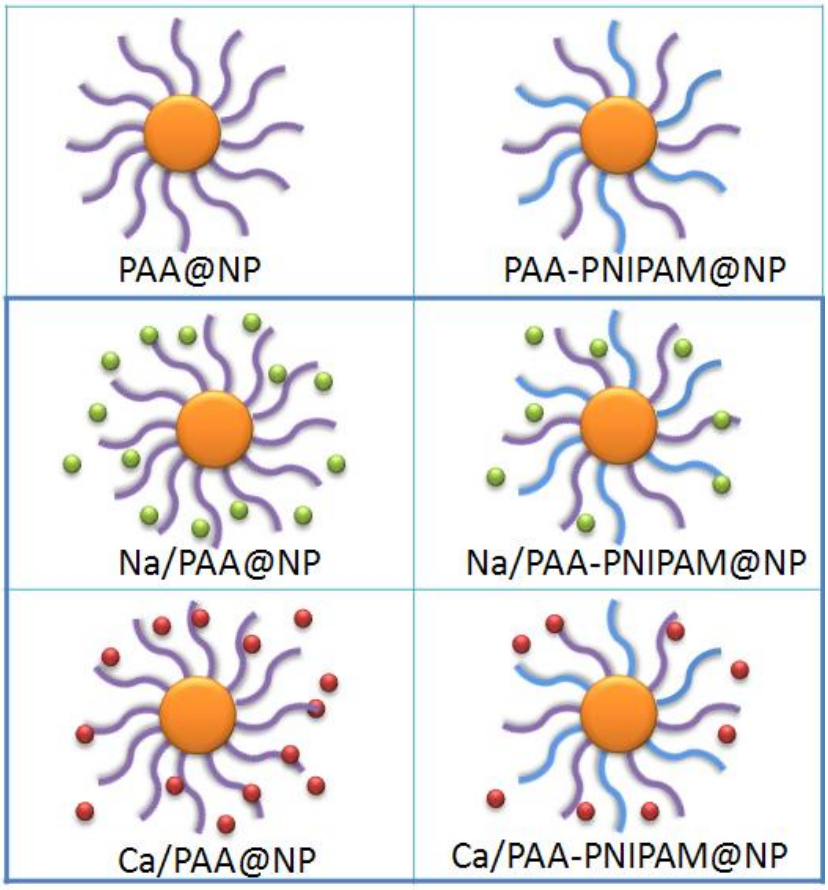

Table 7.1 Illustration of nanoparticles prepared

PAA@NPs were synthesized by a thermal decomposition method in the presence of Iron (III) acetylacetonate, using polyacrylic acid as the capping agent and triethylene glycol as

the solvent. The detailed synthetic procedures and other characterizations can be found in thesis 2.1. Both PAA@NPs and PAA-PNIPAM@NPs were dissolved in DI water. The alkaline solution of either NaOH or $Ca(OH)_2$ was added dropwise in the nanoparticle solution until a constant neutral solution was obtained under mechanical stirring. After that, the resultant nanoparticle solutions were dialyzed for 36 hours to completely remove impurities prior to FO application.

7.2.3 Characterization of Surface-dissociated Nanoparticles

The measurements of size distribution of nanoparticles were conducted by a Nanoparticle Size Analyzer (Nano ZS, ZEN3600). Nanoparticles were imaged using a Transmission Electron Microscope (TEM, JEOL: JEM-3010 model) by drying a dispersion of nanoparticles on amorphous carbon coated copper grids. Spectra of Fourier transform infrared spectroscopy (FTIR) of nanoparticles which were pressed into KBr pellets were obtained on a Bio-Rad Spectrometer of FTS 135. The pH values of nanoparticle solutions were measured by a pH meter (Horiba pH meter D-54, Japan). The osmotic pressures of nanoparticle solutions were converted from osmolality which was obtained from an osmometer (3250, Advanced Instrument, USA).

7.2.4 Forward Osmosis using Surface-Dissociated Nanoparticles as Draw Solutes

Commercially available HTI membranes (Hydration Technologies Inc. previously Osmotek Inc.) were employed as the FO membranes, while both DI water and synthetic brackish water were used as feed solutions. The details of FO test can be found in thesis 2.3.

7.2.5 Nanoparticle Draw Solutes Regeneration via Integrated Eletrophresis-Nanofiltration System

After water extracted from the feed solution in the FO process, the diluted nanoparticle draw solution was regenerated via an integrated electric field and nanofiltration system, as illustrated in Figure 7.1. Two parallel flat metal plates served as electrodes were placed in the diluted nanoparticle draw solution and were connected by a DC power supply from Bio-Rad. In response to an applied electric field, nanoparticles would migrate to the anode, while metal ions towards the cathode. Thus, the nanoparticles turned to their original state without metal ions on the surface and they were collected on the metal plate. Meanwhile, the leftover alkaline solution of metal ions was subjected to a nanofiltration (NF) process to reconcentrate the alkaline solution and retrieve the product water. A flat sheet membrane module made from stainless steel with an effective membrane area of 9.6 cm^2 (3.5cm in diameter) was employed to house the NF membrane. A magnetic stirring bar was placed inside the cell so that the effect of concentration

polarization was minimized. Before conducting experiments, the membrane was rinsed with DI water according to the standard procedures to remove preservatives. The NF process was operated under a trans-membrane pressure of no more than 5 bar. Subsequently, the reconcentrated alkaline solution was employed to dissolve and ionize the pre-collected nanoparticles, which could proceed to the FO process and perform as draw solutes again.

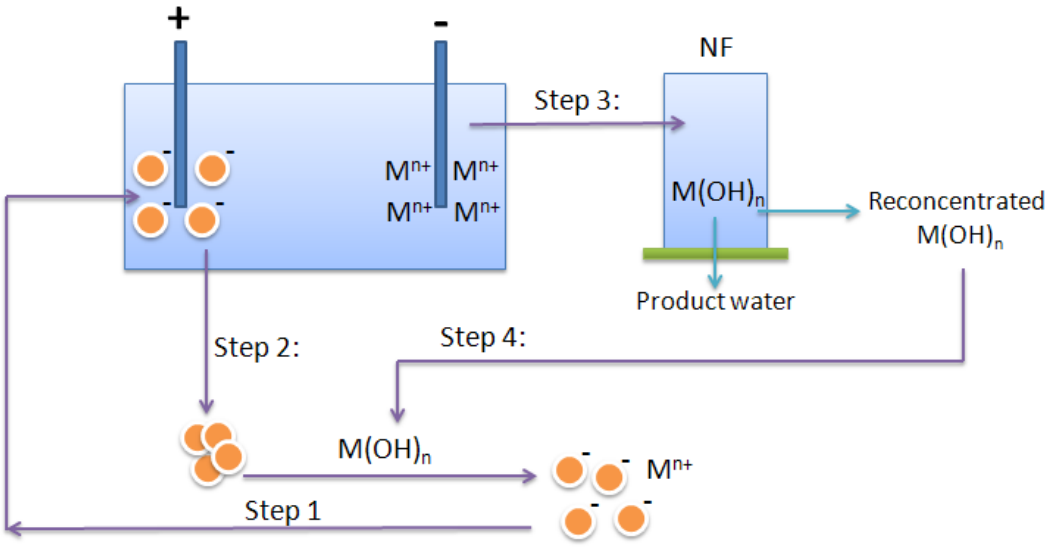

Figure 7.1 Schematic diagram of an electric field and nanofiltration integrated system

7.3 Results and Discussion

7.3.1 Design strategies of surface-dissociated nanoparticles

A primary aim of this work was to design hydrophilic nanoparticle draw solutes by surface modifications in order to induce a higher osmotic pressure than our previous

thermo-responsive magnetic nanoparticles capped with PNIPAM [29]. PAA was therefore introduced together with PNIPAM onto the nanoparticle surface to increase both osmotic pressure and hydrophilic propensity. In addition, PAA can easily anchor on nanoparticle cores with the copious carboxyl groups [35-36]. Thus, PAA-PNIPAM@NPs were expected to exhibit a higher osmotic pressure and water flux than PNIPAM@NPs owing to the existence of PAA. On the other hand, osmotic pressure is a colligative property and PAA has limited dissociation in water at its inherent pH range. As a result, a further increment in osmotic pressure was hindered. Moreover, experimental results showed that the interaction between PAA and PNIPAM polymer chains on the nanoparticle surface resulted in nanoparticle agglomeration, which would not give a fair osmotic pressure and FO performance.

Since the recent research verified that the polyelectrolyte analog of PAA was neutral in water and had a much greater dissociation capacity than PAA [30], a higher osmotic pressure and conductivity were induced in the polyelectrolyte analog of PAA solutions resulting from dissociated carboxyl groups and the grafted cations [30]. Therefore, PAA-PNIPAM@NPs were added with Na^{+} and Ca^{2+} alkaline solution respectively to achieve enhanced dissociation of COOH on nanoparticle surface, in order to eliminate the agglomeration between nanoparticles and to exceed the FO performance of PAA-PNIPAM@NPs. Nanoparticles capped with PAA alone (PAA@NPs) and their surface-dissociated nanoparticles (Na/PAA@NPs; Ca/PAA@NPs) using alkalis were also prepared to systematically investigate their potential as draw solutes.

7.3.2 Characterization of Surface-Dissociated Nanoparticles

Size distributions of PAA-PNIPAM series nanoparticles in Figure 7.2a displayed that PAA-PNIPAM@NPs agglomerated to a size up to 1000 nm in diameter. . Conversely, the nanoparticle size can be decreased to around 20 nm in diameter after the addition of Na^{+} and Ca^{2+} alkaline solutions respectively. The existence of alkali in the solution increased the pH of nanoparticle solutions and facilitated the dissociation of PAA function groups from COOH to COO^{-} . Hence the interaction with PNIPAM on nanoparticle surface was eliminated. As a result, the nanoparticles remained stable as individual particles without agglomeration.

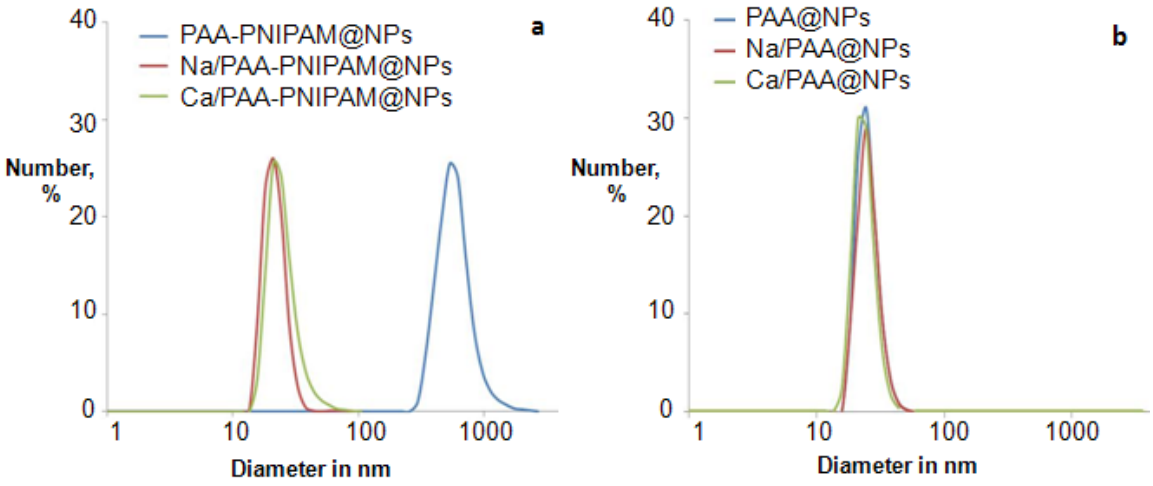

Figure 7.2 Size distributions of surface-dissociated nanoparticles and their originals

The PAA series nanoparticles showed no changes in diameter before and after surface-dissociation. At approximately 20 nm, they are similar in size to the PAA-PNIPAM series nanoparticles. The surface-dissociated nanoparticles possessed an increased zeta potential of -30mV~-40mV compared to PAA@NPs of -25 mV, indicating a higher stability of surface-dissociated nanoparticle draw solutes in water. TEM images of PAA and PAA-PNIPAM series nanoparticles dispersed in water (excluding those agglomerated PAA-PNIPAM@NPs) were shown Figure 7.3. It can be readily discerned that all nanoparticles were sphere in shape but exhibited a slight polydispersity with a size distribution of 7 ±3 nm in diameter. The particle size from TEM seemed to be smaller than the size distribution determined from the Nanoparticle Size Analyzer. This discrepancy was attributed to the existence of ions and extended polymer chains around nanoparticles in aqueous solutions.

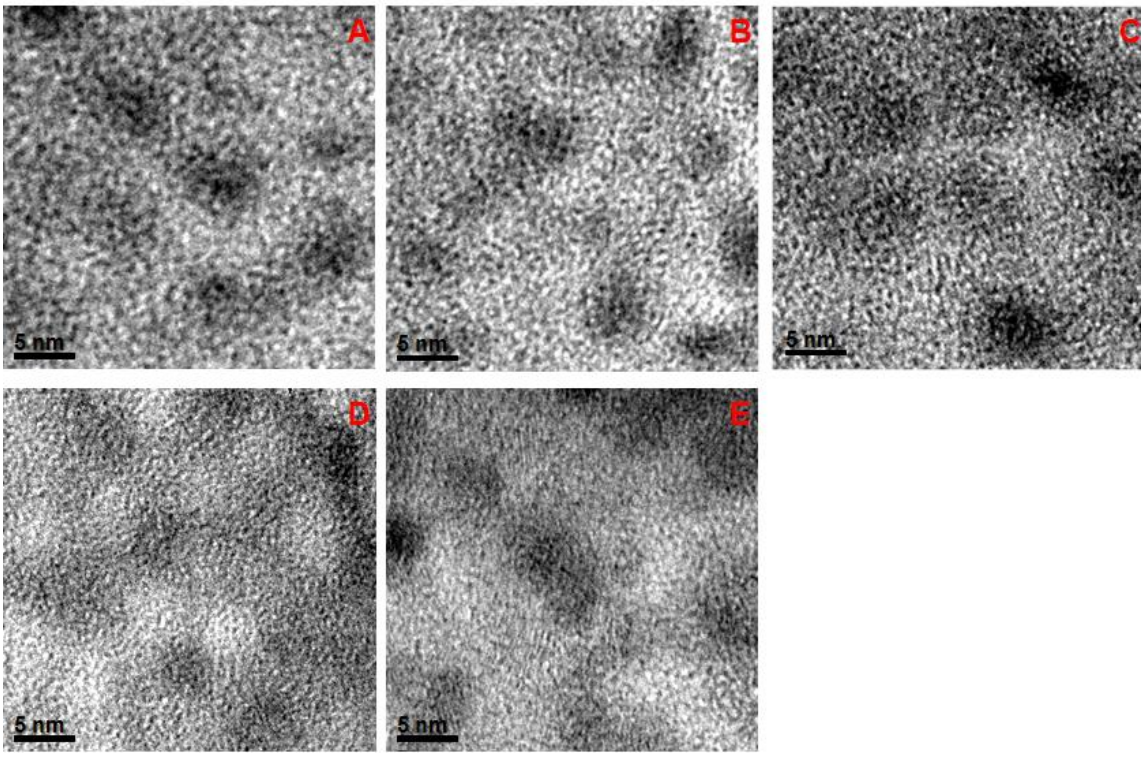

Figure 7.3 TEM imagines: A (Na/PAA@NPs), B (Ca/PAA@NPs), C (PAA@NPs), D (Na/PAA-PNIPAM@NPs) and E (Ca/PAA-PNIPAM@NPs)

Figure 7.4a & b showed the FTIR spectra of PAA series and PAA-PNIPAM series nanoparticles. Typical peaks of PAA groups were found in both figures. The peaks at 1120–1060 cm^{-1} corresponded to C–O stretching of PAA [35-36]. The strong absorption peak of 1735 cm^{-1} was attributed to the C=O stretching mode for carboxylate groups [35-36], which confirmed the successful attachment of PAA on nanoparticle surface. In Figure 4a, peaks at 1650 cm^{-1} and 1570 cm^{-1} were referred to as the secondary amide C=O stretching for amide I and amide II of PNIPAM [37], which verified the presence of PNIPAM on nanoparticle surface. It was also observed that the absorbance of COOH

peaks were relatively decreased after dissociation, indicating COOH groups were dissociated to COO^-groups.

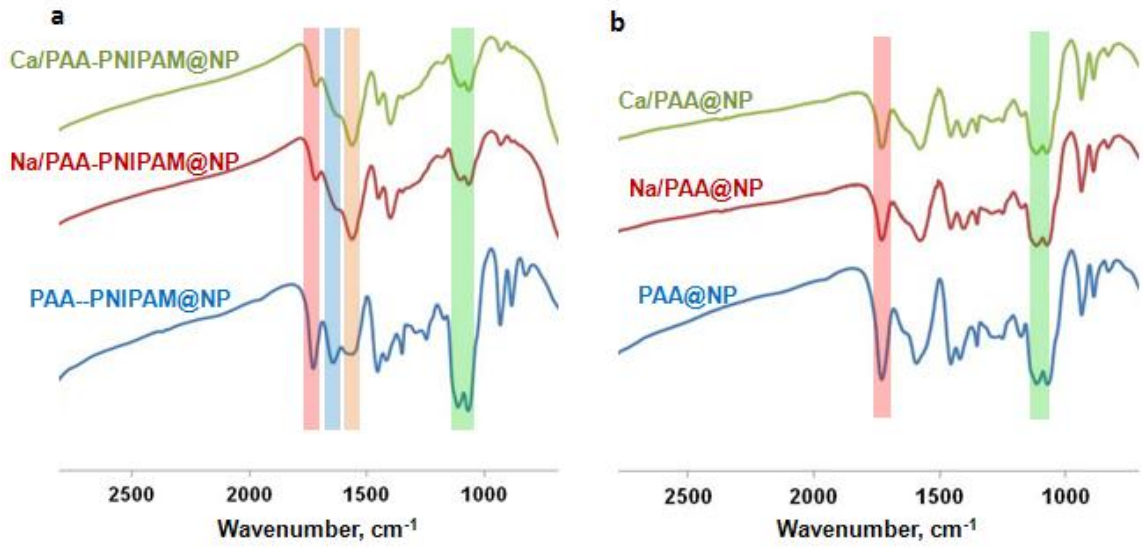

Figure 7.4 FTIR spectra of nanoparticles before and after dissociation

7.3.3 Improved FO Performance using Surface-Dissociated Nanoparticles as Draw Solute

Figure 7.5 showed a comparison in osmotic pressure between original PAA@NPs and surface-dissociated Na/PAA@NPs and Ca/PAA@NPs. With the nanoparticle concentration increased, all the osmotic pressures increased accordingly. It can be seen that the osmotic pressure of surface-dissociated nanoparticles were much higher than that of PAA@NPs without dissociation at the same concentration. The original PAA@NPs had a low degree of dissociation in aqueous solutions and the COOH groups of PAA

contribute to the creation of osmotic pressure. In contrary, the COO^- of PAA capped on the nanoparticle surface co-existed with the metal ions; they both induced the osmotic pressure. As the number of solutes is a key factor in determining osmotic pressure of a solution, the surface-dissociated nanoparticle draw solution generated a higher osmotic pressure than the original nanoparticle draw solution. As shown in Figure 7.6b, Na/PAA@NPs and Ca/PAA@NPs draw solutes were able to draw water from a synthetic brackish water even at a relatively low concentration of 100g NPs per liter, while PAA@NPs could no more draw water from brackish water at the same concentration.

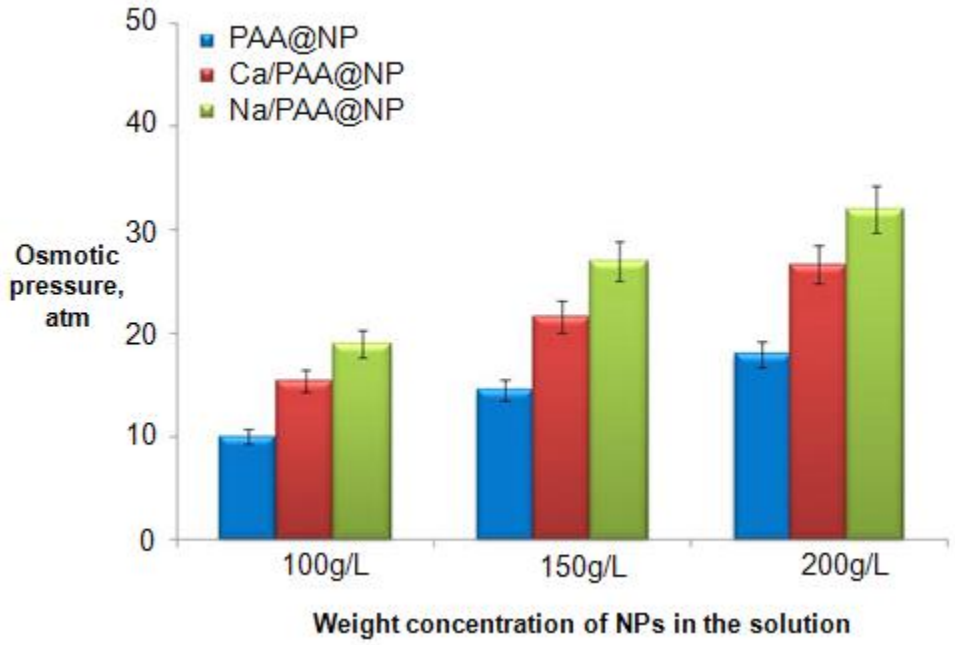

Figure 7.5 Osmotic pressure comparisons of PAA series NPs before and after dissociation

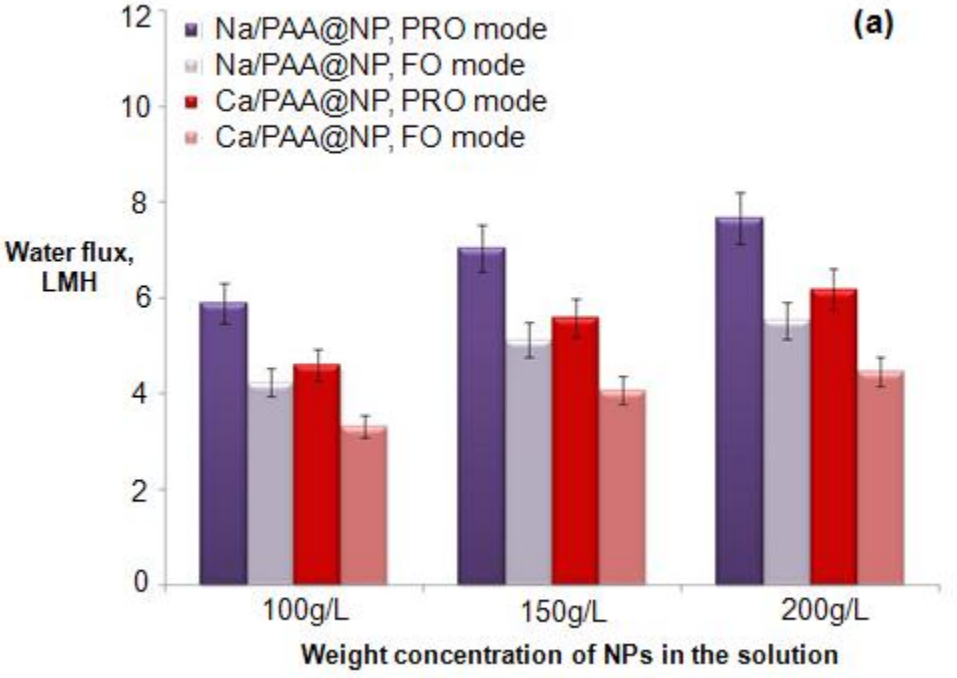
(a)
Na/PAA@NP, PRO mode
Na/PAA@NP, FO mode
Ca/PAA@NP, PRO mode
Ca/PAA@NP, FO mode
Water flux, LMH
0
2
4
6
8
10
12
100g/L
150g/L
200g/L
Weight concentration of NPs in the solution

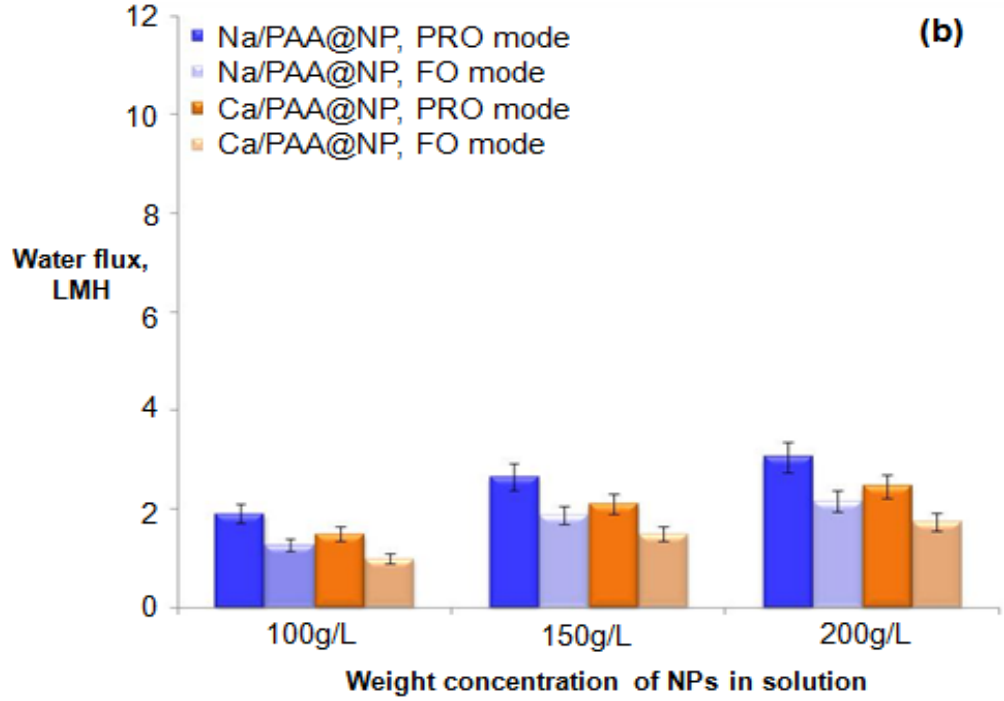
(b)
Na/PAA@NP, PRO mode
Na/PAA@NP, FO mode
Ca/PAA@NP, PRO mode
Ca/PAA@NP, FO mode
Water flux, LMH
0
2
4
6
8
10
12
100g/L
150g/L
200g/L
Weight concentration of NPs in solution

Figure 7.6 A comparison in water flux between surface-dissociated nanoparticles of different ions on PAA@NPs. (a) DI water as feed solution. (b) synthetic brackish water as feed solution

7.3.4 Effect of Different Ions and Ligand Compositions of Nanoparticle Draw Solutes on FO Performance

Figures 7.6 and 7.7 showed the water flux of surface-dissociated nanparticle draw solutes with different alkalis (Na/@NPs; Ca/@NPs) in the solutions using both DI water and synthetic brackish water as feed solutions to compare the FO performance. The water flux of surface-dissociated nanoparticle draw solutes increased with an increase in concentration. It was also observed that the water flux increment was gradually slowed down because a higher concentration multiplied the solution viscosity and resulted in a decrease in the dissociation of PAA analogue on nanoparticle surface [30]. For both PAA and PAA-PNIPAM series, nanoparticles dissociated with NaOH exhibited a higher water flux than $Ca(OH)_2$ using both feed solutions, as illustrated in Figures 7.6 and 7.7. Furthermore, surface-dissociated nanoparticles using NaOH possessed higher osmotic pressures than $Ca(OH)_2$ in both PAA and PAA-PNIPAM series, as summarized in Figure 7.8 a & b. The comparisons of water flux and osmotic pressures were in line with each other, implying that the draw solutions of nanoparticles surface-dissociated using NaOH could generate a higher driving force in FO than $Ca(OH)_2$ surface-dissociated nanoparticles of the same ligand compositions on nanoparticle surface at the same

concentration. This was due to the fact that, in order to neutralize the same amount of COOH groups of PAA on nanoparticles surface, the number NaOH to be used was larger than that of $Ca(OH)_2$ because of the charge differences between Na^+ and Ca^{2+} from the alkaline solutions. Therefore, the draw solutions of surface-dissociated nanoparticles with the addition of NaOH performed superior over $Ca(OH)_2$ in terms of water flux and osmotic pressure as a result of more solutes present in the solution.

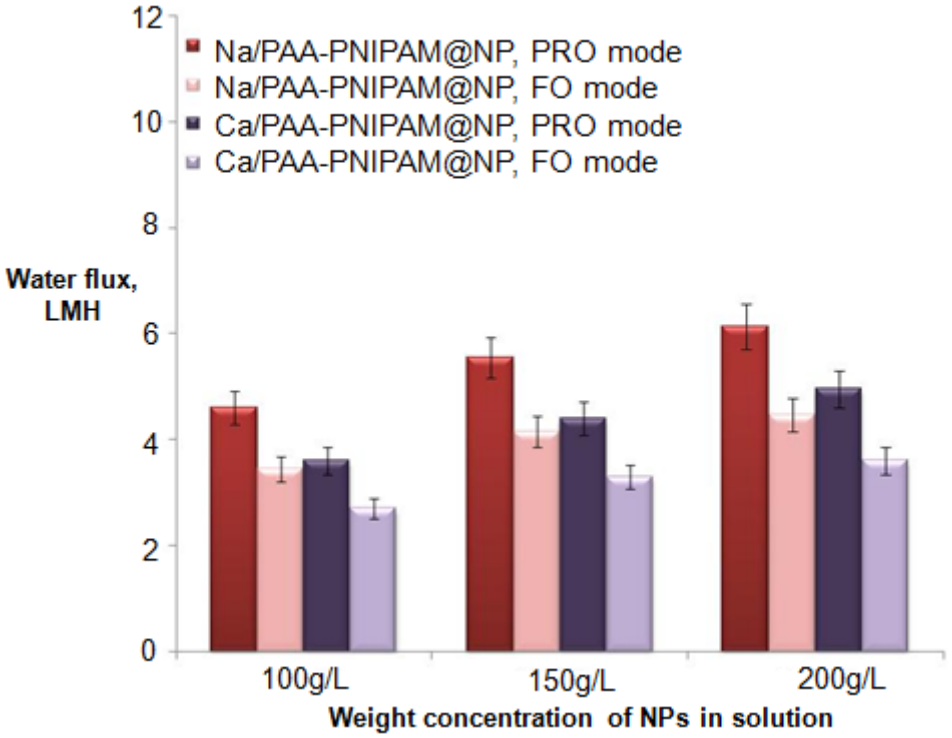

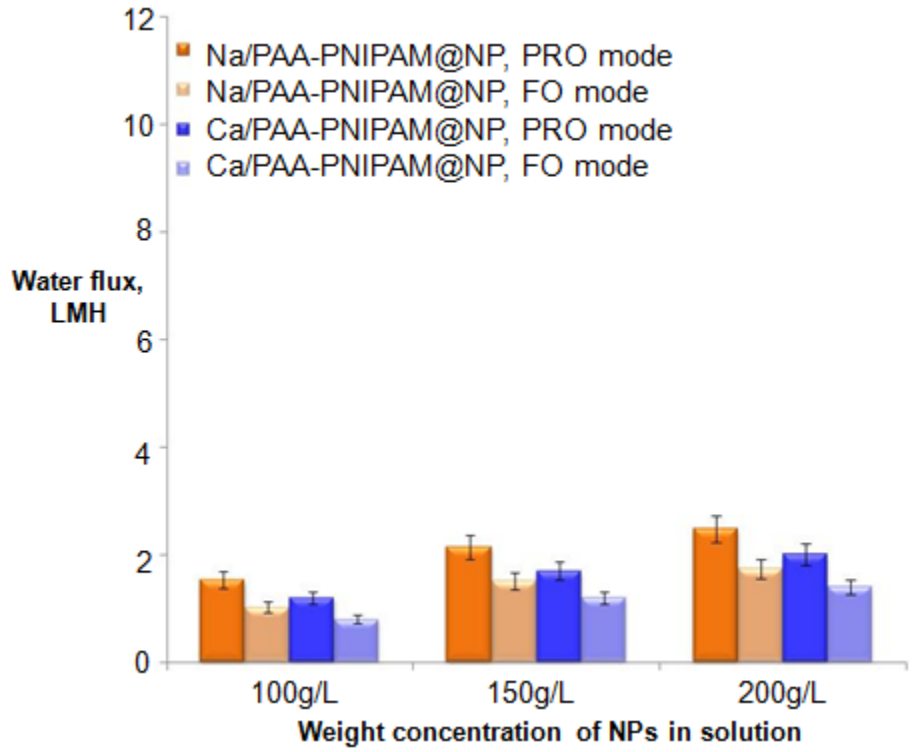

Figure 7.7 A comparison in water flux between surface-dissociated nanoparticles of different ions on PAA-PNIPAM@NPs. (a) DI water as feed solution. (b) synthetic brackish water as feed solution

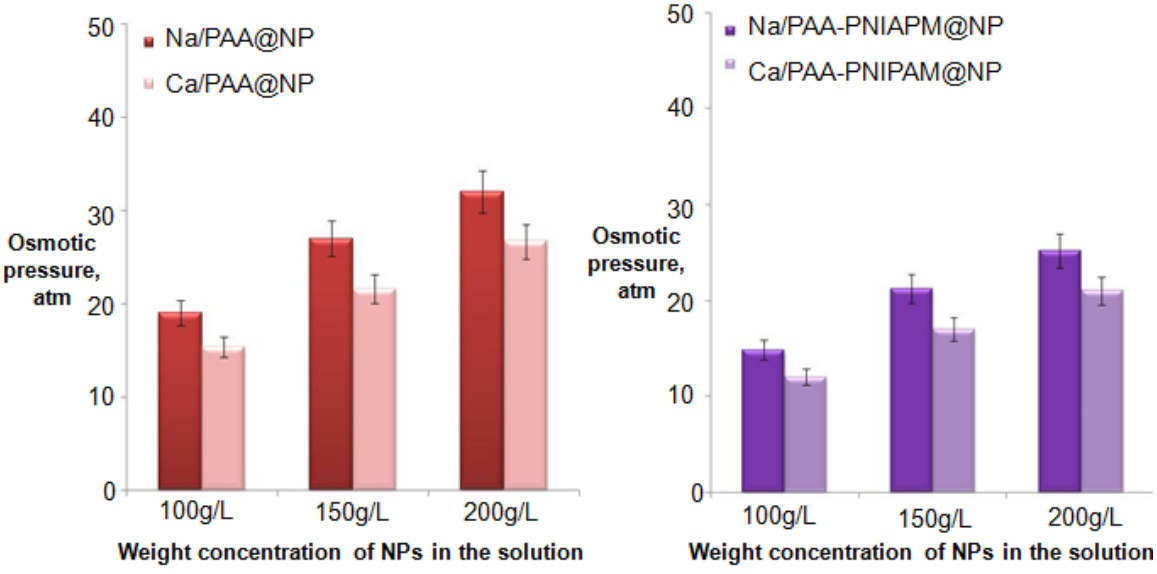

Figure 7.8 A comparison in osmotic pressure comparison between surface-dissociated nanoparticles of Na^{+} and Ca^{2+} in (a) PAA series and (b) PAA-PNIPAM series

Figures 9 and 10 illustrated a comparison in water flux between nanoparticles draw solutes of different ligand compositions but surface-dissociated with the same alkali in the solutions. As seen, draw solutions of surface-dissociated PAA@NPs always produced a higher water flux than PAA-PNIPAM@NPs using both DI water and synthetic brackish water as feed solutions when the surface-dissociations were enhanced with the same alkali. This was due to the fact that the osmotic pressures of surface-dissociated PAA@NPs draw solution were higher than those of surface-dissociated PAA-PNIPAM@NPs regardless either alkali was used in the solutions as shown in Figure 11 a & b. For each nanoparticle, the amount of iron atoms on nanoparticle surface to anchor ligands via chelation was limited. Thus, the numbers of PAA which can be dissociated to increase osmotic pressure on PAA@NPs were higher than PAA-PNIPAM@NPs of the same nanoparticle size and concentration. In addition, PNIPAM was less hydrophilic and could not contribute to water flux increment as much. Therefore, surface-dissociated PAA@NPs draw solutions can effectively generate a higher water flux and osmotic pressure than surface-dissociated PAA-PNIPAM@NP with the same alkali added.

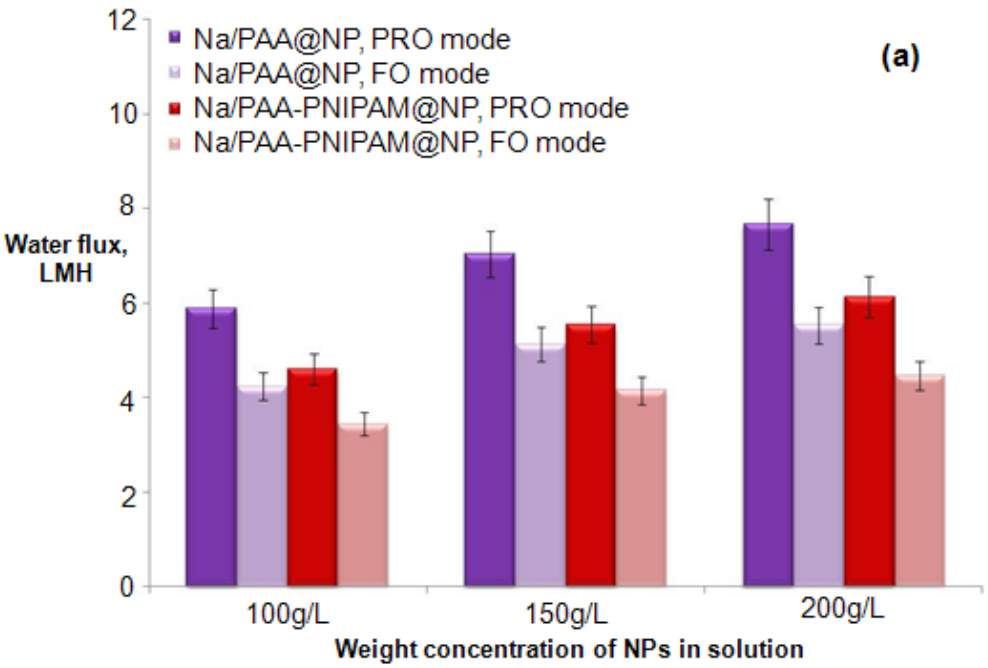
(a)
Na/PAA@NP, PRO mode
Na/PAA@NP, FO mode
Na/PAA-PNIPAM@NP, PRO mode
Na/PAA-PNIPAM@NP, FO mode
Water flux, LMH
0
2
4
6
8
10
12
100g/L
150g/L
200g/L
Weight concentration of NPs in solution

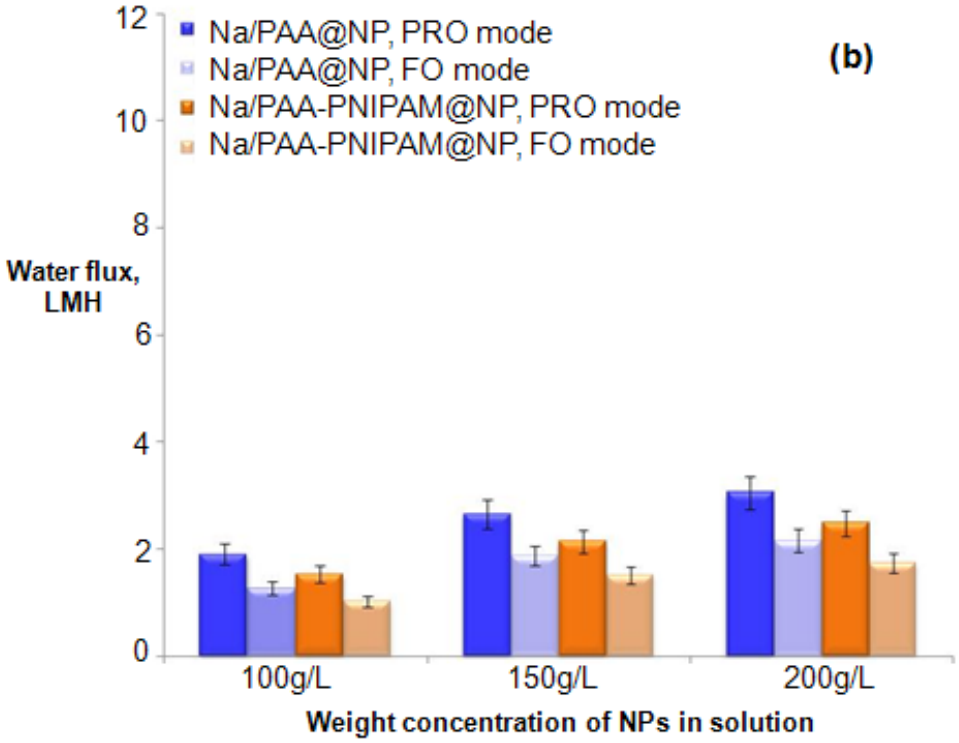
(b)
Na/PAA@NP, PRO mode
Na/PAA@NP, FO mode
Na/PAA-PNIPAM@NP, PRO mode
Na/PAA-PNIPAM@NP, FO mode
Water flux, LMH
0
2
4
6
8
10
12
100g/L
150g/L
200g/L
Weight concentration of NPs in solution

Figure 7.9 A comparison in water flux between surface-dissociated nanoparticles of Na^+ capped with PAA-PNIPAM and PAA. (a) DI water as feed solution. (b) synthetic brackish water as feed solution

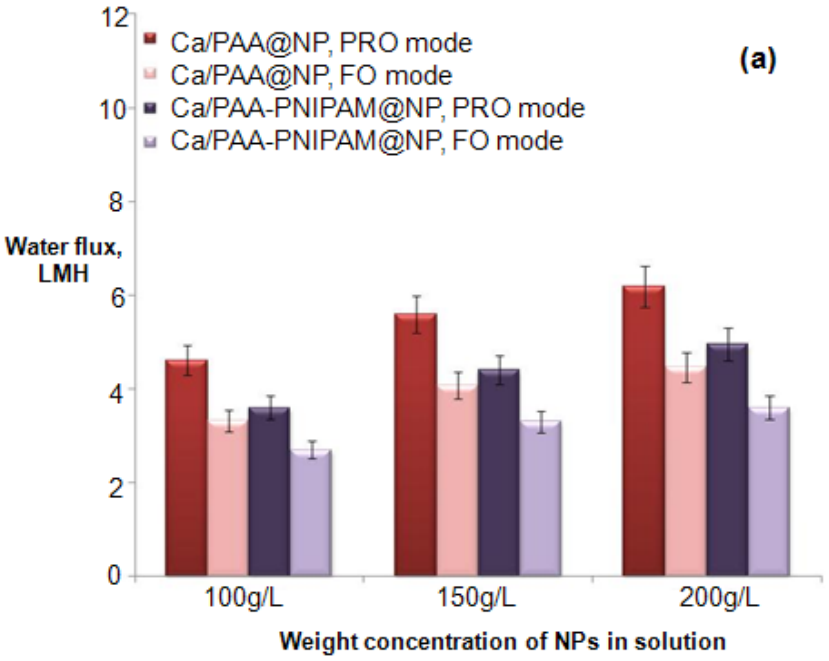

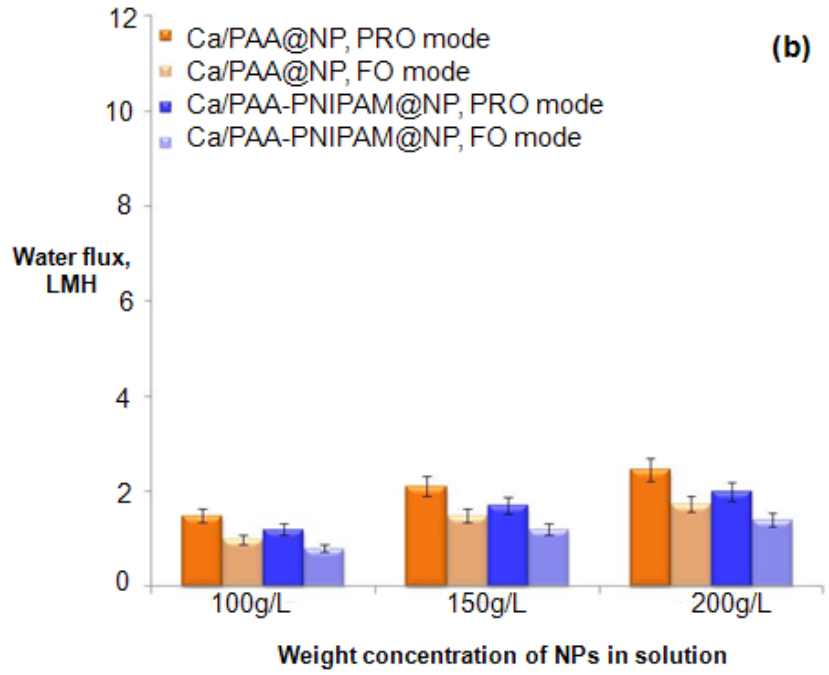

Figure 7.10 A comparison in water flux between surface-dissociated nanoparticles of Ca^{2+} capped with PAA-PNIPAM and PAA (a) DI water as feed solution. (b) synthetic brackish water as feed solution

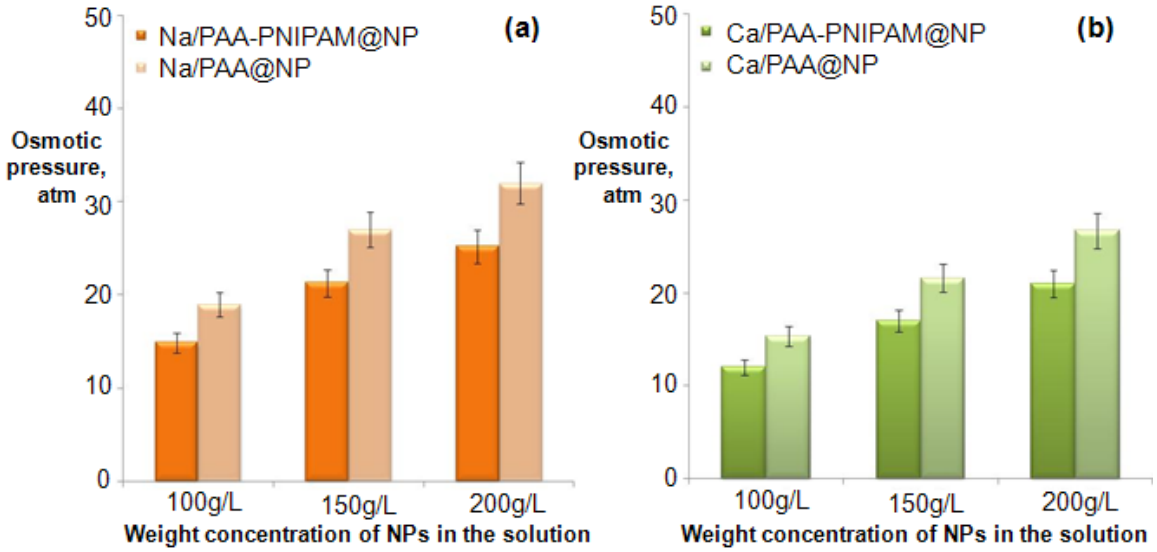

Figure 7.11 A comparison in osmotic pressure between surface-dissociated nanoparticles of different ligand compositions with (a) Na^{+} and (b) Ca^{2+}

7.3.5 Regeneration of Surface-Dissociated Nanoparticle Draw Solutes in an integrated electric field and nanofiltration system

Surface-dissociated PAA-PNIPAM@NPs showed a much lower thermo-responsive property due to the decreased amount of PNIPAM on nanoparticle surface. Hence, a low-strength magnetic field with pre-heating was not able to regenerate surface-dissociated PAA-PNIPAM@NPs. Nonetheless, PAA-PNIPAM@NPs exhibited a higher conductivity after surface-dissociation because of the existence of PAA polyelectrolyte

on nanoparticle surface [30]. With the advantage of improved conductivity, an integrated electric field and nanofiltration system was applied to regenerate diluted draw solutions of surface-dissociated PAA@NPs and PAA-PNIPAM@NPs. It was found that both Na/PAA@NPs and Na/PAA-PNIPAM@NPs could be readily regenerated to draw water from brackish water for water reclamation. The water fluxes were almost constant as shown in Figure 7.12. The collected nanoparticles could be dispersed quickly in the reconcentrated alkaline solution from nanofiltration. The nanoparticles diameters of both surface-dissociated PAA@NPs and PAA-PNIPAM@NPs had almost no changes through recycles as displayed in Figure 7.13, which confirmed that the integrated electric field and nanofiltration system provided an effective method for surface-dissociated nanoparticle regeneration.

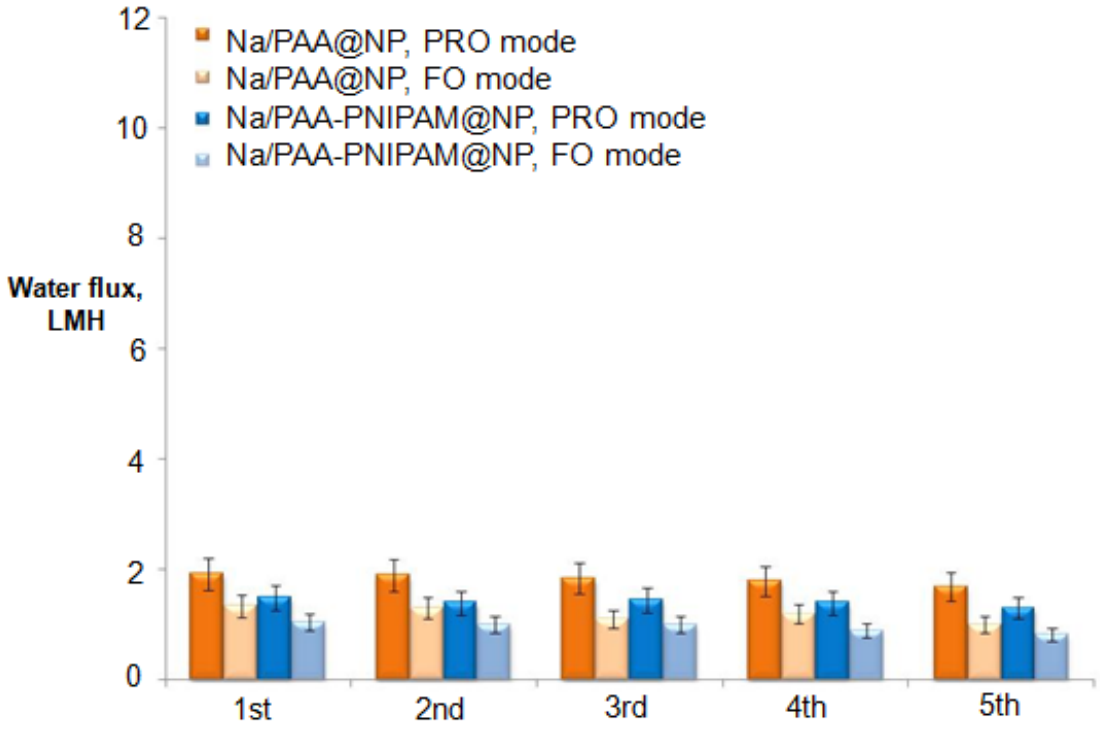

Figure 7.12 Water flux of recycled Na surface-dissociated nanoparticles using synthetic brackish water as feed solution

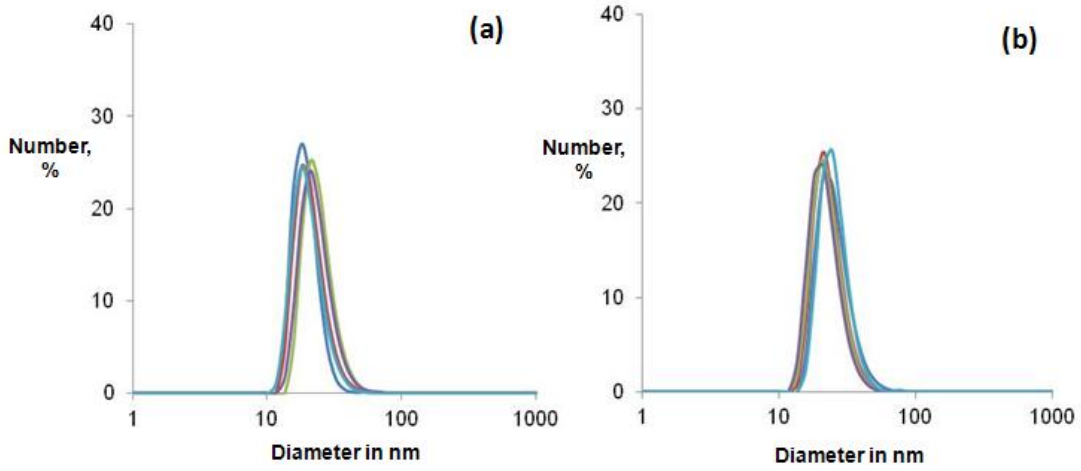

Figure 7.13 Size distributions of recycled NPs (a) Na/PAA@NPs. (b) Na/PAA-PNIPAM@NPs

7.4 Conclusions

Surface-dissociated PAA@NPs and PAA-PNIPAM@NPs have been prepared and applied successfully as draw solutes in FO for water reuse. Nanoparticle draw solutions exhibited higher water fluxes and osmotic pressures after enhanced surface-dissociation using alkaline solutions. Surface-dissociated nanoparticle draw solutions with NaOH added performed superior to $Ca(OH)_2$ surface-dissociated nanoparticles of the same ligand compositions on nanoparticle surface. Draw solutions of surface-dissociated PAA nanoparticles can create a higher driving force than PAA-PNIPAM nanoparticles. The integrated electric field and nanofiltration system was proven to be effective in the regeneration of nanoparticle draw solutes. Future work will be focused on the

optimization and energy evaluation of the regeneration system in the application of water reclamation.

7.5 References

1. I. Escobar, B. V. der Bruggen, Modern Applications in Membrane Science and Technology, Eds. American Chemical Society: Washington, D.C., 2011.
2. T. S. Chung, S. Zhang, K.Y. Wang, J. Su, M.M. Ling, Forward osmosis processes: Yesterday, today and tomorrow, Desalination 287 (2012) 78-81.
3. S. Zhao, L. Zou, C. Y. Tang, D. Mulcahy, Recent developments in forward osmosis: Opportunities and challenges, J. Membr. Sci. 396 (2012) 1-21.
4. T. Y. Cath, A. E. Childress, M. Elimelech, Forward osmosis: principles, applications, and recent developments. J. Membr. Sci. 281 (2006) 70.
5. B. X. Mi, M. Elimelech, Gypsum scaling and cleaning in forward osmosis: measurements and mechanisms, Environ. Sci. Technol. 44 (2010) 2022.
6. E. R. Cornelissen, D. Harmsen, K. F. D. Korte, C. J. Ruiken, J. J. Qin, H. Oo, L.P. Wessels, Membrane fouling and process performance of forward osmosis membranes on activated sludge, J. Membr. Sci. 319 (2008) 158-168.
7. K. Y. Wang, T.S. Chung, J. J. Qin, Polybenzimidazole (PBI) nanofiltration hollow fiber membranes applied in forward osmosis process. J. Membr. Sci. 300 (2007) 6.

8. R. Hausman, B. Digman, I. C. Escobar, M. Coleman, T. S. Chung, Functionalization of polybenzimidizole membranes to impart negative charge and hydrophilicity, J. Membr. Sci. 363 (2010) 195-203.
9. J.C. Su, Q. Yang, J. F. Teo, T.S. Chung, Cellulose acetate nanofiltration hollow fiber membranes for forward osmosis processes. J. Membr. Sci. 355 (2010) 36.
10. R. Wang, L. Shi, C. Y. Tang, S. Chou, C. Qiu, A. G. Fane, Characterization of novel forward osmosis hollow fiber membranes, J. Membr. Sci. 355 (2010) 158-167.
11. N. Y. Yip, A. Tiraferri, W. A. Phillip, J. D. Schiffman, M. Elimelech, High performance thin-film composite forward osmosis, Environ. Sci. Technol. 44 (2010) 3812-3818.
12. Q. Yang, K. Y. Wang, T. S. Chung, A novel dual-layer forward osmosis membrane for protein enrichment and concentration. Sep. Purif. Technol. 69 (2009) 269.
13. M. M. Ling, T. S. Chung, Novel dual-stage FO system for sustainable protein enrichment using nanoparticles as intermediate draw solutes. J. Membr. Sci. 372 (2011) 201–209.
14. E. G. Beaudry, L. A. Lampi, Membrane technology for direct osmosis concentration of fruit juice. Food Technol. 44 (1990) 121.
15. K. Gerstandt, K. V. Peinemann, S. E. Skilhagen, T. Thorsen, T. Holt, Membrane processes in energy supply for an osmotic power plant, Desalination 224 (2008) 64-70.
16. T. Thorsen, T. Holt, Statkraft patents on semi permeable membrane for use in osmosis, and method and plant for providing elevated pressure by osmosis to create

power; WO Patent 03/047733 A1 (2003); US Patent 7,566,402 B2 (2009); US Patent application 2009/0008330 A1 (2009).

17. K. Y. Wang, T. S. Chung, and G. Amy, Developing Thin-film-composite forward osmosis membranes based on the PES/SPSf substrate through interfacial polymerization, AIChE J. 58 (2012) 770.
18. J. C. Su, T. S. Chung, B. J. Helmer, and J. S. de Wit, Enhanced double-skinned FO membranes with inner dense layer for wastewater treatment and macromolecule recycle using Sucrose as draw solute, J. Membr. Sci. 396 (2012) 92.
19. X. Song, Z. Liu, D. D. Sun, Nano gives the answer: Breaking the bottleneck of internal concentration polarization with a nanofiber composite forward osmosis membrane for a high water production rate, Adv. Mater. 23 (2011) 3256-3260.
20. Q. Yang, K. Y. Wang, T. S. Chung, Dual-layer hollow fibers with enhanced flux as novel forward osmosis membranes for water reclamation, Environ. Sci. Technol. 43 (2009) 2800-2805.
21. N. N. Bui, M. L. Lind, E. M.V. Hoek, J. R. McCutcheon, Electrospun nanofiber supported thin film composite membranes for engineered osmosis, J. Membr. Sci. 385-386 (2011) 10-19.
22. R. C. Ong, and T. S. Chung, "Fabrication and positron annihilation spectroscopy (PAS) characterization of cellulose triacetate membranes for forward osmosis," J. Membr. Sci. 394 (2012) 230.

23. H. L. Wang, T. S. Chung, Y. W. Tong, K. Jeyaseelan, A. Armugam, Z. C. Chen, M. H. Hong, W. Meier,"Highly permeable and selective pore-spanning biomimetic membrane embedded with Aquaporin Z," Small. 8 (2012) 1185.
24. S. Qi, C. Q. Qiu, C. Y. Tang, Synthesis and characterization of novel forward osmosis membranes based on layer-by-layer assembly, Environ. Sci. Technol. 45 (2011) 5201-5208.
25. J. R. McChtcheon, R. L. McGinnis, M. Elimelech, A novel ammonia--carbon dioxide forward (direct) osmosis desalination process. Desalination, 174 (2005) 1.
26. M. M. Ling, K. Y. Wang, T. S. Chung, Highly water-soluble magnetic nanoparticles as novel draw solutes in forward osmosis for water reuse. Ind. Eng. Chem. Res. 49(2010)5869.
27. Q. C. Ge, J. C. Su, T. S. Chung, G. Amy, Hydrophilic superparamagnetic nanoparticles: synthesis, characterization, and performance in forward osmosis processes. Ind. Eng. Chem. Res. 50 (2011) 382.
28. M. M. Ling, T.S. Chung, Desalination process using super hydrophilic nanoparticles via forward osmosis integrated with ultrafiltration regeneration, Desalination, 278 (2011) 194–202.
29. M. M. Ling, T.S. Chung, Facile synthesis of thermosensitive magnetic nanoparticles as “smart” draw solutes in forward osmosis, Chem. Commun., 47 (2011) 10788.
30. Q. C. Ge, J. C. Su, G. Amy, T. S. Chung, Exploration of polyelectrolytes as draw solutes in forward osmosis processes, Water Research. 46 (2012) 1318.

31. Q. C. Ge, P. Wang, T. S. Chung, Polyelectrolyte-promoted forward osmosis-membrane distillation (FO-MD) hybrid process for dye wastewater treatment. Env. Sic. Tech In press.
32. S. Phuntsho, H. K. Shon, S. Hong, S. Lee, S. Vigneswaran, A novel low energy fertilizer driven forward osmosis desalination for direct fertigation: Evaluating the performance of fertilizer draw solutions, J. Membr. Sci. 375 (2011) 172-181.
33. M. Y. A. Mollah, R. Schennach, J. R. Parga, D. L. Cocke, Electrocoagulation (EC)—science and applications, J. Hazard. Mater. B 84 (2001) 29.
34. J. D. Bass, X. Ai, A. Bagabas, P. M. Rice, T. Topuria, J. C. Scott, F.H. Alharbi, H.C. Kim, Q. Song, R.D. Miller, An Efficient and Low-Cost Method for the Purification of Colloidal Nanoparticles, Angew. Chem. Int. Ed. 50 (2011) 6538 .
35. J. P. Ge, Y. X. Hu, M. Biasini, C. L. Dong, J. H. Guo, W. P. Beyermann, Y. D. Yin, One-step synthesis of highly water-soluble magnetite colloidal nanocrystals. Chem. Eur. J. 13 (2007) 7153.
36. T. R. Zhang, J. P. Ge, Y. X. Hu, Y. D. Yin, A general approach for transferring hydrophobic nanocrystals into water. Nano Lett. 7 (2007) 3203.
37. T. Isojima, M. Lattuada, J. B. Vander Sande, T. A. Hatton. Reversible clustering of pH- and temperature-responsive Janus magnetic nanoparticles, ACS Nano, 2 (2008) 1799.

CHAPTER 8

CONCLUSION AND RECOMMENDATIONS

8.1 Conclusion

In comparison to conventional draw solutes found in literature, nanoparticles have shown superiorities than others in terms of both FO performance and regeneration methods. However, development of high performance nanoparticle draw solutes has not yet been optimal. In general, nanoparticle draw solutes have exhibited promising perspective in a variety of applications. The first part of thesis has been focused on the exploration of highly water soluble magnetic nanoparticles as draw solute in FO for water reuse. Highly water soluble magnetic nanopaticles have been successfully synthesized and demonstrated them as novel robust draw solute in forward osmosis for the first time. Draw solutions of magnetic nanoparticles capped with polyacrylic acid exhibit the highest water flux among the three different surface functionalized magnetic nanoparticles. It is believed that water flux can be further increased by modifying the surface chemistry. Magnetic nanoparticles after using in the FO process are readily captured in the magnetic field. HGMS provides a facile and fast way to facilitate the recovery of magnetic nanoparticles in a continuous process. In addition, water flux can be enhanced by decreasing the diameters of magnetic nanoparticles.

Ultrasonication was applied to redisperse agglomerated magnetic nanoparticle draw solutes after magnetic separation. Experimental results indicate that the agglomeration of magnetic nanoparticles recovered by magnetic fields can be solved by ultrasonication, but the magnetic properties of nanoparticles may deteriorate. It was conceptually demonstrated that, for the first time, a potentially sustainable integrated FO-UF system for water reuse and desalination with super hydrophilic nanoparticles as draw solutes. The integrated FO-UF process may be better than the FO-magnetic separation process when using super hydrophilic nanoparticles as draw solutes. A novel FO-UF process has been demonstrated and investigated. PAA-NPs draw solutions can be recycled in FO-UF for 5 times to desalinate synthetic seawater without increasing their sizes or reducing its osmotic functionality. UF membranes of small pore diameter and narrow pore size distribution are preferred to enhance recovery efficiency of nanoparticle draw solution. It is believed the proposed FO-UF integrated system using super hydrophilic nanoparticles as draw solutes is a promising technology to desalinate both seawater and brackish water and to reclaim water from wastewater.

Dual-stage FO systems using nanoparticles as intermediate draw solutes was proposed and investigated for protein enrichment The newly developed system can be applicable to various proteins of different sizes and charges. The dual-stage FO system consisting of a large membrane surface and highly osmotic draw solutes can effectively dehydrate protein solutions under athermal conditions. In addition, experimental results show that

(1) The PAA-NPs intermediate draw solution is efficacious to keep protein intact and stable during the enrichment, while concentrated salts as draw solutes may denature proteins; (2) The steady osmotic driving force of PAA-NPs solution can be maintained in the continuous dual-stage FO; (3) The model RO retentate can regenerate PAA-NPs solutions effectively, (4) the PRO PRO model may enrich proteins fast if protein fouling is minimal and (5) Dual-stage FO integrated with nanoparticles exhibits superiority than one-stage FO to enrich protein solutions, considering the aspects of reverse salt flux as well as expense and disposal of draw solutions. The proposal system can be used for the application of other pharmaceutical and bio-molecule enrichments.

In order to further solve the magnetic nanoparticle draw solute agglomeration, thermosensitive superparamenetic nanoparticles was successfully synthesized with improved hydrophilicity in one step. The resultant PNIPAM/TRI-MNPs exhibit uniform particle sizes of less than 20 nm and excellent stability in water. It was demonstrated that PNIPAM/TRI-MNPs can be recycled as a ‘smart’ draw solute in FO processes without losing performance efficiency as a result of their reversible thermosensitive property facilitating the magnetic separation of low strength to assure the integrity of nanoparticle draw solutes. The FO performance can be enhanced with nanoparticle surface engineering and decreasing particle sizes. It is believed that thermosensitive magnetic nanoparticles hold great potential as a novel draw solute in FO processes for water reuse, desalination, protein dehydration and biomedical applications.

So as to improve the FO performance of nanoparticle draw solutes with sustained regeneration efficiency, surface-dissociated PAA@NPs and PAA-PNIPAM@NPs have been prepared and applied successfully as draw solutes in FO for water reuse. Nanoparticle draw solutions exhibited higher water fluxes and osmotic pressures after enhanced surface-dissociation using alkaline solutions. Surface-dissociated nanoparticle draw solutions with NaOH added performed superior to Ca(OH)2 surface-dissociated nanoparticles of the same ligand compositions on nanoparticle surface. Draw solutions of surface-dissociated PAA nanoparticles can create a higher driving force than PAA-PNIPAM nanoparticles. The integrated electric field and nanofiltration system was proven to be effective in the regeneration of nanoparticle draw solutes. Future work will be focused on the optimization and energy evaluation of the regeneration system in the application of water reclamation.

8.2 Recommendations

Based on the experimental results obtained, the discussions presented and the conclusions from this research, the following recommendations may be interesting for future investigation related to this topic:

1) Nanoparticle draw solutes with improved hydrophilicility on the surface so that higher FO performance can be obtained.

2) Nanoparticle draw solutes with tunable particle size so that higher regeneration efficiency can be obtained.

3) Further exploration of novel draw solutes of high osmotic pressure and facile recovery in integrated systems.

4) Energy evaluations and economical calculations of FO process and nanoparticle draw solutes regenerations.

5) Extend of the use of nanoparticle draw solutes in FO in various applications.

Publication list

US Provisional Patent Application No.: 61/302,992

Forward osmosis process using water soluble magnetic nanoparticles as draw solutes

Inventors: **M. M. Ling**, T. S. Chung and K. Y. Wang.

Scientific paper:

(1). **M. M. Ling**, K. Y. Wang, T. S. Chung, Highly water-soluble magnetic nanoparticles as novel draw solutes in forward osmosis for water reuse. Ind. Eng. Chem. Res. 49 (2010) 5869.

(2). **M. M. Ling**, T.S. Chung, Desalination process using super hydrophilic nanoparticles via forward osmosis integrated with ultrafiltration regeneration, Desalination. 278 (2011) 194–202.

(3). **M. M. Ling**, T. S. Chung, Novel dual-stage FO system for sustainable protein enrichment using nanoparticles as intermediate draw solutes. J. Membr. Sci. 372 (2011) 201–209.

(4). **M. M. Ling**, T.S. Chung, Facile synthesis of thermosensitive magnetic nanoparticles as "smart" draw solutes in forward osmosis, Chem. Commun., 47 (2011) 10788.

(5) T. S. Chung, S. Zhang, K.Y. Wang, J. Su, **M.M. Ling**, Forward osmosis processes: Yesterday, today and tomorrow, Desalination 287 (2012) 78-81.

(6). **M. M. Ling**, T.S. Chung, Surface-dissociated nanoparticles draw solutes and their regeneration in an integrated electric field and nanofiltration system, Ind. Eng. Chem. Res, submitted

Conference Paper:

(1) **M. M. Ling**, K. Y. Wang, T. S. Chung, Highly water soluble magnetic nanoparticles as novel draw solutes in forward osmosis for water reuse, NAMS, Washington DC, July 17-22, 2010

(2) **M. M. Ling**, K. Y. Wang, T. S. Chung, Investigations of Using Highly Water-Soluble Magnetic Nanoparticles as Novel Draw Solutes in Forward Osmosis, AIChE Annual Meeting, November 7-12, 2010, Salt Lake City, Utah, USA

(3) **M. M. Ling**, T. S. Chung, Novel dual-stage FO system for sustainable protein enrichment using nanoparticles as intermediate draw solutes, NAMS, Las Vegas, NV, June 6-8, 2011

(4) **M. M. Ling**, T. S. Chung, Novel dual-stage FO system for sustainable protein enrichment using nanoparticles as intermediate draw solutes, U21 Graduate Student Conference, Kuala Lumpur, Malaysia, June 22-26, 2011

(5) **M. M. Ling**, Q. C. Ge, J. Su, G. Amy, T. S. Chung, Molecular designs of novel draw solutes in forward osmosis for desalination, Desalination for the Environment: Clean Water and Energy, Barcelona, Spain April 22–26, 2012